UNIVERSITY OF CALIFORNIA SAN DIEGO

NMR Studies of the G Protein-Coupled Receptor CXCR1

A dissertation submitted in partial satisfaction of the
requirements for the degree Doctor of Philosophy

in

Chemistry

by

Jasmina Radoicic

Committee in Charge:

Professor Stanley J. Opella, Chair
Professor Rommie Amaro
Professor Geoffrey Chang
Professor Edward Dennis
Professor Patricia A. Jennings

2018

The Dissertation of Jasmina Radoicic is approved, and it is acceptable in quality and form for publication on microfilm and electronically:

_____

_____

_____

_____

_____
Chair

University of California San Diego

2018

DEDICATION

To my parents and husband, for your unconditional love and support throughout these years.

EPIGRAPH

“Success is not final; failure is not fatal: it is the courage to continue that counts.”

-Winston Churchill

TABLE OF CONTENTS

LIST OF ABBREVIATIONS

^{1}H	Proton
^{2}H	Deuterium
^{13}C	Carbon -13
^{15}N	Nitrogen - 15
^{31}P	Phosphorous - 31
AMS	Ammonium Sulfate
COSY	Correlation Spectroscopy
CP	Cross Polarization
CSA	Chemical Shift Anisotropy
CXCR1	CXC Chemokine Receptor 1
CXCR2	CXC Chemokine Receptor 2
DC	Dipolar Coupling
DHPC	1,2-dihexanoy-sn-glycero-3-phosphocholine
DMPC	1,2-dimyristoyl-sn-glycero-3-phosphocholine
DMPG	1,2-Dimyristoyl-sn-glycero-3-phosphorylglycerol
DPC	Dodecyl Phosphocholine
EDTA	Ethylenediamine tetraacetic acid
FPLC	Fast protein liquid chromatography
Gαi1	Inhibitory G-protein alpha subunit 1
GDP	Guanosine Di-Phosphate

GMP-PNP	Guanosine 5′-[β,γ–imido]triphosphate trisodium salt hydrate
GPCR	G Protein – Coupled Receptor
GST	Glutathione S - transferase
GTP	Guanisine Tri-Phosphate
GTPγS	Guanosine 5'-O-[gamma-thio] triphosphate
HEPES	4-(2-hydroxyethyl)-1-piperazineethanesulfonic acid
HETCOR	Heteronuclear Correlation
HPLC	High Pressure Liquid Chromatography
HPC	Hexadecyl Phosphocholine
HSQC	Hetronuclear Single Quantum Coherence
HQA	2-amino-3-(8-hydroxyquinolin-3-yl)propanoic acid
IL8	Interleukin - 8
INEPT	Insensitive Nuclei Enhanced by Polarization Transfer
IPTG	Isopropyl β-thiogalactoside
kD	Kilo - Dalton
KSI	Ketosteroid Isomerase
LB	Luria - Bertani
MAS	Magic Angle Spinning
MSP	Membrane Scaffold Protein
NMR	Nuclear Magnetic Resonance
NOE	Nucear Overhauser Effect
NOESY	Nucear Overhauser Effect Spectroscopy

PBS	Phosphate Buffered Saline
PCS	Pseudo Chemical Shift
PDB	Protein Data Bank
PDSD	Proton Driven Spin Diffusion
PISA	Polarity Index Slant Angle
PISEMA	Polarization Inversion Spin Exchange at the Magic Angle
PMSF	Phenylmethanesulfonylfluoride
PRE	Paramagnetic Relaxation Enhancement
SAMMY	Sandwich-Based Separated Local Field Spectroscopy
SDS	Sodium Dodecyl Sulfate
SDS-PAGE	Sodium Dodecyl Sulfate Polyacrylaminde Gel Electrophoresis
SLF	Separated Local Field
SMA	Styrene – Maleic Acid
SMA-EA	Styrene maleic acid-ethanol amine modified
SMALP	Styrene Maleic Acid Lipid Particle
TCEP	Tris(2-carboxyethyl)phosphine
TFE	2,2,2-Trifluoroethanol
TFA	Trifluoroacetic acid
TM	Trans-Membrane
TOCSY	Total Correlation Spectroscopy
Tris-HCl	Tris(hydroxymethyl)aminomethane hydrochloride
TX-100	Triton X - 100

LIST OF FIGURES

ACKNOWLEDGEMENTS

First and foremost, I would like to thank my dissertation advisor Professor Stanley Opella, for giving me the opportunity to be a part of his research group. This dissertation would not be possible without his help, support, and guidance. I am immensely grateful for everything he has taught me and all the instrumentation and facilities which I had available to conduct this research. I would also like to thank my committee members Professor Patricia Jennings, Professor Rommie Amaro, Professor Edward Dennis, and Professor Geoffrey Chang for their support and guidance.

I would like to thank both past and present Opella Lab members for making my experience in the Opella lab so memorable; I have been incredibly lucky to have had the chance to work with so many wonderful people. To Dr. Sang Ho Park, thank you for your patience and mentorship, for teaching me so much about biochemistry and research, and for your support, advice, and friendship over the past years. I would like to thank my office and bench-mate, Dr. Anna De Angelis, for your advice and guidance, for being an incredible support, friend, and a wonderful person to work with. To Dr. Sabrina Berkamp and Zheng Long from “Team GPCR”, thank you for all of our scientific discussions and collaborations, for being such an incredible support system, for all our laughs, and great times together. To my fellow lab-members, past and present, Dr. Lindsay Dawson, Dr. Gabriel Cook, Dr. Ye Tian, Dr. Luis Basso, Dr. Thach (Cody) Can, Dr. Hua Zhang, Dr. Eugene Lin, Dr. George Lu, Megan Chu, Dr. Anna Pavlova, Dr. Andrea Balanceau, Dr. Henry Nothnagel, Dr. Dongtao Cui, Nemil Vora, Youjeong Na, Jiaqian (Emily) Wu, Elena

Vitoshka-Tarasov, Mitchell Zhao and Eric Vetter, I will always remember our time spent together and the great talks, laughs, and experiences that we shared. Thank you for making my time in the Opella lab so memorable. To my colleagues at the NMR “Bubble” Dr. Albert (Chin) Wu, Dr. Bibhuti Das, Dr. Christopher Grant, and Dr. Ratan Rai, thank you for your help and guidance, for teaching me about probes and pulse sequences, for your patience while I was learning and for all the insightful discussions. To Dr. Anthony Mrse and to Dr. Xuemei Huang, thank you for teaching me about solution NMR and for all your support and advice over the years.

Thank you to my undergraduate research advisor, Dr. Francesca Marassi from the Sanford Burnham Prebys Research Institute and Dr. Leigh Plesniak, for opening the door of scientific research for me. Thank you for your patience, guidance, and help and for giving me a strong foundation on which to build my future scientific goals on. I would also like to thank the Marassi Lab members, Dr. Yong Yao, Dr. Luz Meneghini, L. Miya Fujimoto, Dr. Yi Ding, Dr. Chandan Singh, Dr. Kyungsoo Shin, and Pavel Ryzhov for all the great discussions and collaborations we have had over the years. To the Jennings lab members, Dr. Kendra Hailey, Dr. DJ Burban, Dr. Collin Lipper, Dr. Nicholas Tiee, and Jason Stofleth, thank you for being great lab-neighbors, for all our creative happy hours and the fun we have had throughout the years.

Chapter 1, in part, is a reprint of the material as it appears in Quarterly review of Biophysics, “NMR Structures of Membrane Proteins in Phospholipid Bilayers”, by Radoicic J., Lu, G. J., and Opella, S. J., 2014. The dissertation author was the first author of this paper.

Chapter 3, in full, is a reprint of the material as it appears in JBNMR, “Paramagnetic relaxation enhancement of membrane proteins by incorporation of the metal-chelating unnatural amino acid 2-amino-3-(8-hydroxyquinolin-3-yl)propanoic acid (HQA)” by Park, S.H., Wang, V. S., Radoicic, J., De Angelis, A. A., Berkamp, S., and Opella, S. J., 2015. The dissertation author was the third author of this paper.

Chapter 4, in full, is a reprint of the material as it appears in Biophysical Journal, “Interaction of Monomeric Interleukin-8 with CXCR1 Mapped by Proton-detected Fast MAS Solid-state NMR and Intermolecular Paramagnetic Relaxation Enhancement” by Park, S. H., Berkamp, S., Radoicic, J., De Angelis, A. A., and Opella, S. J., 2017. The dissertation author was the third author of this paper.

Chapter 5, in part, is a reprint of the material as it appears in Biophysical Journal, “Macrodiscs Comprised on Styrene-Maleic Acid Lipid Particles (SMALPs) for Oriented Sample Solid State NMR Spectroscopy of Membrane Proteins” by Radoicic, J., Park, S.H., and Opella, S.J., 2018. The dissertation author was the co-first author of this paper.

VITA

2011 Bachelors in Science, University of California San Diego

2018 Doctor of Philosophy, Chemistry, University of California San Diego

PUBLICATIONS

Radoicic J., Lu, G. J., and Opella, S. J. (2014) NMR Structures of Membrane Proteins in Phospholipid Bilayers, *Q. Rev. Biophys*., 47(3):249-83.

Park, S.H., Wang, V. S., **Radoicic, J**., De Angelis, A. A., Berkamp, S., and Opella, S. J., (2015) Paramagnetic relaxation enhancement of membrane proteins by incorporation of the metal-chelating unnatural amino acid 2-amino-3-(8-hydroxyquinolin-3-yl)propanoic acid (HQA), *JBNMR*, 61(3-4):185-96.

Park, S. H., Berkamp, S., **Radoicic, J.**, De Angelis, A. A., and Opella, S. J., (2017) Interaction of Monomeric Interleukin-8 with CXCR1 Mapped by Proton-detected Fast MAS Solid-state NMR and Intermolecular Paramagnetic Relaxation Enhancement, Biophysical Journal, 113(12): 2695–2705.

Radoicic, J., Park, S.H., and Opella, S.J., (2018) Macrodiscs Comprised on Styrene-Maleic Acid Lipid Particles (SMALPs) for Oriented Sample Solid State NMR Spectroscopy of Membrane Proteins, Biophysical Journal, 115(1): 22-25.

ABSTRACT OF THE DISSERTATION

NMR Studies of the G Protein-Coupled Receptor CXCR1

by

Jasmina Radoicic

Doctor of Philosophy in Chemistry

University of California San Diego, 2018

Professor Stanley J. Opella, Chair

Approximately 30% of the proteins expressed from the human genome correspond to membrane proteins. They perform a wide variety of cellular functions and are very attractive drug targets, with almost half of all pharmaceutics targeting these proteins. G protein coupled receptors (GPCRs) are the largest class of integral membrane proteins comprised of seven transmembrane-spanning helices, an extracellular N-terminus, and an intracellular C-terminus. CXCR1 is a class A, rhodopsin-like GPCR which couples to the Gi G-proteins, and has one high-affinity ligand, interleukin-8 (IL8). Many methods used to study membrane protein structure, function, and dynamics require significant

modifications to be made to the protein of interest, resulting in an environment that is far from the native phospholipid bilayer. However, NMR spectroscopy is a powerful technique which allows the study of unmodified membrane proteins in near-native lipid environments and at physiological temperatures and pH.

IL8 interacts with CXCR1 at two sites - the N-terminus (Site I) and the extracellular loops (Site II). To probe these interactions, ^{1}H fast MAS solid-state NMR was used to study IL8 bound to CXCR1 in pnhospholipid bilayers. A majority of the IL8 residues become immobilized upon receptor binding and their chemical shifts significantly perturbed, indicating that the environment and dynamics of the ligand are affected by interactions with CXCR1. Additional long-range distance restraints for the IL8-CXCR1 interaction were obtained via paramagnetic relaxation enhancement (PRE) experiments utilizing incorporation of a metal-chelating unnatural amino acid, 2-amino-3-(8-hydroxyquinolin-3-yl) propanoic acid (HQA), into various CXCR1 constructs positioned at residues near the ligand binding sites.

Sample preparation is challenging because membrane proteins are generally low expressing in heterologous systems, hydrophobic, and difficult to re-fold into their active conformations – any variation from the native structure results in inactive and/or mis-folded protein. The use of detergents can be especially detrimental to membrane proteins. We have developed styrene-maleic acid (SMA) macrodiscs which provide a detergent-free phospholipid bilayer environment for biophysical and functional studies of membrane

proteins under physiological conditions. They are particularly well suited for structure determination by oriented-sample solid-state NMR and high-resolution solid-state NMR spectra of membrane proteins have been obtained in these discs.

Chapter 1. General Introduction

1.1 Membranes and Membrane Proteins

Membranes define the physical boundaries of organelles, cells, unicellular organisms, and some viruses. They allow cells to regulate what enters and exits via membrane proteins. Phospholipids [1] and proteins are the two principal macromolecular constituents of biological membranes. The phospholipids found in biological membranes consist of an amphipathic or charged polar head group attached to two long hydrocarbon chains through a tri-substituted glycerol backbone. A wide range of head groups, chain lengths, number of double bonds, and other chemical characteristics are found in biological membranes. Membrane proteins account for almost one-third of proteins found in the eukaryotic proteome [2]. They are localized in cell surface membranes as well as the integral membranes of organelles such as nuclei, the endoplasmic reticulum, golgi and mitochondria [3]. Membrane proteins have diverse functions including those of transporters, enzymes, ion channels, receptors, and anchoring proteins. Mutations, misfolding, and/or malfunctions of these proteins are implicated in many diseases including diabetes, cancer, cystic fibrosis, cardiovascular disease, immunological disorders, and neurodegenerative diseases [2, 4], and as such, they are the targets for ~40% of all pharmaceuticals [5]. However, given their importance, membrane protein structures are vastly underrepresented in the Protein Data Bank (PDB). Some of the main reasons contributing to the lack of structural information are difficulties in membrane protein expression, purification, and stability. Many methods of membrane protein studies and structure determination require significant modifications to be made to the protein of

interest, resulting in an environment that is far from the native phospholipid bilayer. This further emphasizes the need for development of new and better membrane protein environments, as well as techniques, such as NMR spectroscopy, that can help unravel the structures, function, and interactions of these important proteins without the need for modifications and in a near-native environment.

1.2 NMR Spectroscopy of Membrane Proteins

NMR spectroscopy is a technique which allows for the study of membrane protein structures, dynamics and interactions of a variety of biomolecules and complexes [6]. The nature of the membrane environment used in experimental studies, especially structure determination by NMR, has been a major factor since the beginning of the field [7-11]. With the increasing interest in the analysis of the functions of membrane proteins in terms of their structures, there is a heightened concern about the influence of the surrounding environment as is has been shown that certain environments, such as detergents and organic solvents, can have detrimental effects on membrane protein structure and function [12-18]. Membrane environments including amphipols [19-21], membrane scaffold protein (MSP) nanodiscs [22-24], and peptide [25] and polymer [26] nano- and macro-discs have been developed to facilitate a more native membrane environment.

There are two main approaches used in the NMR studies of membrane protein structure and function: solution and solid-state NMR. We can use both solution and solid-state NMR to study membrane proteins, with the sample size and composition

determining which of the two is appropriate. Larger proteins have slower rates of re-orientation and tumbling, which in turn results in significant line broadening in the spectra, making them poor candidates for solution NMR. Currently, ~50kDa is considered the upper size limit of membrane proteins that can be studied using solution NMR spectroscopy. However, in solid-state NMR spectroscopy there is no such size limit, and large proteins and complexes can be readily studied. The basic approach to determining membrane protein structure in both solution and solid-state NMR is similar; protein samples are isotopically labeled in accordance to the necessary experiments, various multidimensional experiments are performed and spectral parameters, such as NOEs (nuclear-Overhauser effect), RDCs (residual dipolar coupling), J-couplings, and chemical shifts, are recorded. The resonances are then assigned from the spectral data and the protein structure is calculated [27].

1.3 Solution NMR Spectroscopy

Solution NMR techniques can be used for structure determination and studies of membrane proteins in various environments including detergent micelles, detergent/lipid mixed micelles [28-29], bicelles [30-34], as well as nanodiscs [22, 24-25, 35]. One of the key advantages is that molecules in these samples are freely tumbling in a near-native environment, unlike those in crystals. The most commonly utilized solution NMR experiment is the heteronuclear single quantum coherence (HSQC) experiment [36]. It is more commonly referred to as the protein fingerprint spectrum and it is a correlation of the chemical shifts of directly bound nuclei. In this experiment, all ^{1}H-^{15}N correlations from

the protein backbone amide residues for each residue of the protein are observed with the exception of proline and the first N-terminal residue; the sidechains of Asn, Gln, Arg, and Trp residues, which have nitrogen-bound protons, are also readily detected. Well dispersed peaks in an HSQC spectrum are indicative of a properly folded protein and in many cases, most of the individual resonances can be distinguished. The individual peaks of the HSQC can be assigned and the spectra used to map the interactions of a given protein with its ligands, drugs, or other proteins. Experiments commonly used in solution NMR for assignments and structure determination include the nuclear Overhauser effect spectroscopy (NOESY) [37-38], HNCO [39-41], HNCA [39-40, 42], HN(CA)CO [43], HN(CO)CA [40, 44], and CBCA(CO)NH / HN(CO)CACB [40] experiments which provide information for backbone resonance assignments, and the total correlation spectroscopy (TOCSY) [45-46] and correlation spectroscopy (COSY) [39, 44, 47] experiments, which can be used for sidechain assignments. NOESY spectra can also be used to obtain structural restraints and the CO chemical shifts from HNCO experiments can help with secondary structure calculation. Solution NMR samples of micelles and small bicelles can also be weakly aligned [48-50] providing orientation restraints.

To obtain high resolution spectra in solution NMR, the molecules being studied must undergo rapid isotropic tumbling. However, long correlation times of larger proteins and protein complexes limit the number and types of proteins which can be studied by solution NMR [6]. Larger samples such as membrane proteins embedded in lipid bilayers (liposomes) or in large bicelles or macrodiscs [25-26] are difficult to study using solution

NMR; however, they are amenable to solid-state NMR methods, which, in theory, have no size imitation.

1.4 Solid State NMR Spectroscopy

In 1973, Urbina and Waugh described the first application of high resolution solid-state NMR to membranes and after many years of development, solid-state NMR has matured into an approach fully capable of determining the structures of membrane proteins in their native phospholipid bilayer environment under physiological conditions, and is the only method with this capability. The initial structures of membrane proteins obtained under near-native conditions are providing a basic understanding of their structures, dynamics, and functions in biological membranes. Solid-state NMR is essential for studies of membrane proteins associated with lipid bilayers because they are effectively ‘’immobilized” by their interactions in this large supramolecular membrane structure and it allows for the study of membrane proteins in lipid bilayers, which provide a near-native environment. The development of techniques which facilitate studying internuclear distances, torsion angles, anisotropy, molecular dynamics, exchange processes, and atomic orientations have also contributed to the success of solid-state NMR [51] and a variety of solid-state NMR approaches have been applied to membrane proteins [17, 52-68]. The primary focus of this introduction will be magic angle spinning (MAS) solid-state NMR and oriented-sample (OS) solid-state NMR spectroscopy. MAS solid-state NMR provides local structural parameters, such as interatomic distances, side-chain conformations, and backbone torsion angles. In contrast, OS solid-state NMR provides

primarily angular constraints measured relative to a single external axis, such as the magnetic field. In all cases, the quality of the structures benefits from the complementary measurements from the various techniques, with the primary issue being that the samples provide comparable membrane environments.

1.4.1 Magic Angle Spinning (MAS) Solid-State NMR

Three main interactions in samples lead to the broadening of signals in NMR spectra; they include the chemical shift anisotropy, dipole-dipole, and quadrupolar interactions. These interactions are averaged out in solution NMR due to rapid reorientation of the molecules and only the isotropic component is detectable. In solid state NMR, where the samples do not undergo unrestricted isotropic motions, the experiments have very broad lines, termed powder patterns, which reflect all the orientations of the molecules in the sample [69], which results in severe loss of resolution [70]. However, by spinning the samples at the magic angle (54.74^{o}) relative to the direction of the magnetic field [71-72], we can alleviate some of these effects in solid-state NMR spectroscopy. At this angle, these orientation-dependent interactions can be averaged out. The MAS frequency determines whether an interaction will be completely or partially averaged out [70]. This averaging of interactions results in narrowing of linewidths and better resolution in the NMR spectra.

A plethora of multidimensional MAS NMR experiments, ranging from 2D to 4D, have been developed to facilitate structural studies [73-100]. Some of the more common

MAS experiemnts include insensitive nuclei enhanced by polarization transfer (INEPT) [101], proton-driven spin diffusion (PDSD) [102], NCO [103], NCA [103], and proton-detection experiments. The INEPT experiment in solid-state NMR is used for detection of mobile residues; it enhances the sensitivity of low γ nuclei. Two dimensional PDSD spectra can be regarded at the solid-state NMR equivalent of the HSQC experiment; magnetisation is transferred from ^{1}H to ^{13}C and then to surrounding ^{13}C nuclei and all ^{13}C atoms in close proximity to one another are correlated by crosspeaks in the spectrum. The NCO and NCA experiments are used as part of the assignment scheme, with the NCA providing information on N-Cα linkage and the NCO information on the N-CO linkages. In both experiments magnetization is transferred via cross polarization (CP) from ^{1}H to ^{15}N and then to either ^{13}CO or $^{13}C\alpha$, for the NCO and NCA experiments, respectively.

1.4.2 Oriented Sample (OS) Solid-State NMR

Solid-state NMR spectra of aligned samples allow for the determination of complete three-dimensional protein structures by measurement of multiple orientation-dependent frequencies for the nuclei at each residue [27, 104-105]. These methods are particularly well suited for proteins which are not compactly folded, as is the case for helical proteins [106]. Bilayer samples (large bicelles, macrodiscs) are particularly well suited for use in static, uniaxially aligned samples [107] since the proteins are immobilized, in terms of NMR timescales, and provide a high degree of alignment, comparable to that observed for single crystals [27, 108]. There are two approaches which can be used to align samples in the magnetic field: mechanical and magnetic alignment. In mechanical

alignment, protein samples are physically aligned between glass plates to the desired orientation [108-110]. For the latter approach, large bicelles and peptide and polymer macrodiscs will spontaneously align with their bilayer normals perpendicular to the direction of the applied magnetic field at temperatures above the gel-to-liquid phase transition of the lipids. Notably, it is possible to "flip" the orientation of the magnetically aligned samples from perpendicular to parallel by addition of lanthanide ions [31, 111].

Separated local field (SLF) spectroscopy [112-113] is the key method used in oriented solid-state NMR spectroscopy. These experiments allow for the "mapping" of protein structures onto the spectra and are the foundation of aligned sample structure determination [105, 107]. An additional feature of SLF spectra is that measurements of all frequencies are independent of one another, meaning that errors will not propagate and accumulate throughout the experiment [106]. Two of the most common variations of the experiment are PISEMA (polarization inversion spin-exchange at the magic angle) [114] and SAMMY (sandwich-based separated local field spectroscopy) [115]. From the two-dimensional PISEMA experiment, information about the structure and topology of a membrane protein can be obtained from the observed resonances [116-117]. There is a very characteristic feature of the PISEMA experiment and that is the observation of a PISA (polarity index slant angle) wheel [106, 117-118]. PISA wheels are a result of the helical wheel projections of the residues in the alpha helices of the protein; they provide information on both the secondary structure and topology of the protein. Both the chemical shift and dipolar coupling dimensions of PISEMA spectra are dependent on helix orientation and

backbone dihedral angles [27]. Multidimensional experiments yield better spectral resolution and additional orientation constraints, which can be especially useful for larger proteins [108, 119-127].

Chapter 1, in part, is a reprint of the material as it appears in Quarterly review of Biophysics, “NMR Structures of Membrane Proteins in Phospholipid Bilayers”, by Radoicic J., Lu, G. J., and Opella, S. J., 2014. The dissertation author was the first author of this paper.

Chapter 2. G Protein-Coupled Receptors, CXCR1, and Interleukin-8

2.1 Abstract

G protein – coupled receptors (GPCRs) are the largest class of integral membrane proteins and have many vital roles, including signal transduction. They share a common topology of seven trans-membrane spanning helices, an extracellular N-terminus and an intracellular C-terminus. The GPCR CXCR1 is a potential breast cancer and anti-inflammatory drug target. It has one high-affinity ligand, interleukin-8 and activates the Gi family of heterotrimeric G proteins. Studies using various CXCR1 and G-protein constructs are used to map the IL8-CXCR1 and CXCR1-G protein binding interactions, with the final goal of studying the complete signaling process.

2.2 G Protein-Coupled receptors, CXCR1 and Interleukin-8

The G protein – coupled receptors (GPCRs) are a class of integral membrane proteins which account for ~2% of the total genes encoded by the human genome [128] and they are the largest class of proteins in the mammalian genome [129-131]. GPCRs are seven transmembrane spanning alpha helical proteins involved in signal transduction, which are defined by conserved structural features [132] and are divided into three broad families based on their sequence similarities, and members of each family share at least 25% sequence similarity; the families are further divided into subfamilies [129, 133]. The largest family is the Class-A rhodopsin-like GPCRs, which encompass all the olfactory receptors (~500) in addition to almost 200 other GPCRs [129, 133-134]. Class B and C GPCRs have far fewer members [133]; members of Class B GPCRs couple mainly to the Gs G proteins and

Class C GPCRs have a notably larger N-terminus than other GPCRs [133]. GPCRs interact with, and can be activated by, a variety of ligands including lipids, peptides, proteins, light, odorants, nucleotides, amino acids, ions, as well as biogenic amines [128]. They control a plethora of physiological functions including hormone and enzyme release, immune responses, blood pressure regulation, neurotransmission, cardiovascular and pulmonary systems, just to name a few [128]. Malfunction of GPCRs leads to the onset of some of the most prevalent human diseases; it has also been discovered that they are key players in tumor growth and metastasis and interfering with GPCRs may provide an avenue towards cancer prevention and treatment [128]. As such, it is no surprise that ~40% of all therapeutics aim to target GPCRs, directly or indirectly [5].

The chemokine receptor CXCR1 is a class-A rhodopsin-like GPCR which binds to the chemokine Interleukin-8 (IL-8) and activates the G-protein Gi signaling cascade. CXCR1 has the primary role of mediating the migration of neutrophils [135]; it is also involved in defending against pathogen invasion during innate immune response [135], activation phospholipase D and respiratory burst [136-139], regulation of tumor growth and vasculogenesis [137-138], acute and chronic inflammation, developments of lymphocytes and proliferation [135, 140-141]. IL-8 is a chemokine produced by macrophages and other cell types. It is released as a response to inflammatory stimuli by multiple cell types and results in the migration of leukocytes, monocytes, T- and B- lymphocytes and basophils to the sites of inflammation [139, 142]. IL-8 has two high affinity receptors, CXCR1 and CXCR2, however it has a stronger affinity for CXCR1 [136, 143-144]. The two receptors share

~77% sequence identity and differ primarily in their N-termini, fourth transmembrane domain (TM4), ECL2, and their C-termini [145-148]. It is believed that the IL8 monomer and dimer can differentially activate and regulate the two receptors [143]; rates of receptor internalization also regulate their different cellular functions [136].

As their name implies, GPCRs couple to G – proteins and it is this specificity which determines the downstream effectors of each receptor. All GPCRs will couple to at least one G protein, however others can couple to two or more [149-150]. GPCR – G protein interaction efficiency is significantly influenced by the ratios, conformations, and proximities of these proteins [151]. However, it is very difficult to precisely achieve these ratios in vitro. To facilitate this interaction, the use of GPCR-G protein fusion proteins has been employed [152-158]. In these constructs, the N-terminus of the $G\alpha$ subunit, or parts of the $G\alpha$ subunit, usually the C-terminal end, is covalently fused to the C-terminus of the GPCR, ensuring a 1:1 stoichiometry of GPCR:G protein; this also ensures that the two interaction partners are in close proximity to one another, further facilitating their interaction. These fusions enhance coupling efficiency and specificity and allow for studies of GPCR-G protein interactions that may not readily be done if the proteins were to be either individually or co-expressed [154]; a variety of GPCR-G protein fusions have been studied [153, 158-182]. We have also designed a CXCR1-$G\alpha_{i22}$ fusion construct for our research, where we covalently attached the last 22 C-terminal residues of the $G\alpha_{i1}$ G-protein subunit to the C-terminal end of CXCR1; this construct will be discussed in later sections.

Studies have found that activation of CXCR1 by IL8 involves binding of the chemokine to two distinct regions of the receptor, the N-terminus (biding site I) and residues in the second (ECL2) and third (ECL3) extracellular loops (binding site II) [183-193]. Ligand binding to GPCRs induces a conformational change in the receptor via movement of transmembrane helices; this change allows certain areas of the receptor to be accessible to G-protein binding, thus activating the GPCR. Upon ligand binding, there is a conformational change in the GPCR which results in activation of the heterotrimeric G-protein, with the receptor essentially acting like a guanine nucleotide exchange factor [194]. The third (TM3) and sixth (TM6) transmembrane helices have been found to be especially important in GPCR-G protein interaction and activation [195]; specifically, the region between TM3 and ICL2, including the highly conserved E/DRY motif, and the region on TM6 which is near ICL3 have been found to be crucial for G protein interactions [196-200]. The D of the DRY motif in GPCRs plays a role in stabilizing the GPCR conformation via ionic and hydrogen bonding to other amino acids that impact GPCR activation and coupling [197-198, 201-204]. Residues M241, V247, and F251 are thought to be very important for the GPCR-G protein interaction [135]. There is also movement in TM6 and TM7 that opens a pocket for G-protein binding [205-206]; outward movement of TM6, moves it away from TM3, and exposes the binding pocket [205].

However, given the importance of GPCRs, structural and dynamics studies have had a slow start. The large size, low expression levels, and membrane association of these receptors have made structure determination challenging. The first high-resolution

structure of a GPCR was that of rhodopsin [207] and many crystal structures of GPCRs have since emerged [208-216]. The structures have greatly contributed to our understanding of these receptors and crystallography continues to be one of the main methods of choice for GPCR structure determination. It must be noted, however, that amino acid sequence modifications, truncations, as well as attachment of T4 lysozyme and nanobodies are necessary to facilitate crystallization. Moreover, crystallography does not allow observation of protein dynamics. NMR spectroscopy can provide insight into both structure and dynamics of unmodified proteins in a near native environment. The field has seen an exponential rise in both technology and methodology and structures of numerous membrane proteins have been determined using both solution and solid-state NMR spectroscopy (http://www.drorlist.com/nmr/MPNMR.html; [217]).

A number of NMR structural studies have been carried out on CXCR1. Using solution NMR, assignments of the mobile N- and C-termini of the receptor were obtained using NOE and HNCA/HNCOCA experiments [218]. This aided in the sequential resonance assignments of the termini and chemical shift perturbations were used to identify the residues responsible for the interaction of CXCR1 with its ligand IL-8 [219]; this has allowed for a multi-step model for this interaction to be proposed. The structure of the unmodified receptor in phopspholipid bilayers using rotationally aligned (RA) solid state NMR spectroscopy was determined by our group [220]; this was the first structure of a GPCR determined via NMR spectroscopy. Proton detection and paramagnetic relaxation enhancement methods have also provided additional information on the CXCR1-IL8

interaction [221-222]. It has also been shown that IL-8 stimulates self-renewal of breast cancer stem cells [223], making CXCR1 an attractive target that could potentially block formation of these cancer stem cells [224] thus halting metastasis and tumor growth. As IL-8 also targets the recruitment and activation of polymorphonuclear (PMN) cells which can result in reperfusion injury (delayed graft function) [225], a drug which targets CXCR1, repertaxin (reparixin) has been found to be a noncompetitive allosteric inhibitor of the receptor. Studies have shown it to be a potential therapeutic agent in the treatment of reperfusion injury [225-228].

2.3 Heterotrimeric G – Proteins

Heterotrimeric guanine-nucleotide binding proteins (G-proteins) which couple to GPCRs are a highly conserved ancient protein family comprised of three non-covalently associated subunits: the α, β, and γ subunits. They essentially function as on/off switches for a myriad of cellular functions [194, 229] and are similar to other protein GTPases [194]. The networks regulated by this system include metabolic enzymes, ion channels, and transporters and they control a host of cellular functions including motility, transcripition, contractility and secretion, ultimately affecting systemic functions such as embryonic development, gonadal development, learning and memory, and organismal homeostasis [230]. Over 35 genes in the human genome code for G-proteins; 16 encode α-subunits, five encode β–subunits, and 14 encode γ–subunits [194]. The most prevalent disease that can be attributed to alterations in heterotrimeric G-protein activity is cholera [194]. However,

changes in G-protein activity have also been implicated in heart failure, rare endocrine conditions [231], metabolic syndrome, and acromegaly [229].

The Gα subunits perform a wide range of functions including interaction with receptors, effectors, the Gβγ dimer, guanine nucleotide exchange factors, and GTPase activating proteins and, as such, they must have very specific interfaces which allow for these interactions [194]. The Gα subunits have two domains – the G-domain, which is involved in binding and hydrolyzing GTP, and the helical domain, which buries GTP in the core of the Gα subunit [232-234]. There is almost 50% sequence identity between the most diverse Gα subunits [194]. Based on their sequence similarity, the G-protein alpha subunits have been divided into four main classes: $G\alpha_s$, $G\alpha_i$, $G\alpha_{q/11}$, and $G\alpha_{12/13}$ [194, 230] and the four groups are further divided into specific isotypes. The Gα subunit functions as an intrinsic GTPase by hydrolyzing GTP to GDP in the nucleotide binding pocket to allow for re-association of the G-protein heterotrimer and completion of the signaling cycle [194]. Based on their cDNA sequences, the Gα subunits would appear to be essentially soluble proteins, however, it was hypothesized that they would need to be present at or near the membrane in order to facilitate interactions with their receptors [194]. It was found that the N-terminus of the Gα subunit and the C-terminus of the Gγ subunit are sites of lipid modifications [232, 235]. These two sites are in relatively close proximity in the heterotrimer, suggesting that these may be sites of membrane attachment or interaction [232]. Interestingly, only members of the Gαi family are targets for N-terminal myristoylation whereas all of the other Gα subunits are targets for post-translational palmitoylation [194].

In the inactive state, G-proteins exist as GDP-bound heterotrimers. Upon activation by their cognate receptors, GDP is exchanged for GTP in the Gα subunit and the heterotrimer dissociates into the Gα and Gβγ subunits [232, 236-237]. These individual components then go on to interact and regulate a host of effectors including second messenger enzymes and a variety of ion channels [194]. Once they are in the active, GTP-bound conformation, the Gα subunits interact with their effectors with a 20-100-fold higher affinity than in the GDP-bound, inactive state [238]. Gα effectors include adenylyl cyclase, Src tyrosine kinases, ERK/MAPkinases, K^+/Ca^{2+} channels, phospholipase cβ, Protein kinase D, and PI-3 kinases [194]. Initially, it was thought that the Gβγ dimer simply acted as a binding partner for the Gα subunit and it has been confirmed that the Gβγ subunits enhance interaction of the Gα subunit with the receptor [232, 239]. It has also been suggested that the Gβ subunit rigidly holds the Gα subunit in place in order for GDP release to occur [240]. However, the Gβγ dimer also activates a variety of effectors [241] including include K^+ channels, PLC-β, adenylyl cyclase, and phosphatidylinositol 3-kinase (PI3K) [230]. Unlike the Gα subunit, the conformation of the Gβγ dimer is the same in both the inactive, GDP-bound heterotimeric state and in the active, GTP-bound dissociated signaling state [242], which suggests that the Gα subunit inhibits Gβγ signaling via the Gα binding site on the Gβγ dimer [240, 243].

In the heterotrimeric G-protein, the extreme C-terminus of the Gα subunit is believed to be the primary receptor interaction/recognition site [244-253], especially the last

~10 residues [239, 251, 254]. The C-terminus of Gα becomes highly immobilized upon interaction with receptor [248, 255-256]. However, multiple other regions of the G-protein have been shown to be involved in interaction with the receptor as well. The N-terminal domain [244, 246], the αN and αN/β1 hinge [256-260], the α2 helix and α2/β4 loop regions [244], the α4 helix and α4-β6 loop domain [244, 246, 250-251, 257, 259, 261-265], the α5 helix [244, 266-267], the α3-β5 region [268] and a small segment within the loop that links the N-terminal α-helix to the β1 strand of the GTPase domain [257] of the Gα subunit have all been reported to interact with the receptor. Due to their high degree of conformational variability, the loop and hinge regions of the Gα are proposed to fine-tune receptor-G protein interactions [205]. There are also binding interactions between the receptor and the Gβγ subunits [269-271] and the C-terminal region of Gγ has also been shown to be involved in receptor coupling and specificity [232, 270-271]. Upon binding, the receptor induces a significant conformational change of the C-terminus of Gα, altering the interaction with the guanine ring of the bound nucleotide [261, 272-273] and leading to nucleotide release. This is achieved via movement of the α5 helix [249] as well as movement of α5, αG, α4, and the αN/β1 hinge of the Gα subunit [206, 274]. Binding of the nucleotide to Gα reduces conformational flexibility and restores contacts between the domains of Gα [233-234, 275], resulting in a decrease in conformational flexibility which may stabilize subunit conformations that favor interaction with binding partners [205].

Given the large size of both the G-protein heterotrimer and Gα subunit alone, small peptides corresponding to specific areas of the G-protein, usually the extreme C-

terminus, have also been utilized in studying GPCR-G protein interactions. These peptides have been shown to mimic the conformational changes in GPCRs induced by heterotrimeric G proteins and can be used to not only study the active or inactive conformations of the GPCR but also in drug discovery [250-251, 262, 276-279]. Almost all the reported G-protein peptides have been synthetic peptides, however, we have cloned and overexpressed a Gαi peptide in *E. coli* corresponding to the last 22 residues of the Gαi subunit, termed $G\alpha_{i22}$, to use for our studies; this peptide will be discussed in more detail in later sections of the chapter.

Much progress has also been made in structural studies of heterotrimeric G-proteins. Although a large majority of the initial structural studies were done using x-ray crystallography [248, 256, 280-285], significant progress has also been made to study both the G-proteins as well as their interaction with cognate GPCRs using NMR spectroscopy. Initial solution NMR spectra were done on small fragments of the G-proteins [276, 286-288] however recently, high resolution NMR spectra of the complete $G\alpha_{i1}$ subunit have been reported [289] and Shimada and co-workers have obtained backbone resonance assignments for an N-terminally truncated construct of the $G\alpha_{i3}$ subunit (Δ31 $G\alpha_{i3}$) in both the active (GTPγS bound)[290] and inactive (GDP-bound)[291] conformations. Others have also studied the N-terminally truncated construct of $G\alpha_{i1}$ (Δ31 $G\alpha_{i1}$); they obtained backbone assignments for a majority of residues of Δ31 $G\alpha_{i1}$ bound to two GTP analogs, GMP-PNP and GTPγS, GDP, and the nucleotide-free apo form of the subunit and interactions between rat neurotensin receptor and the Δ31 $G\alpha_{i1}$ were analyzed [292].

2.4 Methods and Materials

2.4.1 Expression and Purification of Monomeric Interleukin-8

Monomeric interleukin-8 (1-66) was prepared as described previously [293]. In brief, the IL-8(1-66) plasmid was cloned into the pET32 vector with a thioredoxin fusion partner, an N-terminal FactorXa cleavage site and an N-terminal hexa-histidine tag. The plasmid was over-expressed in BL21(DE3)pLysS competent *E. coli* cells using M9 minimal media, supplemented with trace elements (13.4mM EDTA, 3.1mM $FeCl_3$-$6H_2O$, 0.62mM $ZnCl_2$, 76uM $CuCl_2$-$2H_2O$, 42uM $CoCl_2$-$2H_2O$, 162uM H_3BO_3, and 8.1uM $MnCl_2$-$4H_2O$), using ^{15}N ammonium sulfate (Cambrige Isotope Laboratories, Inc, isotope.com) as the nitrogen source. The IL8(1-66)-plasmid containing *E. coli* cells were grown at 37^{o}C until they reached an OD ~0.6 after which they were induced with a final concentration of 100mM isopropyl β-D-1-thiogalactopyranoside (IPTG) and grown for another 4-5 hours following which the cells were pelleted via centrifugation at ~5,000 rpm in the Beckman JLA 8.1000 rotor. The cells were lysed via sonication in lysis buffer (20mM Tris-HCl, 500mM NaCl, 20mM imidazole, pH 7.4) with phenylmethane sulfonyl fluoride (PMSF) and lysozyme and the cell debris was pelleted by centrifugation at 17,000 rpm in the Beckman JA 20 rotor. The protein-containing supernatant was bound to Ni-NTA resin (Qiagen, Ni-NTA Superflow) for approximately one hour following which the column was washed with 5 bed-volumes of wash buffer 1 (20 mM Tris, 300 mM NaCl, 30 mM imidazole, pH 7.4) and wash buffer 2 (20 mM Tris, 150 mM NaCl, 30 mM imidazole, pH 7.4). The fusion protein was eluted with elution buffer (20 mM Tris, 150 mM NaCl, pH 7.4) using a gradient

of 150-300mM imidazole. The fusion-protein containing elution fractions were cleaved with FactorXa and further purified using reverse-phase high performance liquid chromatography (HPLC) with a C18 column (Waters DeltaPak 15uM, 300Å) using an acetonitrile gradient. The purified IL-8 was lyophilized and stored at -20^{o}C until further use.

2.4.2 Expression, Purification, and Reconstitution of CXCR1 and its Constructs

CXCR1 and all its related constructs were prepared as described previously [144, 294]. The CXCR1 constructs were cloned into the pGEX2a vector with a GST-fusion partner, an N-terminal thrombin cleavage site, and a C-terminal hexa-histidine tag. The plasmid was over-expressed in BL21 competent *E. coli* cells using M9 minimal media, supplemented with trace elements, using ^{15}N ammonium sulfate (Cambrige Isotope Laboratories, Inc, isotope.com) as the nitrogen source. The CXCR1-plasmid containing *E. coli* cells were grown at 37^{o}C until they reached an OD ~0.6 after which they were induced with a final concentration of 100uM IPTG and grown for another 4-5 hours following which the cells were pelleted via centrifugation at ~5,000 rpm in the Beckman JLA 8.1000 rotor. The cell pellets were re-suspended in ~35mL of lysis buffer (20mM Tris-HCl, 500mM NaCl, 15% v/v Glycerol, pH=8) with ~5mg of lysozyme and sonicated for 5 minutes (5 seconds on/10 seconds off) to lyse the cells. The sonicated cells were spun down at 17,000 rpm in the Beckman JA 20 rotor to pellet the protein-containing inclusion bodies. The supernatant was discarded and the protein-containing inclusion bodies solubilized via sonication (5 minutes, 5 seconds on/10 seconds off) in ~30mL of binding

buffer (1X PBS, 1% SDS, 0.1% TCEP, pH=8) and then loaded onto a Ni-NTA column (~10mL bed-volume) equilibrated with binding buffer and left to bind for at least 1 hour at room temperature with gentle agitation. The column was washed with 5 bed-volumes of binding buffer followed by 20 bed-volumes of thrombin cleavage buffer (20mM Tris-HCl, 250mM NaCl, 0.1% HPC) and cleaved, on column, with 1000 units (per liter cells) of thrombin re-dissolved in thrombin cleavage buffer, for at least two hours to remove the GST fusion partner. Following cleavage, the column was washed with 10 bed-volumes of wash buffer (20mM HEPES, 0.5% DPC, 50mM NaCl, pH=7.3) and the protein was eluted with 30 bed-volume of elution buffer (20mM HEPES, 0.5% DPC, 500mM imidazole, pH=7.3). The protein-containing elution fractions were pooled and further purified using size exclusion chromatography on a HiLoad 26/60 Superdex 200 column (GE Lifesciences, www.gelifesciences.com) in 20mM HEPES, 50mM NaCl, and 0.5% SDS pH=7.5 buffer. The monomeric protein was pooled and lipids were added at a 1:5 or 1:10 protein:lipid w/w ratio; the mixture was incubated for at least 1 hour. The proteliposomes were then dialyzed in 10kDa cutoff dialysis tubing in 20mM HEPES, pH=7.3 overnight and for an additional ~6 hours in 20mM HEPES, 20mM KCl, pH=7.3 the following day to remove residual SDS. After dialysis, the proteoliposomes were spun down via ultracentrifugation for 2 hours at 40k rpm in a Beckman Ti.45 rotor, the pellet washed and re-suspeneded in 20mM HEPES, pH 7.3, and then spun for another 2 hours at 60k rpm in a Beckman Ti.70 rotor. The proteoliposome pellet was re-suspened in 20mM HEPES, pH 7.3 to a final concentration of 1mg/mL, aliquoted, frozen in liquid nitrogen and stored at -80C until further use. For the 1TM_CXCR1 construct, after Ni-column, the protein-

containing elution fractions were dialyzed against ddH_2O until the protein precipitated out of solution. The precipitated protein was further purified using reverse-phase high performance liquid chromatography (HPLC) with a C18 column (Waters DeltaPak 15uM, 300Å) using an acetonitrile gradient. Protein containing fractions were dried under nitrogen gas to remove residual organic solvents, lyophilized, and stored at -20^oC until further use.

2.4.3 Expression and Purification of Gα_{i1}

The Gα_{i1} construct was cloned into the pGEX2a vector containing the GST-fusion partner, with an N-terminal thrombin cleavage site and C-terminal hexa-histidine tag. The plasmid was over-expressed in BL21 competent *E. coli* cells using M9 minimal media, supplemented with trace elements, using ^{15}N ammonium sulfate (Cambrige Isotope Laboratories, Inc, isotope.com) as the nitrogen source. The Gα_{i1}-plasmid containing *E. coli* cells were grown at 37^oC until they reached an OD ~0.4; the temperature was then lowered to 25^oC and at an OD~0.6 the cells were induced with a 100uM final concentration of IPTG and left to growth at 25^oC overnight. The following morning, the cells were pelleted by centrifugation at ~5,000 rpm in the Beckman JLA 8.1000 rotor. The resulting cell pellet was solubilized in ~35mL of lysis buffer (20mM Tris-HCl, 500mM NaCl, 15% v/v Glycerol, pH=8) with lysozyme and sonicated for 5 minutes (5 seconds on/10 seconds off) to lyse the cells. After centrifugation, the cell debris was spun down by centrifugation at 17,000 rpm in a Beckman JA 20 rotor, and the protein-containing supernatant was bound to Ni-NTA or Talon resin (~10mL bed volume), equilibrated with

5 column volumes of lysis buffer, for at least two hours. The column was washed with 5-bed volumes of lysis buffer, equilibrated with 20 bed volumes of thrombin cleavage buffer (20mM Tris-HCl, 50mM NaCl, pH=8) and cleaved with ~10 units of thrombin re-dissolved in 20mL of thrombin cleavage buffer, to remove the GST fusion. Following cleavage, the column was washed with 5 bed-volumes of wash buffer (20mM HEPES, 50mM NaCl, 20mM imidazole, pH=7.3) and $G\alpha_{i1}$ was eluted from the column with three bed-volumes of elution buffer (20mM HEPES, 50mM NaCl, 500mM Imidazole, pH=7.3). The eluted protein was further purified using size exclusion chromatography (SEC) on a HiLoad 16/60 Superdex 200 PrepGrade column in 20mM HEPES, 50mM NaCl, pH=8 buffer.

2.4.4 Expression and Purification of the $G\alpha_{i22}$ Peptide

The $G\alpha_{i22}$ peptide was cloned into the pET31b(+) vector with a KSI-fusion partner, with N-terminal thrombin cleavage site and a hexa-histidine tag. The plasmid was over-expressed in BL21(DE3) competent *E. coli* cells into inclusion bodies using M9 minimal media, supplemented with trace elements, using ^{15}N ammonium sulfate (Cambrige Isotope Laboratories, Inc, isotope.com) as the nitrogen source. The $G\alpha_{i22}$ plasmid containing *E. coli* cells were grown at 37°C until they reached an OD ~0.6 after which they were induced with a final concentration of 100uM IPTG and grown for another 4-5 hours following which the cells were pelleted via centrifugation at ~5,000 rpm in the Beckman JLA 8.1000 rotor. The cell pellets were re-suspended in ~35mL of lysis buffer (20mM Tris-HCl, 500mM NaCl, 15% v/v Glycerol, pH=8) with lysozyme and sonicated for 5 minutes (5 seconds on/10 seconds off) to lyse the cells. The sonicated cells were spun down at

17,000 rpm in the Beckman JA 20 rotor to pellet the protein-containing inclusion bodies. The supernatant was discarded and the inclusion bodies solubilized via sonication (5 minutes, 5 seconds on/10 seconds off) in ~30mL of binding buffer (1X PBS, 1% SDS, 0.1% TCEP, pH=8) and then loaded onto a Ni-NTA column (~10mL bed-volume) equilibrated with binding buffer and left to bind for overnight at room temperature with gentle agitation. The column was washed with 5 bed-volumes of binding buffer followed by 20 bed-volumes of thrombin cleavage buffer (20mM Tris-HCl, 250mM NaCl, 0.1% HPC) and cleaved, on column, with 1000 units (per liter cells) of thrombin re-dissolved in thrombin cleavage buffer, for at least two hours to remove the KSI fusion partner. Following cleavage, the $G\alpha_{i22}$ peptide was eluted into the thrombin cleavage flow through. The protein-containing fractions were pooled and further purified using size exclusion chromatography on a HiLoad 26/60 Superdex 200 column (GE Lifesciences, www.gelifesciences.com) in 20mM HEPES, 50mM NaCl, and 0.5% SDS pH=7.5 buffer.

2.4.5 NMR Spectroscopy

Solution NMR experiments were done on a Bruker Avance 600 MHz spectrometer equipped with 5-mm triple-resonance cryoprobe with a z-axis gradient or on a Bruker Avance Neo 800MHz spectrometer with a triple resonance TXO cryoprobe. One-dimensional ^{15}N-edited ^{1}H NMR and two dimensional ^{1}H-^{15}N HSQC NMR spectra were obtained at 40^{o}C for interleukin-8 spectra, 50^{o}C for all CXCR1 constructs, 40^{o}C for $G\alpha_{i1}$, and 35^{o}C for the $G\alpha_{i22}$ peptide. Solid-State NMR experiments were performed on a spectrometer with a ^{1}H resonance frequency of 900 MHz (21.1T). The Bruker Avance III

HD console and magnet were interfaced to a $^{1}H/^{13}C/^{15}N$ 3.2 mm MAS probe. All 2D ^{13}C-^{13}C correlation PDSD spectra were obtained using a 3 second recycle delay, 100 ms mixing time, and a 10 ms acquisition time at 5^{o}C. 1D INEPT spectra were obtained by averaging 2024 transients using a 2 second reaxation delay and 10ms acquisition time at 25^{o}C. The sample-spinning rate was controlled to 11.1 kHz. The NMR data were processed using TopSpin 3.5 (http://www.bruker.com).

2.5 Results and Discussion

The goal of this work is to study the IL-8, CXCR1, and G-protein signaling cascade and how each of the binding partners are affected by one another. However, the sheer size of this complex, as well as each of the constituents, makes this a very difficult feat. As this is the case, we have decided to employ a 'divide and conquer' approach. It has been well established that IL-8 has two sites of interaction with CXCR1 – binding Site I, located at the N-terminus of the receptor, and binding Site II – located in the extracellular loops. To look at these binding sites we have utilized three different CXCR1 constructs (Fig. 2.1A): WT-CXCR1(1-350), which contains binding Sites I and II, 1TM-CXCR1(1-72), which contains only binding Site I, and NT-CXCR1 (39-350), which only contains binding Site II. We have also utilized two receptor-G protein fusions (CXCR1_Gα_{i22} and NT-CXCR1_Gα_{i22}) to study the effect of the G-protein bound to CXCR1 as well as the effects of G-protein binding on the IL8-CXCR1 interaction.

Wild-type IL-8 (1-72) exists as a dimer at high concentrations and as a monomer at lower concentrations [185, 295-296]; however, it has been found that IL8 binds to CXCR1 as a monomer [297] and with high affinity [298]. Because of this, we have used a truncated, monomeric form of interleukin-8, IL-8 (1-66), in which the dimerization interface, residues 67-72, has been removed. The IL-8 (1-66) monomer is easily expressed and purified and is properly folded, as can be observed using solution NMR (Fig. 2.2). Preliminary two-dimensional solid-state MAS NMR ^{13}C-^{13}C correlation PDSD spectra (Figure 2.3) and one-dimensional INEPT spectra (fig. 2.5), which only detect mobile residues, of CXCR1 and CXCR1 bound to IL-8(1-66), show noticeable changes in the receptor upon ligand binding. Further comparison of the same spectra with those of CXCR1_$G\alpha_{i22}$ show that different areas of the receptor are affected by ligand binding versus G-protein binding, which is especially noticeable in the aromatic residues of the INEPT spectra. These data support the different interaction sites of IL-8 and $G\alpha$ with CXCR1. More detailed interaction studies using these various constructs are discussed in Chapter 4.

CXCR1 and CXCR2 are the two high-affinity receptors of IL-8, sharing almost 77% sequence identity with their most divergent regions being their termini and loop regions. We have done preliminary studies comparing the two receptors using MAS solid-state NMR. The ^{13}C-^{13}C correlation PDSD spectra of the two proteins are shown in Fig. 2.3 and we can observe that there are noticeable differences in the spectra of the two receptors, however more detailed analysis is necessary to provide a comprehensive comparison of the two receptors.

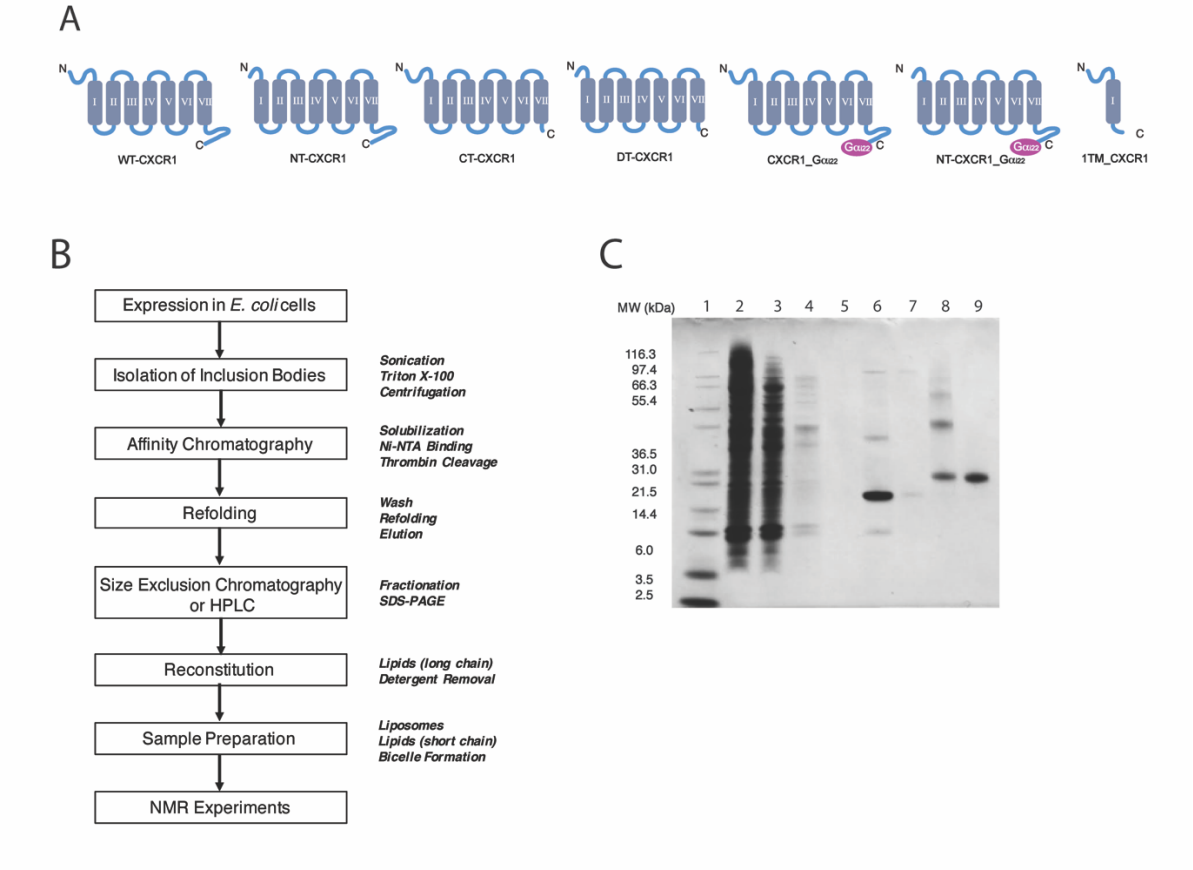

Figure 2.1. Purification of CXCR1 and its constructs. (A) Topology models of the various CXCR1 constructs used. (B) General purification scheme. (C) SDS-PAGE of a typical WT-CXCR1 purification; lane 1: Mark12 Standard, lane 2: Inclusion Bodies, lane 3: Post Ni-NTA binding flow through, lane 4: bind buffer wash, lane 5: thrombin cleavage buffer wash, lane 6: thrombin cleavage flow-through, lane 7: wash flow-through, lane 8: Ni-NTA pure CXCR1, lane 9: monomeric CXCR1 obtained after size exclusion chromatography.

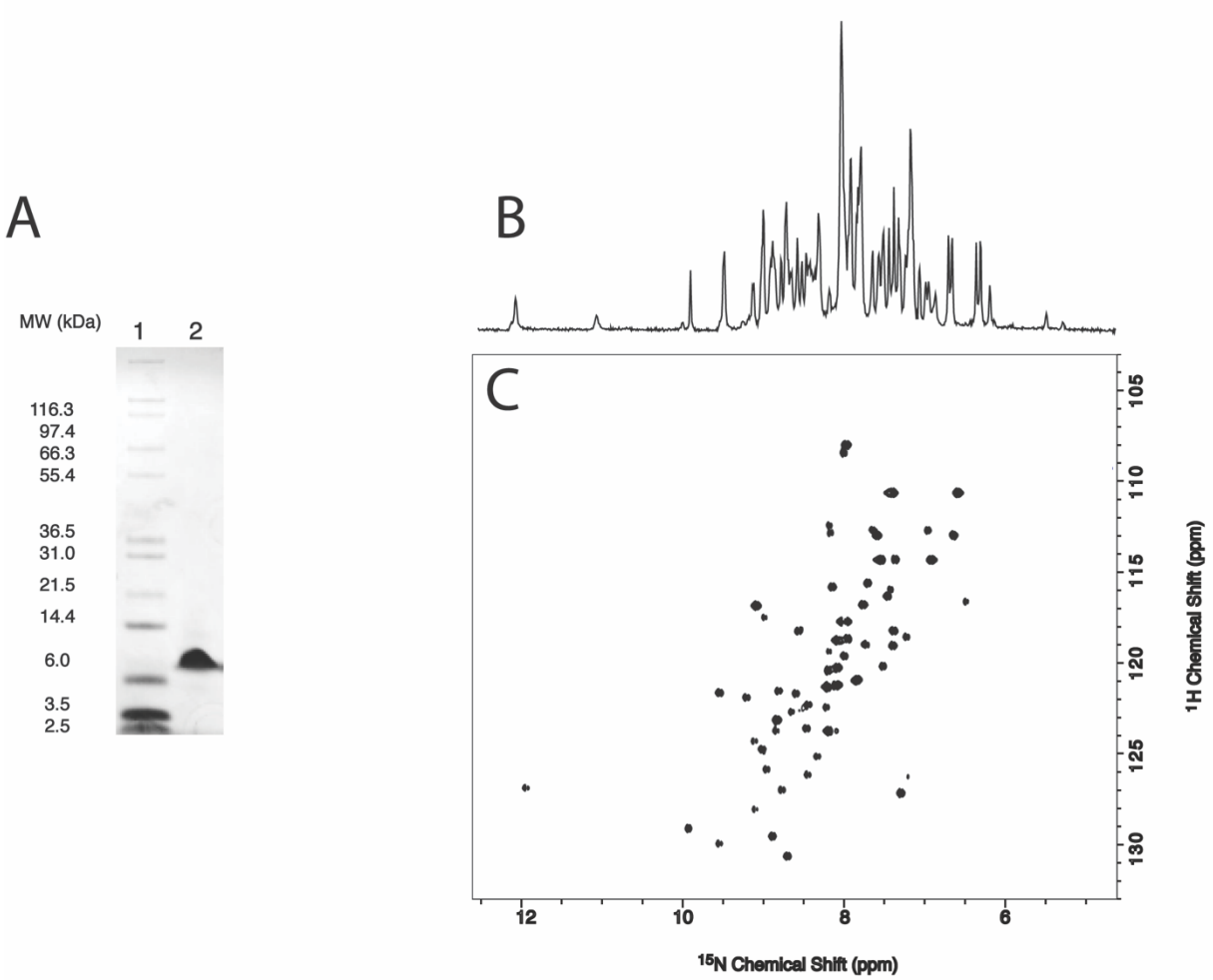

Figure 2.2. Purification and NMR spectra of IL8(1-66). (A) SDS-PAGE of pure, monomeric interleukin-8(1-66); lane 1: Mark12 Standard, lane 2: IL8(1-66). (B) 1D ^{1}H-^{15}N solution NMR spectrum. (C) 2D ^{1}H-^{15}N HSQC spectrum.

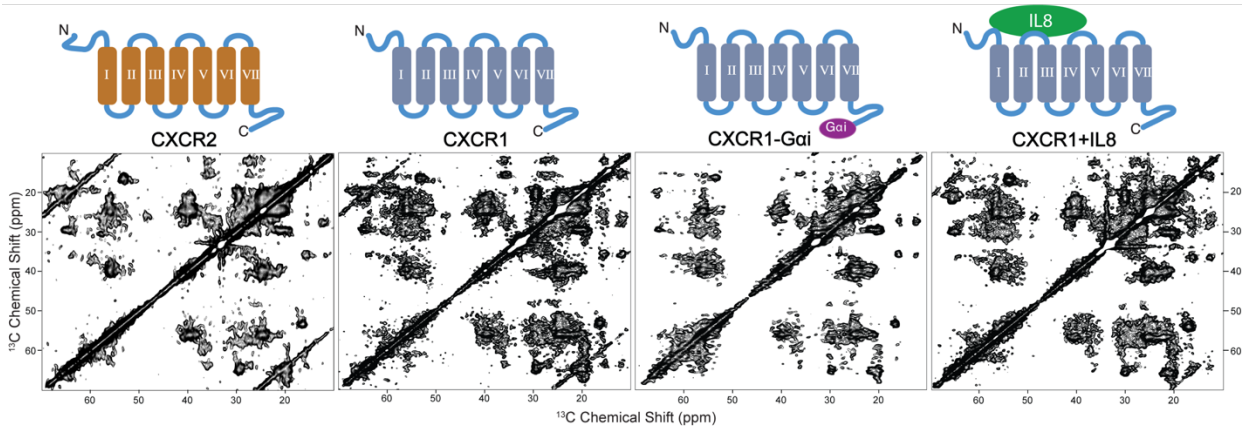

Figure 2.3. ^{13}C-^{13}C Correlation PDSD MAS solid-state NMR spectral comparison of CXCR2, CXCR1, CXCR1_Gα_{i22}, CXCR1 bound to IL8(1-66).

For our initial CXCR1-G protein interaction studies, we looked at a CXCR1_Gα_{i22} fusion protein, where we covalently fused the last 22 C-terminal residues of the Gα_{i1} protein to the extreme C-terminus of CXCR1 and express this fusion protein as a whole. As mentioned in the introduction, this portion of the Gα subunit is one of the primary areas involved in receptor-G protein interaction. These GPCR-G protein fusion constructs ensure the correct stoichiometry and proximity of the binding partners, in turn enhancing the coupling efficiency. Initial studies of the CXCR1_Gαi_{22} construct using solution NMR are shown in Fig. 2.4. In Fig. 2.4 A-D, four different solution NMR HSQC spectra of CXCR1 constructs are shown; WT-CXCR1, NT-CXCR1, CT-CXCR1, and CXCR1_Gα_{i22}. Fig. 2.4. E-H show the mapped-out residues belonging to the C-terminus in red (Fig. 2.4F) and those belonging to the N-terminus in blue (Fig. 2.4G). Fig. 2.4E shows both the N- and C-terminal mapped residues. Using this scheme, we mapped the same residues from the CXCR1_Gα_{i22} spectra in Fig. 2.4H. Overall, the CXCR1_Gα_{i22} spectra show that most

of the C-terminal CXCR1 residues are broadened beyond detection in the CXCR1_Gαi_{22} construct when compared to wild type CXCR1, and that most peaks appear to be stemming from the N-terminal part of the receptor. We also do not observe any extra signals from the attached peptide indicating that it is immobilized; the extra peaks that can be observed in the HSQC spectra are residues left-over from cleavage of the protein from its fusion partner. Further studies of the CXCR1_Gα_{i22} fusion construct were done using MAS solid-state NMR. Preliminary ^{1}H-^{13}C 1D correlation spectra with INEPT magnetization transfer (Fig. 2.5) also show similar changes at the C-terminus of the receptor indicating a change in dynamics due to interaction of the peptide with the receptor or as a result of conformational changes. Comparisons of the two-dimensional ^{13}C-^{13}C correlation MAS spectra of WT-CXCR1 to that of CXCR1_Gα_{i22} and CXCR1 bound to IL-8(1-66) (Fig. 2.3) also confirm these changes. More detailed solid-state NMR experiments will provide greater insight into this interaction.

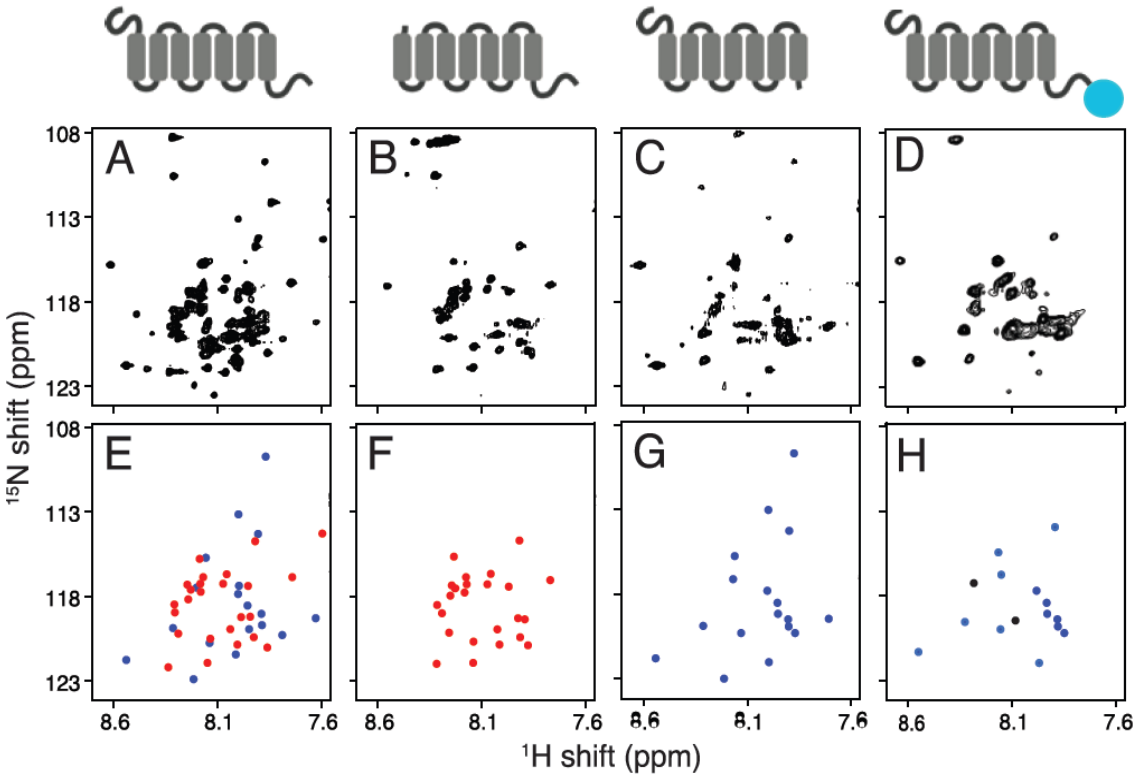

Figure 2.4. Comparison of ^{1}H-^{15}N edited HSQC spectra of wild-type CXCR1, NT-CXCR1 (38-350), CT-CXCR1 (1-319), and CXCR1-Gα_{i22}. (A-D) HSQC spectra of WT-CXCR1, NT-CXCR1, CT-CXCR1, and CXCR1_Gα_{i22}, respectively, obtained at 600MHz. (E-H) mapping of respective N-terminal (blue) and C-terminal (red) residues of the HQSC spectra.

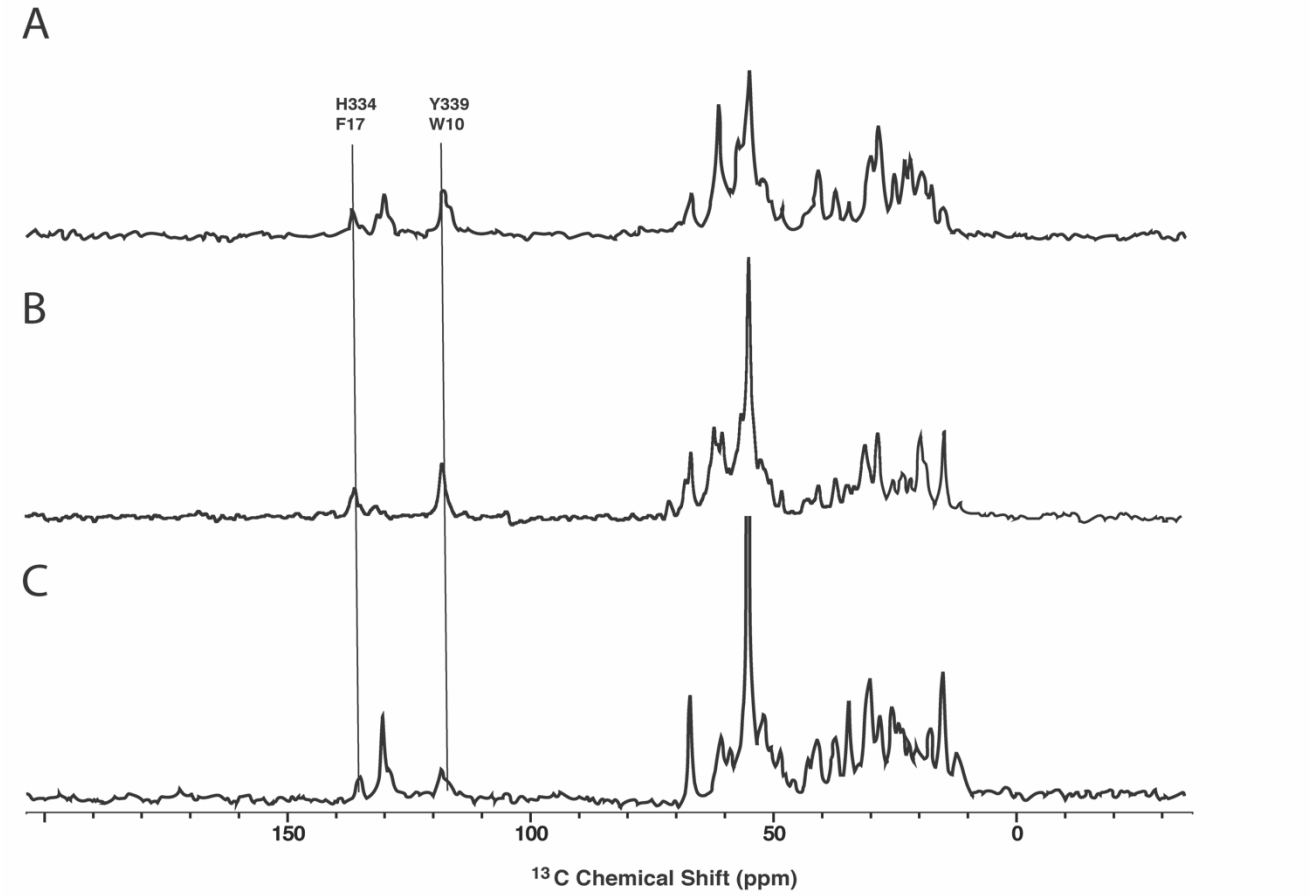

Figure 2.5. ^{1}H-^{13}C INEPT solid-state NMR spectra of (A) WT-CXCR1, (B) WT-CXCR1 bound to unlabeled IL8(1-66), and (C) CXCR1_$G\alpha_{i22}$. Previously assigned [220] aromatic residues W10, F17, H334, and Y339 are indicated.

Further studies of the CXCR1-G protein interaction were done using two different G-protein constructs: (1) a peptide corresponding to the C-terminus of the $G\alpha_i$ subunit and (2) the full-length unmodified $G\alpha_{i1}$ subunit. Initial expression and purification of the $G\alpha$-peptide was done using a $G\alpha_{i22}$ construct (Fig. 2.6A, construct #1) where the peptide was expressed as a KSI-fusion protein into inclusion bodies. Methionine residues present at the N- and C-termini facilitated cleavage of tags via cyanogen bromide (CNBr) cleavage. The peptide was purified using guanidine buffers and the fusion partner cleaved

with cyanogen bromide (CNBr). Fusion protein expression and yields were excellent however significant issues with peptide oligomerization were encountered upon CNBr cleavage of the KSI fusion partner. After cleavage, the peptide would extensively oligomerize with no sign of monomeric protein (Fig. 2.6C). Many approaches were taken to stop the oligomerization of this construct including working with the peptide in very dilute conditions, re-solubilizing in organic solvents, and addition of various reducing agents, however pure, monomeric $G\alpha_{i22}$ could not be obtained. Following this, multiple $G\alpha_i$-peptide constructs were designed, including constructs having a Cys → Ser mutation in KSI as well as in both KSI and the peptide, as well as an extended $G\alpha_{i27}$ construct, which contained five more residues to ensure the complete C-terminal helix of the $G\alpha_i$ peptide was forming, and a short, $G\alpha_{i11}$ construct, all with the aim of reducing oligomerization. However, the same patterns were observed for all the different constructs. Finally, we decided to take a different approach and include an N-terminal thrombin cleavage site in the $G\alpha_{i22}$ construct and purify the protein in the same manner as our CXCR1 constructs. Using this method, we were able to obtain pure, monomeric $G\alpha_{i22}$ peptide (Fig. 2.7A) and obtain high resolution solution NMR spectra (Fig. 2.7B and C). The spectra show well-dispersed peaks indicating that the peptide is properly folded.

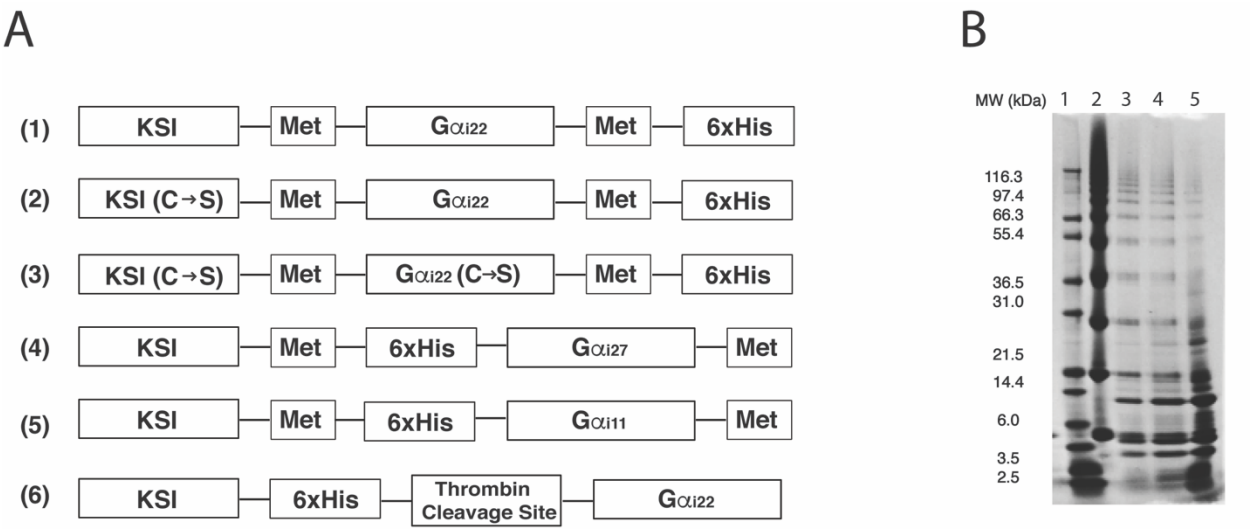

Figure 2.6. $G\alpha_{i22}$ Constructs and Purification. (A) schematic showing $G\alpha_{i22}$ peptide constructs. (B) SDS-PAGE gel of typical $G\alpha_{i22}$ peptide purification using CNBr cleavage; lane 1: Mark2 Standard, lane 2:

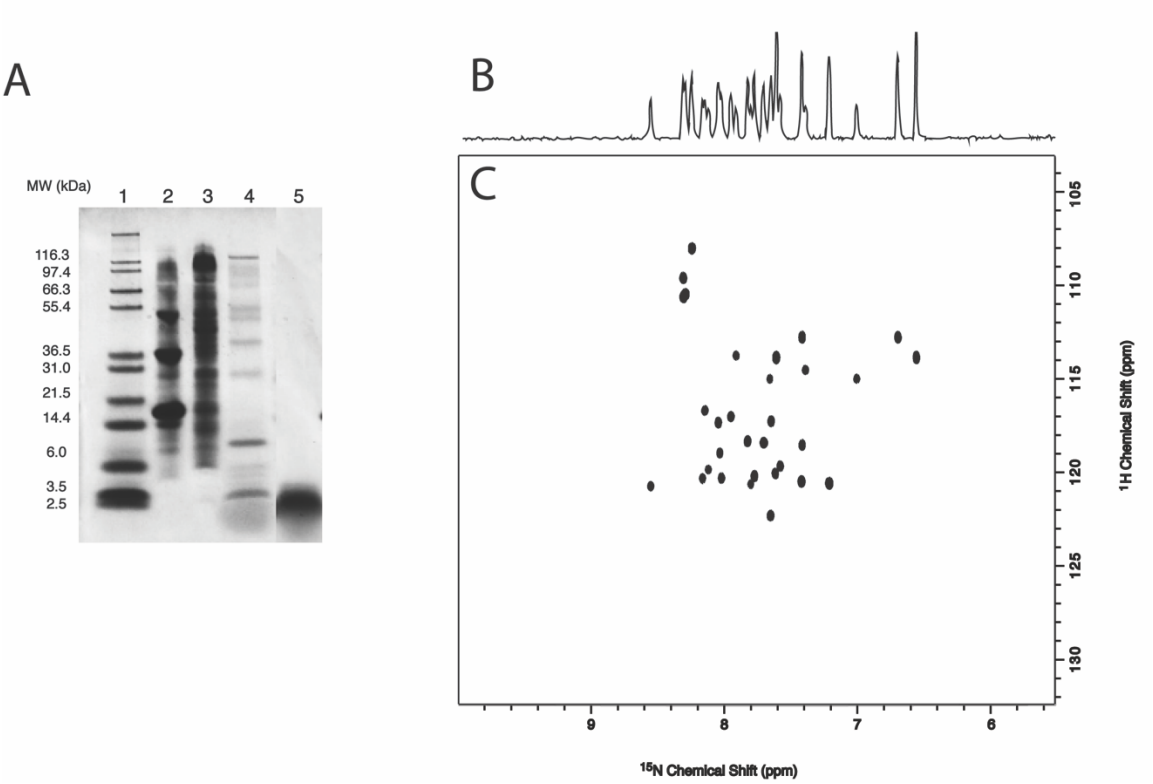

Figure 2.7. Expression, purification, and solution NMR of the $G\alpha_{i22}$ peptide construct containing thrombin cleavage site. (A) SDS-PAGE analysis of $G\alpha_{i22}$ peptide purification; lane 1: Mark12 Standard, lane 2: Solubilized inclusion bodies containing fusion protein, Lane 3: Flow-thru post Ni-column binding, lane 4: protein-containing flow-thru post cleavage with thrombin, lane 5: concentrated pure, monomeric $G\alpha_{i22}$ peptide post size exclusion chromatography.

The expression and purification of the full-length unmodified $G\alpha_{i1}$ subunit were straightforward. The subunit was expressed as a soluble protein via a GST-fusion in a pGEX2a vector with a thrombin cleavage site to facilitate cleavage of the fusion partner. We were able to obtain pure, monomeric $G\alpha_{i1}$ in quantities sufficient for NMR studies (Fig. 2.8A) and solution NMR data show the protein to be structured and well folded (Fig. 2.8B and C), although issues with sample stability were encountered. We next went on to look at the interaction of $G\alpha_{i1}$ with CXCR1.

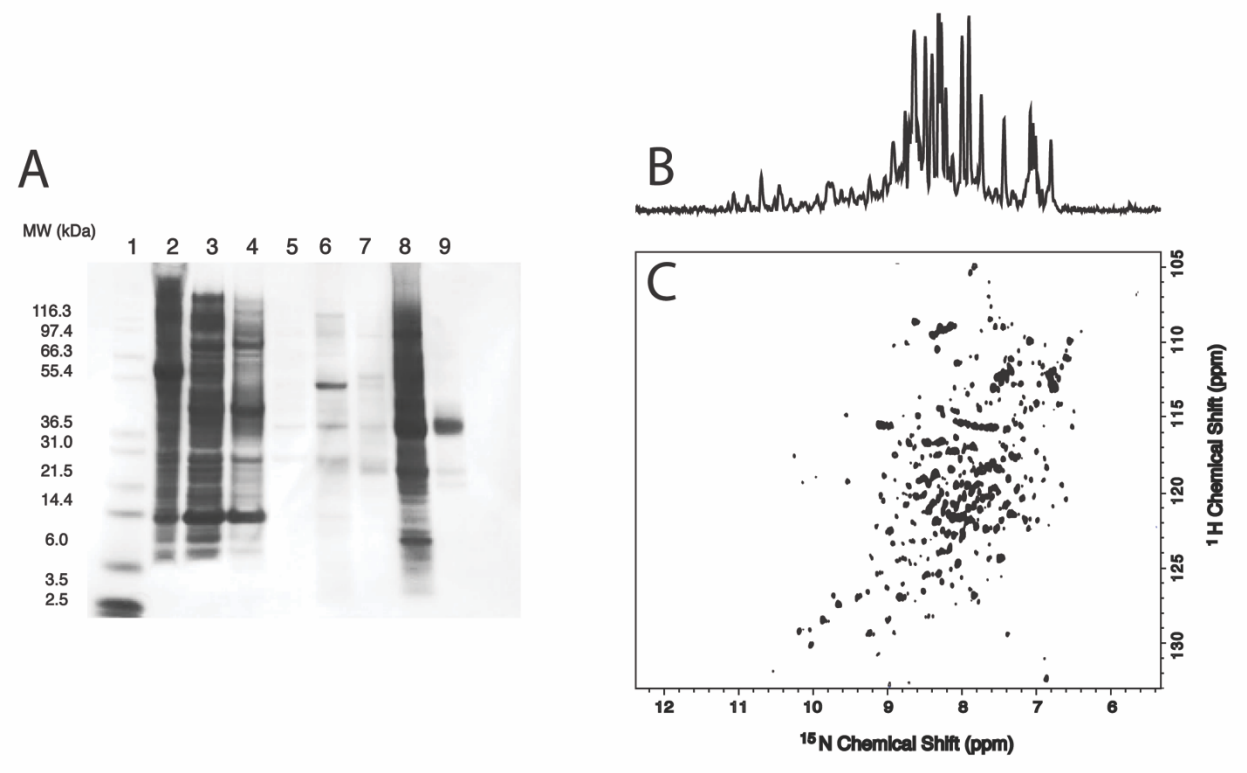

Figure 2.8. Expression, purification, and solution NMR of $G\alpha_i1$. (A) SDS-PAGE gel of $G\alpha_i1$ purification. (B) 1D solution NMR spectrum and (C) 2D ^{1}H-^{15}N HSCQ spectrum of $G\alpha_i1$.

Chapter 3. Paramagnetic relaxation enhancement of membrane proteins by incorporation of the metal-chelating unnatural amino acid 2-amino-3-(8-hydroxyquinolin-3-yl) propanoic acid (HQA)

3.1 Abstract

The use of paramagnetic constraints in protein NMR is an active area of research because of the benefits of long-range distance constraints (>10 Å). One of the main issues in its successful execution is the incorporation of a paramagnetic metal ion into diamagnetic proteins. The most common metal ion tags are relatively long aliphatic chains attached to the side chain of a selected cysteine residue with a chelating group at the end where it can undergo substantial internal motions, decreasing the accuracy of the method. An attractive alternative approach is to incorporate an unnatural amino acid (UAA) that binds metal ions into a specific site on the protein using the methods of molecular biology. Here we describe the successful incorporation of the unnatural amino acid 2-amino-3-(8-hydroxyquinolin-3-yl) propanoic acid (HQA) into two different membrane proteins by heterologous expression in *E. coli*. Fluorescence and NMR experiments demonstrate stable metal chelation of the mutated proteins and complete replacement of the natural amino acid with HQA. Evidence of site-specific intra- and inter-molecular PREs by NMR in micelle solutions set the stage for the use of HQA incorporation in solid-state NMR structure determinations of membrane proteins in phospholipid bilayers.

3.2 Introduction

Many analogies can be drawn between the earliest protein NMR studies and present day studies of proteins in biological supramolecular assemblies, such as membrane proteins, amyloid fibrils, chromatin, etc. Both were severely limited by resolution and sensitivity of the spectra, and the ability to interpret the data in terms of the three dimensional structures of the proteins, which has always been the major goal of protein NMR spectroscopy. Starting with the initial NMR spectrum of a protein in solution [299], which consisted of four broad, overlapping signals, it was clear that additional steps were needed to extract the underlying spectroscopic and structural information. Some gains resulted from increasing the ^{1}H resonance frequency and the introduction of signal averaging of the continuous wave signals [300]. Nonetheless, the early demonstrations of protein NMR were limited to a few residues whose resonances could be resolved in the spectra of the most favorable globular proteins available in large quantities at the time, for example ribonuclease and lysozyme. The introduction of isotopic labeling of proteins was a major step forward in attaining both improved spectral resolution and resonance assignments [301] but was restricted to selected examples, such as Staphylococcal nuclease because heterologous expression of proteins was not yet feasible. The only available spectral parameters were the isotropic chemical shift frequencies, which varied among amino acid residues because of the differences in environment resulting from protein folding and resonance line widths that reflected protein dynamics. The first spectra of membrane proteins were not reported for another ten years [302-305].

In the early 1970s the addition of directly bound paramagnetic species made a substantial difference in the prospects for NMR of proteins. Two similar, parallel paths were introduced. McConnell and coworkers [306-307] exploited the stable paramagnetic center of 1-oxyl-2,2,6,6,-tetramethyl-4-piperidinyl (TEMPO) (Figure 4.1A) to covalently label lysozyme and then measure the broadening effects on resonances of bound ligands. The goal then, as now, was to make direct distance measurements between the electron spin-label and nuclei at covalently bonded sites on the protein. However, this was not possible because the studies were limited by the experiments being performed at the relatively low field strength corresponding to a ^{1}H resonance frequency of 100 MHz and other technical issues. Around the same time, Campbell and coworkers [308] were able to convincingly demonstrate the ability of a lanthanide ion (Gd^{3+}) bound to lysozyme to selectively broaden resonances from residues proximate to the binding site, aided in large part by performing the experiments at the significantly higher ^{1}H resonance frequency of 270 MHz. These early experiments that exploited the broadening effects of paramagnetic species, whether TEMPO-containing spin labels or lanthanide ions bound to protein ligands, were key predecessors for the current activity in paramagnetic NMR of proteins.

Solution NMR of proteins has advanced significantly over the past forty years based on improvements in instrumentation, implementation of new spectroscopic techniques, and the application of sophisticated computational methods to both the processing of experimental data and structure calculations. Nonetheless, limitations remain for structure determination of several important classes of proteins, especially

large proteins in complexes in aqueous solution and membrane proteins in various detergent/lipid environments [217]. Both classes of proteins present difficulties for the resolution of individual resonances that result from both the number of overlapping resonances and the broad line widths of the resonances associated with slowly reorienting proteins. Even as these problems have been incrementally addressed, there remains the problem of resolving and assigning a sufficient number of $^{1}H/^{1}H$ NOEs for structure determination with conventional approaches that measure inter-proton distances of < 5 Å. Membrane proteins with multiple trans-membrane helices have the additional problem of identifying the correct alignment and relative positioning of the helices, which is difficult to do with only measurements of short-range distances. Further progress in NMR spectroscopy of these classes of proteins would be greatly aided by the ability to measure relatively long-range (>10 Å) distances. Such long-range distance constraints have many benefits, including improving the resolution of protein structure determination, defining the overall folding topology, and identifying residues in binding sites. They are especially advantageous in offering a method for positioning multiple trans-membrane helices in membrane proteins [309-310].

This Perspective focuses on membrane proteins, in particular, the use of paramagnetic metals attached by tags to otherwise diamagnetic proteins. Our primary research interest is in structure determination of membrane proteins in their native environment of phospholipid bilayers [311]. However, on the path towards this goal, aspects of membrane protein sample preparation and, to some extent, experimental methods are

first worked out with micelle [312], bicelle [34], or nanodisc [25] samples that are tractable for solution NMR. This is the situation for the examples described here, as we demonstrate the applicability of the genetically incorporated unnatural amino acid (UAA) 1-amino-3-(8-hydroxyquionolin-3-yl)-propanoic acid (HQA) (Figure 3.1C) [313] as a metal-binding tag to enable the use of paramagnetic ions to provide long-range PREs that serve as intra- and inter- molecular distance measurements in membrane proteins.

3.2.1 Paramagnetic protein NMR

The unpaired electron on a paramagnetic ion has spectroscopic effects that are several orders of magnitude larger than those of the spin S=1/2 nuclei (^{1}H, ^{13}C, ^{15}N) that are commonly observed in NMR studies of proteins [314-315]. Briefly, paramagnetic ions induce three effects on the diamagnetic spectra of proteins, only two of which are generally observed and incorporated into the experiments – paramagnetic relaxation enhancements (PREs) and pseudocontact shifts (PCSs). In addition, there are through-bond contact shifts; however, because they only occur in close proximity to the metal ions, their effects are typically overwhelmed by strong PRE broadening of the resonances. In general, both PREs and PCSs are widely used in paramagnetic NMR studies of proteins. Their occurrence and properties can be controlled by the selection of the metal ions, the ligands, and other factors. The magnetic susceptibility tensor is a key parameter. The two metals used here, Mn^{2+} and Gd^{3+}, have isotropic magnetic susceptibility tensors and therefore induce only PRE effects. Nitroxide spin labels also only induce PRE effects [316]. Many other metals, especially the lanthanides (with the

exception of gadolinium) and Co^{2+} have highly anisotropic susceptibility tensors. This gives rise to PCSs, which can result in large changes in chemical shifts at distant sites.

There are other beneficial effects of adding paramagnetic metals to the samples in a controlled manner. They can reduce the longitudinal relaxation times so that data can be acquired much more quickly [317-319], and they can weakly align proteins in solution [320], providing an alternative to conventional alignment media for the measurement of residual dipolar couplings (RDCs). Much of the groundwork for the use of paramagnetic ions in protein NMR was laid by Bertini and coworkers on metalloproteins, which contain a natural paramagnetic center [321-322]. For convenience, in appropriate cases, the metal ion can be exchanged for one with more favorable properties for the studies of interest. As an example, Bertini and Pintacuda have used metal ions in structural studies of superoxide dismutase [323]. They were able to measure many ^{15}N and ^{13}C PREs based on the high-resolution two-dimensional heteronuclear correlation 'fingerprint' spectrum of the protein. In addition to the PREs, they were able to measure many PCSs. These paramagnetic constraints significantly reduced the RMSD of the calculated protein structure. However, most proteins, especially the membrane proteins of interest, are not metalloproteins. Because of the advantages of introducing a paramagnetic ion, there has been a great deal of activity in the design and implementation of tags that attach a paramagnetic ion to proteins. There are three main strategies for specifically attaching a paramagnetic metal to a protein. One is to attach residues corresponding to a natural or engineered metal binding site to the C- or N- terminus or a loop of the protein, the second

is to attach a chemical linker to a reactive site, almost universally a surface cysteine side chain, which can bind a metal ion, and the third is to incorporate an unnatural metal-binding amino acid into the sequence at a specific location. These three options are illustrated in Figure 3.1 and are briefly discussed below. The incorporation of an unnatural metal-binding amino acid (Figure 3.1C) into membrane proteins is the principal subject of this Perspective.

In the first case, twelve amino acid residues corresponding to an “EF-hand” calcium binding site were added to the N-terminus of the membrane protein Vpu from HIV-1 [48]. This provided a covalently attached lanthanide ion binding site. The protein itself was not altered by the added residues, as evidenced by a lack of perturbation of the chemical shifts, and it was possible to observe long-range paramagnetic effects in the spectra. In addition, the added lanthanide served to weakly align the protein for measurement of residual dipolar couplings. Imperiali and Schwalbe designed seventeen residue lanthanide binding tags (LBTs) for proteins with improved properties over native calcium binding sites [324]. Subsequently, they inserted LBTs into protein loops [325], which were shown to give complementary results. In a similar vein, Gaponenko et al [326] fused zinc fingers to the N- and C- termini of a protein and demonstrated that they could be substituted with paramagnetic cobalt and manganese.

Most paramagnetic NMR studies of proteins have placed the metal ion on the surface of the protein with a covalent tag [327]. Generally, this has been done through a

linkage to a selected cysteine side chain. In many cases this requires the removal of competitive reactive sites through mutation. It has also become a very active area of research with the development of linkers to two cysteine residues to reduce the local dynamics of the metal ion in order to increase the precision of the measurements. There have also been examples where other protein functional groups are involved in the chelation for the same reason. As a result of this activity, this area has been the subject of a number of reviews, including by Ubbink [328], Otting [315], Emsley and Pintacuda [329]. The tables and figures of these reviews provide a thorough listing of the wide variety of tags that have been utilized to tag proteins with paramagnetic ions. Figure 3 of the review by Otting [315] is particularly helpful in understanding and planning paramagnetic NMR experiments. It shows the relative paramagnetism and asymmetry of the magnetic susceptibility tensors in a way that facilitates direct comparisons.

Using covalent paramagnetic tags, Otting and coworkers have utilized pseudocontact shifts in their studies [330]. They discussed how the assignment problem caused by the large shifts could be addressed. One way is to take advantage of the shifts for two bonded nuclei, e.g. ^{1}H and ^{15}N, which shift along parallel frequencies from the same metal ion. Fast exchange between diamagnetic and paramagnetic species enables titration of the protein and the resulting paramagnetic ion-induced chemical shifts. Pseudocontact shifts can be used as constraints for calculations of protein structures. With the use of multiple tags, significant improvements in the precision of structures result from the measurement of PCSs.

Ubbink and coworkers have also focused on the use of PCSs in the structure determination of protein complexes [323]. Their results have been facilitated by the development of metal binding tags. The magnetic properties of lanthanides are relatively insensitive to variations in the coordination. However, since many tags are more flexible than a typical chemical coordination site, it is essential to restrict their dynamics. This has been achieved with bulky tags, including peptide tags as discussed above, two-point attached tags [331], and tags that interact with protein side chains [332]. With dynamically restricted lanthanide tags, significant PCSs can be observed over large distances, perhaps beyond 100 Å [328]. Jaroniec and coworkers have used both nitroxide and EDTA-Cu^{2+} -tagged mutants of the protein GB1 as a model polycrystalline protein [333-334]. They observed substantial PRE effects in well resolved magic angle spinning spectra by comparing samples with and without free electrons on the TEMPO moiety. Significantly, some of the strong signals in the control sample are missing in the corresponding spectrum of the spin-labeled protein. A key feature of their experimental samples is that the spin-labeled protein was diluted with unlabeled protein to enable the intramolecular effects of interest to be separated from any intermolecular effects of nearby protein molecules. Although clearly beneficial in certain applications, the use of nitroxides as relaxation agents suffers from a major draw-back, namely the presence of large transverse PREs, which lead to severely attenuated signal intensities for numerous residues; this precludes quantitative PRE and distance measurements. They overcame this problem by using tags containing a more rapidly relaxing paramagnetic center, namely Cu^{2+} [335], that does not elicit significant paramagnetic shifts due to its effectively

isotropic magnetic susceptibility tensor. The longitudinal PREs could be used to determine the global fold of GB1. They were able to calculate the backbone fold of GB1 based solely on PREs using only six mutants.

Paramagnetic NMR has been applied to a number of membrane proteins. Building on the structure of the Anabaena sensory rhodopsin (ASR) [336] Ladizhansky and co-workers employed nitroxide spin labels and PRE data to map the oligomerization interface of the receptor [337]. Gottstein et al [338] have summarized the alpha helical membrane proteins whose structures have been determined with the aid of PREs. Other notable studies of membrane proteins using paramagnetic NMR include: protein-lipid interactions of outer membrane protein X (OmpX) and DHPC using various nitroxide spin labels [339], improvements of the outer membrane protein A (OmpA) backbone structure via 'parallel spin labeling' [340], characterization of the Influenza M2 proton channel [341], topology determination in DPC micelles of SCO3063 and YbdK, two bacterial histidine kinase membrane proteins [342], DsbB [343], structural studies of the M. tuberculosis RV1761C protein [344], and the characterization of an 80 residue region of the GPCR Ste2p using PREs in solution NMR [345].

Perhaps the most powerful approach to introducing tags into proteins is unnatural amino acid incorporation [346-347]. This very promising method for paramagnetic NMR will be discussed in more depth in the following section along with a sampling of recent studies performed in our laboratory using membrane proteins and unnatural amino acid

incorporation of a novel paramagnetic tag. The best currently available metal-binding unnatural amino acid, HQA, is shown in Figure 3.1C, which we used in our studies.

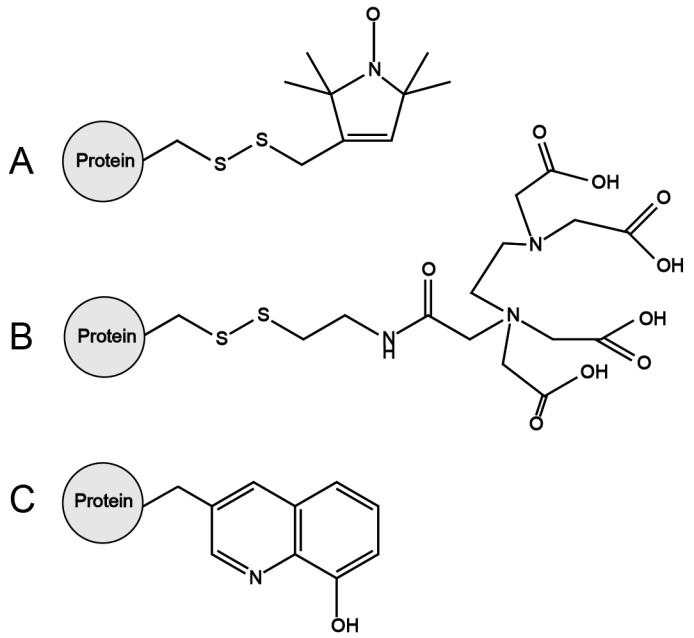

Figure 3.1. Paramagnetic probes for site-specific incorporation of protein. (A) Nitroxide spin label. (B) Ethylenediaminetetraacetic acid (EDTA). (C) 2-amino-3-(8- hydroxyquinolin-3-yl)propanoic acid dihydrochloride(HQA). Nitroxide spin labels and EDTA tags are mobile containing multiple rotatable bonds and are incorporated by chemical reaction at a surface exposed cysteine residue, while HQA is approximately the size of tryptophan and is incorporated genetically at any position in the protein of interest.

3.3 Experimental Section

3.3.1 Synthesis of HQA

The synthesis of 2-amino-3-(8-hydroxyquinolin-3-yl)propanoic acid dihydrochloride (HQA) was carried out as previously reported [313] with a few minor changes. The synthesis of 8-methoxy-3-methylquinoline was carried out according to

Patent DE 3719014 C2, the reflux time in the bromination of 3-methylquinolin-8-yl acetate was decreased to 4-5 hours, and all silica flash column chromatography solvent systems used ethyl acetate and hexanes rather than dichloromethane.

3.3.2 Protein preparation

1TM-CXCR1 [144, 218, 294] and p7 [348] were purified and refolded as described previously for similar constructs of the proteins. For the 1TM-CXCR1 construct an original pET31b(+) vector was modified by including a thrombin cleavage site with a 6-Gly linker between the KSI fusion partner and the polypeptide of interest to facilitate enzymatic cleavage. Interleukin-8 (IL-81-66), a monomeric construct with the 6 C-terminal residues of IL-8 removed, was expressed and purified as previously described [293]. For expression of uniformly ^{15}N-labeled 1TM-CXCR1 and p7 constructs with HQA incorporated (Figure 3.1C), 500 mL Luria-Bertani (LB) media with chloramphenicol/carbenicillin was inoculated with 10% overnight LB starter culture and grown in a shaker/incubator at 37^{o}C. At OD600 ~0.4 the cells were induced with a final concentration of 0.02% L-arabinose and grown for two hours at 37^{o}C. They were then spun down by centrifugation at 3000 rpm. The cell pellets were gently re-suspended in 500 mL minimal media with ^{15}N-labeled ammonium sulfate as the sole nitrogen source, induced with 0.02% final concentration of L-arabinose and grown at 37°C for one more hour following which 1 mM HQA and 100 µM IPTG were added. Cells were grown for four hours, after which they were harvested via centrifugation at 5000 rpm and stored at -80^{o}C prior to further purification. Purification and refolding

procedures of HQA incorporated 1TM-CXCR1 and p7 constructs were identical to those of their wild-type counterparts.

3.3.3 Fluorescence experiments

The fluorescence experiments were performed on a FluoroMax-4 spectrofluorometer (Horiba Scientific, New Jersey, NY) at room temperature with excitation at 400 nm. Fluorescence of the wild-type and HQA-incorporated proteins at 20-50 μM (200 μL) was measured in 300 mM SDS or 150 mM DPC detergent micelles, 20 mM HEPES (pH 7.0) and different concentrations of $ZnCl_2$ (0, 50, 100, 150, and 200 μM). Fluorescence quenching experiments were performed on Zn^{2+} -bound W48HQA p7 by titrating EDTA to final concentrations of 0, 200, 400, and 600 μM.

NMR experiments NMR samples were prepared by dissolving the lyophilized proteins in a solution containing 150 mM DHPC, 20 mM HEPES, pH 7.0 at a final protein concentration of 50 μM -100 μM. For the PRE experiments, aliquots of stock solutions of 10 mM or 100 mM $MnCl_2$ were added to the protein samples at final Mn^{2+} concentrations of 0.1 mM for 1TM CXCR1 samples and 0.5 mM for p7 samples. For the IL-8 and 1TM CXCR1 binding experiments, unlabeled W10HQA 1TM CXCR1 was complexed with uniformly ^{15}N-labeled IL-8 in a 1:1 molar ratio. The NMR experiments were performed on a Bruker Avance 600 MHz spectrometer equipped with 5-mm triple-resonance cryoprobe with zaxis gradient. One-dimensional ^{15}N-edited ^{1}H NMR and ^{1}H-^{15}N HSQC [36] NMR

spectra were obtained at 50°C for the 1TM-CXCR1 and p7 samples, and at 40°C for IL-8-containing samples.

3.4 Results and Discussion

3.4.1 Metal-chelating Unnatural amino acid

Although the use of fusions with cysteines and metal-binding peptides for site-specific paramagnetic labeling of proteins has helped probe protein structure determination, analysis of protein-ligand binding, and descriptions of molecular dynamics, their use is limited by their bulk, local dynamics, and potential sample heterogeneity. Large conformational spaces for the paramagnetic center lead to observed PRE measurements whose properties may be influenced by the flexibility of the probe itself. Rigid paramagnetic probes have been introduced into proteins to counter this problem [349-350], but the location of anchoring cysteine residues in the protein limit their placement and their often-bulky structure can also affect native protein structure. The incorporation of unnatural amino acids (UAAs) easily addresses both the issues of bulk and local dynamics and allows for homogeneous protein samples. They can be placed anywhere in the protein without being limited by disulfide bonds, cysteine residues, and attachments to the protein termini [315]. In addition, a paramagnetic metal ion can be introduced anywhere in the protein with minimal protein structure perturbation [351] due to a single amino acid substitution with a UAA with high metal affinity in the protein sequence.

Site-specific genetic incorporation of HQA involves an orthogonal aminoacyl-tRNA/tRNA synthetase pair specific to the HQA that reads the amber TAG codon [313]. Under normal circumstances, E. coli would recognize TAG as a stop codon. With the addition of the orthogonal pair, however, HQA is added to the growing protein chain. The orthogonal tRNA synthetase is not recognized by endogenous tRNA/amino acid and vice versa [347]. Of the more than 100 unnatural amino acids incorporated successfully, a small fraction is useful for NMR. These include isotopically labeled p-methoxy-phenylalanine and its fluorinated analogs [352-353], photocaged unnatural amino acids for site-specific labeling [351], metal-chelating unnatural amino acids [313, 350, 354], and an amino acid that ligates with a lanthanide tag [346]. Incorporation of isotopically labeled amino acids at specific residues have helped identify ligand binding sites and conformational changes of large proteins [353]. Aside from these, to date, only four unnatural amino acids that have been successfully incorporated into proteins can be used as paramagnetic probes. Three are metal chelating and one is used to ligate with a lanthanide tag [351]. Protein engineering with unnatural amino acids has been discussed [355], and it is possible for site-directed spin labeling of a genetically encoded unnatural amino acid [356].

The use of lanthanides for PRE studies are of particular interest because of their varying magnetic properties; different lanthanides can be incorporated into the same metal-chelation site [351]. Previous lanthanide tags could only be noncovalently bound to the N- or C- termini of a protein, resulting in flexibility of the tag and poor measurements. While the lanthanide-p-azido-L-phenylalanine (AzF) fusion allowed for placement of the

tag independent of the location of other residues in the protein, there are limitations that hinder its widespread application [350]. The lanthanide tag is also limited by the need for known structural data for tether optimization. Using metal-chelating unnatural amino acids, on the other hand, provides a straightforward way to introduce a paramagnetic ion for PRE measurements [354]. For example, the UAA bipyridylalanine (BpyAla) was successfully incorporated into the West Nile virus NS2B-NS3 protease and bound to cobalt (II) to obtain PCS measurements. Of the three metal-chelating unnatural amino acids, only HQA chelates to lanthanides [313, 351], making it the best candidate for PRE studies. Moreover, HQA is the smallest of the three UAA, making it an ideal replacement of the similarly sized aromatic canonical amino acids. It is also fluorescently active, allowing for easy detection of metal-bound protein.

Successful efforts to obtain NMR spectra of HQA-incorporated protein have not been reported previously [351]. Here we show by solution NMR the successful incorporation of HQA into two membrane proteins: the cytoplasmic N-terminal region of the G-protein coupled receptor (GPCR) CXCR1 and the second transmembrane helix of viroporin p7 from the hepatitis C virus. We were also able to successfully obtain NMR data showing specific binding of a paramagnetic ion to the HQA-incorporated proteins, offering powerful insight to protein-ligand binding and protein structure.

3.4.2 Genetic incorporation of HQA into membrane proteins

Genetic incorporation of the unnatural amino acid 2-Amino-3-(8-hydroxyquinolin-3-yl)propanoic acid (HQA) was done via amber codon suppression as demonstrated by Schultz and co-workers [313]. For the 1TM-CXCR1 construct the tryptophan at position 10 in the amino acid sequence was chosen as the site of mutation due to its location in the binding region of the receptor and its ligand, interleukin-8 (IL-8). For the p7 construct, the tryptophan at residue 48 in the sequence was chosen as the site of mutation due to its location in the second transmembrane helix, with the ultimate goal of obtaining intramolecular PRE data.

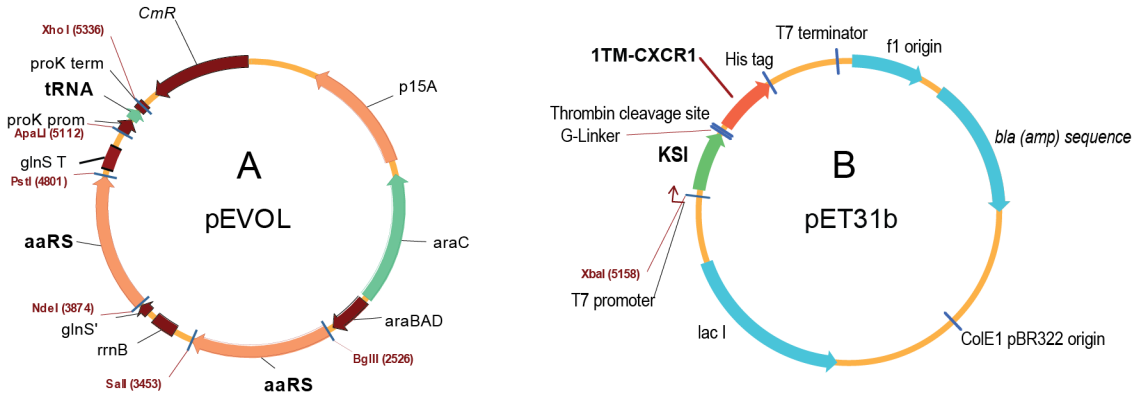

Figure 3.2. Vector maps for unnatural amino acid incorporation into proteins in E. coli. (A) The pEVOL vector optimized for efficient expression of orthogonal pairs (Young et al. 2010). (B) Modified pET31b(+) vector for HQA-incorporated 1TM-CXCR1 expression as a KSI-fusion protein containing a thrombin cleavage site between KSI and the target membrane protein.

The plasmid containing the orthogonal tRNA/tRNA synthetase pair (pEVOL) and that containing our target (pET31b+) (Figure 3.2) were co-expressed in minimal media and we were able to obtain high yields of mutant, HQA incorporated, protein for both the

1TMCXCR1 and p7 constructs. Growth and incorporation protocols for both the orthogonal pair and target genes were optimized and included testing various growth temperatures, induction times and concentrations, as well as optimizing the growth media itself (data not shown). Following growth and induction both the truncated and incorporated forms of the protein were produced, as can be seen in Figure 3.3, lane 1. Due to the presence of a C-terminal histidine tag, which is only present in the full-length mutant and not in the truncated form (Figure 3.3, top), the two could be successfully separated via Ni-immobilized metal affinity chromatography (IMAC). Further purification by HPLC resulted in high yields of pure protein (Figure 3.3).

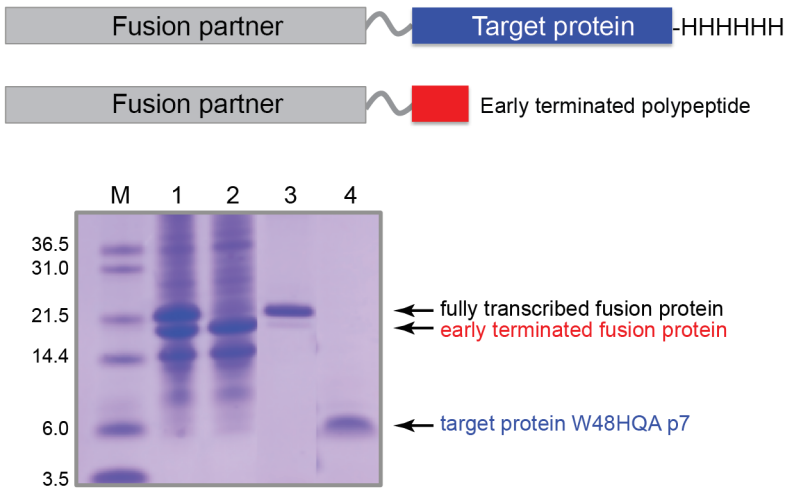

Figure 3.3. Schematic drawings of the proteins prepared by using the expression vectors shown in Fig. 4.2 and a SDS-PAGE showing the purification of a HQA-incorporated membrane protein p7: lane 1, inclusion bodies solubilized in detergents; lane 2, flow through of the Ni-affinity chromatography; lane 3, elution from the Ni-affinity chromatography; lane 4, HPLC pure W48HQA p7 after CNBr cleavage. Note that the His-tag attached to the C-terminus of the target protein facilitates the separation of the fully transcribed proteins from the early-terminated proteins using Ni-affinity chromatography.

In the ^{15}N HSQC spectra obtained at 600 MHz for both W10HQA 1TM-CXCR1 and W48HQA p7 in DHPC micelles at pH 7 (Figure 3.4) it was observed that the resonances from the tryptophan indole nitrogen sites, which were mutated at positions 10 and 48, respectively, were noticeably absent in the spectra of the mutant proteins, indicating that the unnatural amino acid was successfully incorporated into the proteins and at the correct positions. Furthermore, the overlap between the spectra of the wild type and mutant proteins is very significant for both mutants (Figure 3.4) indicating that incorporation of the unnatural amino acid did not cause any significant chemical shift perturbations in the spectra and that the native structures and conformations are retained.

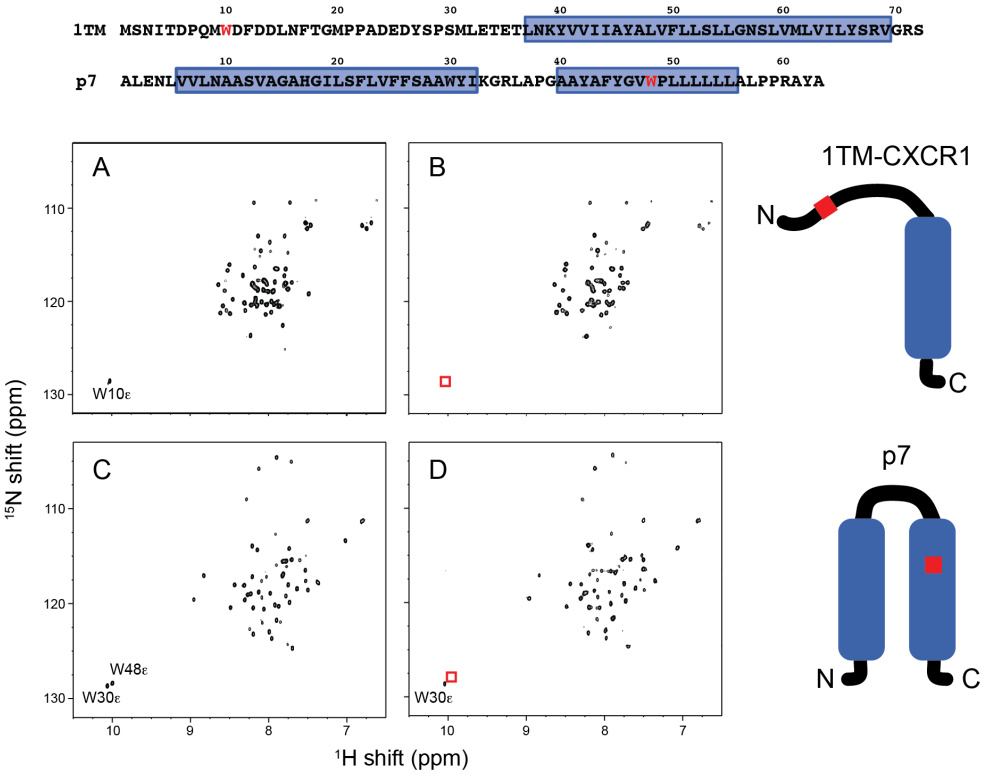

Figure 3.4. Comparison of ^{1}H-^{15}N HSQC spectra of uniformly ^{15}N-labeled membrane protein constructs in DHPC micelles. (A) Wild-type 1TM-CXCR1. (B) W10HQA 1TM-CXCR1. (C) Wild-type p7. (D) W48HQA p7. Absence of Trp indole NHε signals shown in red boxes indicates complete incorporation of the unnatural amino acid HQA into residue Trp 10 in 1TM-CXCR1 and into residue Trp 48 in p7. The mutation site is colored in red in the amino acid sequences and schematic drawings of proteins. Note that the amide chemical shifts for wild-type and HQA incorporated proteins are identical except in the vicinity of the mutated site.

4.4.2 Fluorescence induced by HQA-metal chelate

8-hydroxyquinoline forms chelate compounds with many metal ions including lanthanides, and Cd^{2+}, Mg^{2+}, and Zn^{2+} form a strong fluorescent complex with 8-hydroxyquinoline [357]. In order to investigate site-specific fluorescence from binding of metal ions to HQA-incorporated membrane proteins in detergent micelles, W10HQA 1TM-CXCR1 and W48HQA p7 proteins were titrated with Zn^{2+} ions and fluorescence was measured (Figure 3.5). No fluorescence of the HQA-incorporated proteins was observed

in the absence of Zn^{2+}, but the fluorescence increased with increasing the concentrations of Zn^{2+}, and was saturated at about 5:1 (Zn^{2+}:HQA) molar ratio. As a control, the fluorescence of the wild-type proteins was examined; however, they showed no fluorescence in the presence of 200 μM Zn^{2+}.

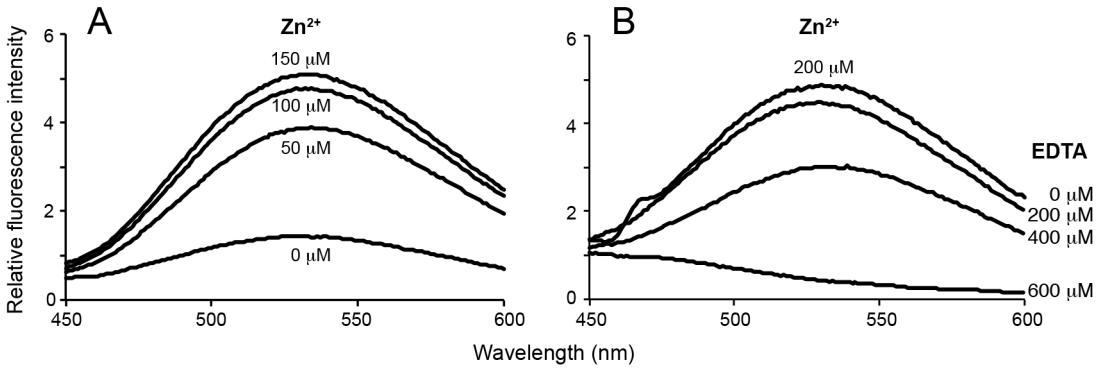

Figure 3.5. Fluorescence spectra of HQA-incorporated membrane proteins in detergent micelles. (A) W10HQA 1TM-CXCR1 complexed with varying concentrations of ZnCl2. (B) W48HQA p7 complexed with 200 uM ZnCl2 and with varying concentrations of EDTA. Protein concentration was approximately 50 uM.

In figure 3.5B, complete quenching of fluorescence of Zn^{2+}-HQA chelates was observed at a 3:1 (EDTA:HQA-Zn^{2+}) molar ratio, suggesting that Zn^{2+} forms stable chelates with HQA in the transmembrane region of p7 in micelles. These results prove that genetic incorporation of the unnatural amino acid HQA into membrane proteins can serve as a powerful site-specific biophysical probe for studies of the structures and dynamics of membrane proteins in membrane environments.

3.4.3 Intramolecular PREs by HQA-metal chelate

In Figure 3.6, the comparison of HSQC spectra of p7 constructs demonstrates the different PRE effects on the wild type and HQA-incorporated p7 samples. All of the p7 resonances, except for the first three N-terminal residues, were observed and assigned in DHPC micelles at pH 7 (Figure 3.6A). When paramagnetic Mn^{2+} ions were titrated to the wild-type p7, several resonances (residues 4, 17, 18, and 63) were significantly broadened, indicating these residues are located in the solvent accessible regions of the molecular surface of p7 in detergent micelles (Figure 3.6B).

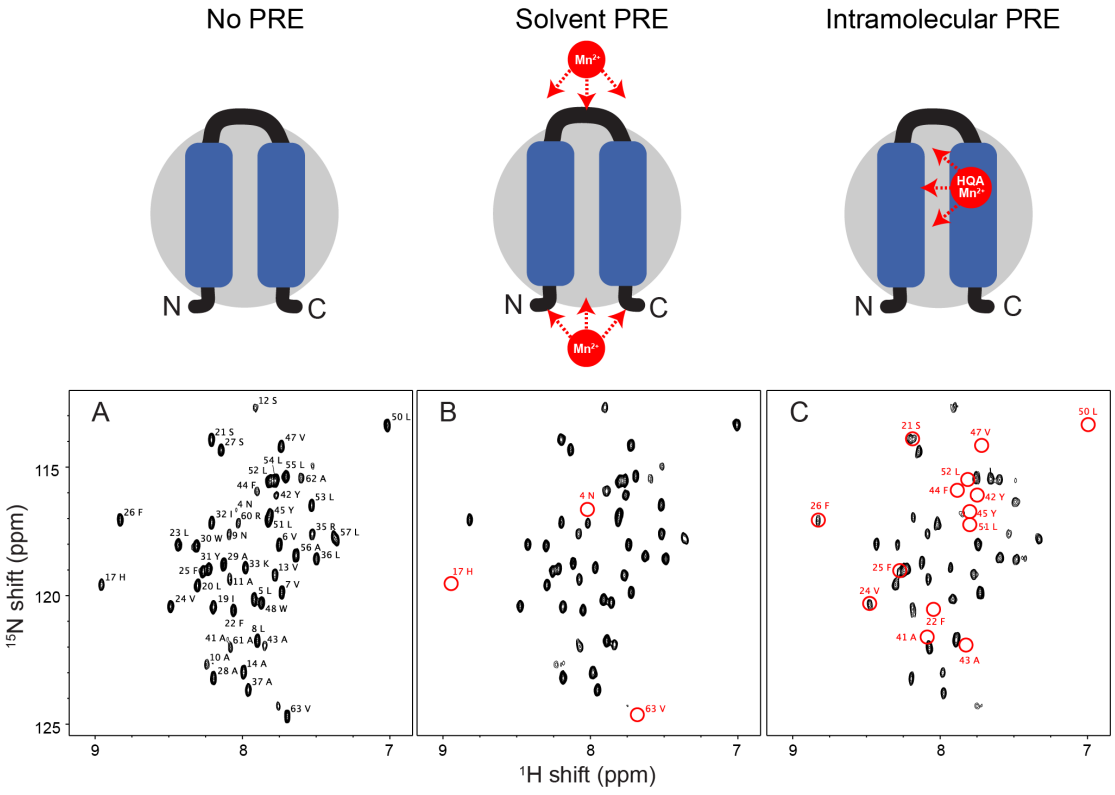

Figure 3.6. Expanded region of the ^{1}H-^{15}N HSQC spectra of uniformly ^{15}N-labeled p7 in DHPC micelles. (A) Wild-type p7 alone. (B) Wild-type p7 in the presence of 0.5 mM MnCl2. (C) W48HQA p7 in the presence of 0.5 mM MnCl2. The resonances broadened by solvent PREs or intramolecular PREs are indicated by red circles. Note that glycine residues 15, 18, 34, and 46 do not lie in the expanded region.

When Mn^{2+} ions were titrated in the W48HQA p7 sample at an approximately 5:1 (Mn^{2+}:W48HQA p7) molar ratio, many more signals were broadened or disappeared compared to the wild-type p7 (Figure 3.6C). This result suggests that Mn^{2+} can specifically bind to the HQA located in the second transmembrane helix of p7 in detergent micelles, and therefore yields intramolecular PREs. Many of the disappeared resonances (residues 41-47 and residues 50-52) are near the mutated position of the residue 48 as expected. However, it is noteworthy that the residues 21-26 were also significantly broadened or disappeared, indicating that these residues, which are located in the first transmembrane helix are in close proximity to residue 48 which is located in the second transmembrane helix of p7. These intramolecular PREs are very helpful in structure determination of membrane proteins, since they provide long-range distance restraints that are very challenging to obtain by conventional NOE experiments.

1TM-CXCR1 consists of the ligand binding N-terminal domain, which is mobile and solvent accessible, and the first transmembrane helix of CXCR1, which is buried in the membrane environments [218]. Therefore, the resonances of the N- terminal domain of wild type 1TM-CXCR1 and several C-terminal residues were broadened beyond detection in the presence of Mn^{2+} or Gd^{3+}, while only 7 residues near the HQA mutation site of W10HQA 1TM-CXCR1 were broadened by the titration of paramagnetic ions due to a site-specific HQA and metal ion interactions. Although successful efforts to obtain NMR spectra of HQA-incorporated protein have not been reported previously due to metal mediated protein oligomerization [351], we do not observe any evidence of oligomerization

or aggregation of HQA-incorporated membrane proteins in detergent micelles. Optimization of experimental conditions was straightforward.

3.4.4 Intermolecular PREs by HQA-metal chelate

The N-terminal domain of the chemokine receptor CXCR1 contains the major binding site of the ligand IL-8 [219]. Figure 3.7 shows that the HQA in 1TM-CXCR1 serves as an excellent probe for intermolecular PREs, providing crucial long-range distance restraints for structure determination of the IL-8 and 1TM-CXCR1 complex. The binding sites of IL-8, identified by chemical shift perturbation upon interaction with W10HQA 1TM-CXCR1 (Figure 3.7B), were identical to those of the IL-8 interaction with wild-type 1TM-CXCR1. Adding Mn^{2+} ions to the complex selectively broadened the residues of the binding sites (e.g. residues K20 and W52ε) beyond detection because of the site specific intermolecular PREs (Figure 3.7C), providing the distance restraints between IL-8 and 1TM-CXCR1 that are essential for structure determination of the ligand-receptor complex.

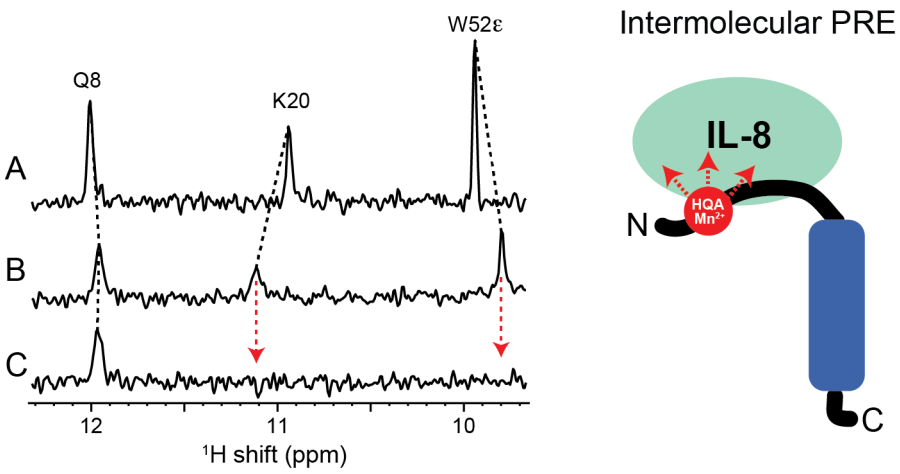

Figure 3.7. Expanded region of the ^{15}N-edited ^{1}H spectra of uniformly ^{15}N-labeled IL-8 in DHPC micelles. (A) IL-8 alone. (B) IL-8 bound to unlabeled W10HQA 1TM-CXCR1. (C) IL-8 bound to unlabeled W10HQA 1TM-CXCR1 in the presence of $MnCl_2$. Close proximity between residues K20 and W52ε of IL-8 and the paramagnetic HQA-Mn^{2+} Group at residue 10 of CXCR1 is shown by observation of select intermolecular PREs.

3.5 Conclusions

The research described here is a prelude to the use of paramagnetic tags on membrane proteins in phospholipid bilayers. This involves the use of solid-state NMR because the membrane proteins are immobilized by their interactions with the phospholipids in the bilayer environment. Thus, significant background comes from prior solid-state NMR studies of paramagnetically tagged proteins. The in vivo incorporation of unnatural amino acids into proteins is a well-established technique requiring an orthogonal tRNA/aminoacyl-tRNA synthetase pair specific for the unnatural amino acid that is incorporated at a position encoded by a TAG amber codon. Recently developed metal-chelating unnatural amino acid 2-Amino-3-(8-hydroxyquinolin-3-yl)propanoic acid (HQA) forms highly stable complexes with various transition metal ions and lanthanides,

serving as an excellent probe for paramagnetic relaxation enhancement NMR experiments. Although poor protein yields hamper its application in the protein NMR field, optimization of the expression of orthogonal aminoacyl-tRNA synthetases/suppressor tRNA pairs from the pEVOL vector and target proteins from the KSI-fusion expression system allows for significant improvement of the yield of HQA-incorporated proteins to the degree of obtaining yields equivalent to those for wild type proteins. NMR spectral comparisons of the wild type and HQA incorporated mutants demonstrate complete incorporation of HQA into the membrane proteins. Zn^{2+}-HQA induced fluorescence confirms a stable metal chelation.

Chapter 3, in full, is a reprint of the material as it appears in JBNMR, “Paramagnetic relaxation enhancement of membrane proteins by incorporation of the metal-chelating unnatural amino acid 2-amino-3-(8-hydroxyquinolin-3-yl)propanoic acid (HQA)” by Park, S.H., Wang, V. S., Radoicic, J., De Angelis, A. A., Berkamp, S., and Opella, S. J., 2015. The dissertation author was the third author of this paper.

Chapter 4. Interaction of Monomeric Interleukin-8 with CXCR1 Mapped by Proton-detected Fast MAS Solid-state NMR and Intermolecular Paramagnetic Relaxation Enhancement

4.1 Abstract

The human chemokine interleukin-8 (IL-8; CXCL8) is a key mediator of innate immune and inflammatory responses. This small, soluble protein triggers a host of biological effects upon binding and activating CXCR1, a G protein coupled receptor, located in the cell membrane of neutrophils. Here, we describe ^{1}H-detected magic angle spinning solid-state NMR studies of monomeric IL-8 (1-66) bound to full-length and truncated constructs of CXCR1 in phospholipid bilayers under physiological conditions. Cross-polarization experiments demonstrate that most backbone amide sites of IL-8 (1-66) are immobilized and that their chemical shifts are perturbed upon binding to CXCR1, demonstrating that the dynamics and environments of chemokine residues are affected by interactions with the chemokine receptor. Comparisons of spectra of IL-8 (1-66) bound to full-length CXCR1 (1-350) and to N-terminal truncated construct NT-CXCR1 (39-350) identify specific chemokine residues involved in interactions with binding sites associated with N-terminal residues (binding site-I) and extracellular loop and helical residues (binding site-II) of the receptor. Intermolecular paramagnetic relaxation enhancement broadening of IL-8 (1-66) signals results from interactions of the chemokine with CXCR1 (1-350) containing Mn^{2+} chelated to an unnatural amino acid assists in the characterization of the receptor-bound form of the chemokine.

4.2 Introduction

More than 800 G protein-coupled receptors (GPCRs) are encoded in the human genome. These membrane proteins have seven transmembrane helices and each binds to one or multiple extracellular molecular signals, typically small molecules, but in some cases proteins. Their activation triggers many physiological processes through interactions with intracellular proteins. The structures, dynamics, and functions of GPCRs are of keen interest to both physiology and medicine, especially because they are receptors for a large fraction of the drugs in current use and provide fertile ground for the targeted development of new drugs [358]. Although there has been significant progress in recent years in the characterization of static structures of crystalline GPCRs at low temperatures [359-361], relatively little is known about their binding to, and activation by, naturally occurring agonists, especially proteins, under physiological conditions where both agonist and receptor dynamics are likely to play important roles. Here we examine the interactions between a chemokine agonist and its receptor in the near-native environment of hydrated phospholipid bilayers by NMR spectroscopy.

About 50 chemokines and 20 chemokine receptors constitute an important part of the innate immune system [362]. Not only do these proteins play key roles in the defense against microbial infections, but they are also associated with responses to inflammatory diseases such as arthritis, asthma, and cancer [363]. The chemokine interleukin-8 (IL-8; CXCL8) binds to and activates the GPCR CXCR1 in the cell membranes of neutrophils, which then interact with G-proteins, arrestins, and other intracellular proteins to initiate

biochemical responses of the cell. IL-8 and CXCR1 serve as a prototypical chemokine system because they are the first of their types to be discovered and are among the best characterized [364]. IL-8 is a small soluble protein with 72 residues. Its structure, determined by solution NMR spectroscopy [365] and x-ray crystallography [366], is characterized by having a flexible N-terminal segment containing a conserved Glu-Leu-Arg (ELR) motif just before the characteristic CXC arrangement of cysteine residues (X represents another type of amino acid) that participate in the two disulfide bonds that stabilize the tertiary fold of the three β-strands and single α-helical segment. Most CXC chemokines have between 70 and 130 residues with substantial variation of sequences. However, they share the characteristic three-dimensional chemokine fold first described for IL-8, which suggests that there may be commonality in how they interact with their receptors.

At the high concentrations used in NMR spectroscopy and x-ray crystallography, most chemokines form noncovalent dimers or larger oligomers. IL-8 has been shown to exist and function both as a monomer and dimer [297, 367-368]. The monomer binds to the N-terminal domain of CXCR1 with higher affinity than the dimer [184-185, 295], and is believed to be the biologically active form of the protein. Modification, mutation, or truncation of residues at the dimer interface stabilize the monomeric form of IL-8 [192, 368]. The structure of monomeric IL-8 (1-66), obtained by truncation of the last six C-terminal residues, using solution NMR is shown in Fig. 4.1A [298]. Overall, the structure of monomeric IL-8 is very similar to that of each subunit in the wild-type IL-8 (1-72) dimer [369]. CXCR1 and CXCR2 were the first chemokine receptors to be identified and cloned [370], and were originally

referred to as IL-8RA [145] and IL-8RB [371] respectively. They share 80% sequence identity. Most of the differences are in the N- and C-terminals, which bind chemokines and G-proteins, respectively. Both receptors have high affinity for IL-8, with a low nanomolar dissociation constant [143, 220]. Finding that two similar but distinct receptors bind the same chemokine, and that CXCR1 almost exclusively binds to IL-8 whereas CXCR2 also binds to several other chemokines, provided an early indication of the complexity of the chemokine defense system. At present, the structures of six chemokine receptors have been reported: the crystal structures of CXCR4 [212, 372], CCR2 [373], CCR5 [374], CCR9 [375], and viral US28 [376], and our NMR structure of CXCR1 in lipid bilayers [220], which is shown in Fig. 4.1B. Although none of the structures represent complexes of a receptor with one of its native chemokine agonists, the structures of receptors bound to viral chemokines provide information that is complementary to the many mutagenesis and binding studies of their interactions. There have been many solution NMR and other biophysical studies of IL-8 interacting with polypeptides whose sequences correspond to N-terminal residues of CXCR1 [184-187, 192, 219, 295, 377]. The current model for chemokine-receptor interactions involves two binding sites on the receptor. Residues in both the N-terminal domain (binding site-I) and in one or more extracellular loops (binding site-II) of CXCR1 have been shown to interact with IL-8 [184, 188, 190, 193, 219].

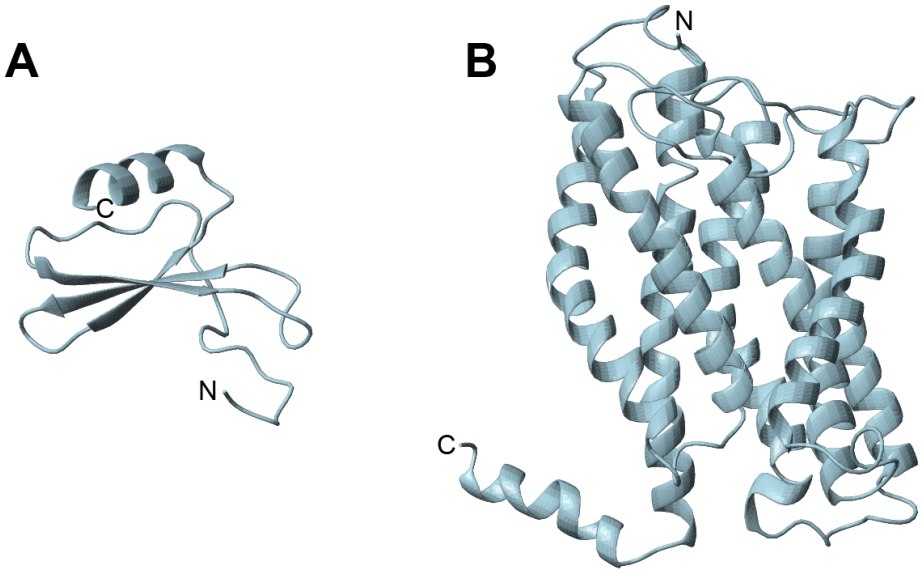

Figure 4.1 Structures of the chemokine IL-8 and its receptor CXCR1. (A) Structure of the monomeric chemokine IL-8 (1-66) in aqueous solution (PDB: 5WDZ). (B) Structure of the chemokine receptor CXCR1 (1-350) in phospholipid bilayers (PDB: 2LNL). Extracellular N-terminal and intracellular C-terminal residues of CXCR1 involved in ligand and G-protein interactions, respectively, are not included in the Figure because they are mobile on the timescales of the NMR experiments used to determine the structure of the receptor.

Solid-state NMR spectroscopy enables studies of the structure and dynamics of membrane proteins in near-native phospholipid bilayer environments [378-381]. There are several examples where solid-state NMR methods have been used to characterize the structures of ligands bound to GPCRs [382-385] as well as GPCRs themselves. Most prior studies of membrane proteins or their ligands have involved the direct detection of signals from labeled ^{13}C or ^{15}N sites; this continues to be a fruitful approach and we applied it in our earlier studies of CXCR1 [219-220, 386]. However, dramatic improvements in sensitivity have been obtained by the implementation of ^{1}H-detected magic angle spinning (MAS) solid-state NMR methods [387-388], especially when fast MAS is combined with

perdeuteration of the samples [387, 389-392]. This approach is being applied to an increasing number of membrane proteins [393-396].

Here, we describe the effects on IL-8 when it binds to CXCR1 in phospholipid bilayers using ^{1}H-detected MAS solid-state NMR. We prepared uniformly ^{2}H and ^{15}N labeled monomeric IL-8 (1-66) [298], and examined its interactions with unlabeled full-length CXCR1 (1-350), which contains both binding site-I and binding site-II, and an N-terminal truncated construct of CXCR1, NT-CXCR1 (39-350), which lacks binding site-I associated with the N-terminal region but retains binding site-II associated with the extracellular loops. Changes observed in spectra of IL-8 (1-66) upon binding CXCR1 (1-350) and NT-CXCR1 (39-350) identify chemokine residues involved in the interactions with CXCR1. In addition, we incorporated the metal-chelating unnatural amino acid 2-amino-3-(8-hydroxyquinolin-3-yl)propanoic acid dihydrochloride (HQA) into full-length CXCR1, expanding upon earlier work [222], to observe intermolecular paramagnetic relaxation enhancement (PRE) between IL-8 (1-66) and CXCR1 (1-350). This provides additional information about the structures and spatial arrangement of the complexed proteins.

4.3 Materials and Methods

4.3.1 Incorporation of HQA

The unnatural amino acid HQA was purchased from BOC Sciences (http://www.bocsci.com). The replacement of tryptophan by HQA at position 10 in the sequence of full-length CXCR1 (1-350) was performed as previously described for a

different construct of CXCR1 [222]. The complete replacement of tryptophan by HQA was confirmed by NMR and fluorescence spectroscopies. Purification and refolding procedures of HQA-containing CXCR1 (W10HQA CXCR1) were identical to those applied to the wild-type protein [220].

4.3.2 Sample preparation

Monomeric IL-8 (1-66) containing residues of 1-66 of the wild-type human protein was expressed and purified using the protocol described previously [296]. Uniformly ^{2}H- and ^{15}N-labeled samples were obtained by growing bacteria in BioExpress cell growth media (U-^{2H}, 98%; U-^{15}N, 98%) and deuterium oxide (^{2}H, 99.9%) (Cambridge Isotope Laboratories, Tewksbury, MA; http://www.isotope.com). High deuteration levels (>90%) were verified by comparing the ^{1}H solution NMR spectrum of perdeuterated IL-8 (1-66) to that of an unlabeled sample. The proteoliposome samples of 1,2-dimyristoyl-sn-glycero-3-phosphocholine lipid bilayers containing full-length CXCR1 (1-350) or N-terminal truncated construct NT-CXCR1 (39-350) were prepared as described previously [218, 220]. The lipid/protein molar ratio was 300:1.

4.3.3 NMR experiments

The solution NMR experiments were performed at 40^{o}C on a Bruker 600MHz spectrometer equipped with 5 mm triple-resonance cryoprobe with z-axis gradient. The concentration of monomeric IL-8 (1-66) was 50 mM in 20 mM HEPES buffer (pH 7.3). One-dimensional ^{15}N-edited ^{1}H NMR spectra of uniformly ^{15}N-labeled monomeric IL-8 (1-

66) were obtained by signal-averaging 128 transients in the absence and presence of CXCR1-containing proteoliposomes at a molar ratio of 1:1. The samples for solid-state NMR experiments contained 30–50 ug of uniformly ^{2}H- and ^{15}N-labeled IL-8 (1-66) in 3 mL of 20 mM HEPES buffer in 100% $^{1}H_2O$. Spectra were obtained in the absence and presence of various unlabeled CXCR1 constructs in liposomes at a receptor to IL-8 (1-66) molar ratio of 1:1. Samples were prepared by adding an appropriate amount of isotopically labeled IL-8 (1-66) in solution to proteoliposomes containing unlabeled CXCR1 constructs in 5 mL of 20 mM HEPES buffer (pH 7.3). The mixtures were incubated for 30 min at room temperature before ultracentrifugation for 20–40 h at 645,000 g at 15^{o}C. Approximately 3 mL of fully hydrated proteoliposomes containing IL-8 (1-66) bound to the receptor was transferred into a 1.3 mm MAS rotor. For the PRE experiments, a 200-fold molar excess of $MnCl_2$ was added to the proteoliposome samples before ultracentrifugation.

Solid-state NMR experiments were performed at 900 MHz (21.2 Tesla) on a Bruker Avance III HD spectrometer equipped with a triple-resonance 1.3 mm MAS probe. The sample-spinning rate was controlled to 60 kHz (52 Hz). The probe temperature was maintained at 8^{o}C using nitrogen cooling gas at 30^{o}C and a flow rate of 1500 L/h; the actual sample temperature, as monitored by the resonance frequency of the water signal, was estimated to be 30^{o}C due to frictional heating. Two-dimensional ^{1}H-detected ^{1}H-^{15}N chemical shift correlation spectra were acquired using either a ^{1}H-^{15}N heteronuclear single quantum correlation (HSQC) pulse sequence via double insensitive nuclei

enhanced by polarization transfers (INEPT) [101] with presaturation for water signal suppression, or via double cross-polarization (CP) transfers [222, 387] with multiple intense solvent suppression intended for sensitive spectroscopic investigation of protonated proteins instantly [388]. ^{15}N globally optimized alternating phase rectangular pulse [397] decoupling with irradiation of 22.6 kHz was applied during ^{1}H signal acquisition. In these pulse sequences, the hard $\pi/2$ pulses had nutation frequencies of 100 and 55.6 kHz for ^{1}H and ^{15}N, respectively. The delay τ was set to 1/4 J (2.5 ms) for INEPT transfers. The contact time was 1 ms for the first CP transfer from ^{1}H to ^{15}N, and 0.4 ms for the second CP transfer from ^{15}N to ^{1}H. Two-dimensional INEPT correlation spectra were acquired using 64 complex time-domain points with a total acquisition time of 10ms in the indirect ^{15}N chemical shift dimension, and 2048 complex time-domain points with a total acquisition time of 56.8 ms in the directly detected ^{1}H chemical shift dimension. Two-dimensional CP correlation spectra were acquired using 64 complex time-domain points with a total acquisition time of 10ms in the indirect ^{15}N chemical shift dimension, and 1024 complex time-domain points with a total acquisition time of 11.3 ms in the directly detected ^{1}H chemical shift dimension. The relaxation delay for all experiments was 1.2 s. The NMR data were processed using TopSpin 3.5 (http://www.bruker.com) and the structures were visualized using PyMol (http://www.pymol.org).

4.4 Results

4.4.1 Immobilization of IL-8 bound to CXCR1 in phospholipid bilayers

Although IL-8 exists as a homodimer in solution [365], monomeric IL-8 has been shown to bind to CXCR1 with similar or higher affinity than the dimer [185, 295]. Truncation of the last six C-terminal residues results in a stable monomeric form of IL-8 (1-66) [188]. Studies of IL-8 (1-66) avoid potential complications due to dimer-to-monomer interconversion of either the free or bound forms of IL-8. Binding of IL-8 (1-66) to full-length CXCR1 (1-350) is tight enough that IL-8 (1-66) can be found in the insoluble proteoliposome pellet along with CXCR1 (1-350) after ultracentrifugation (Fig. 4.2A, lane 3). Similar results were obtained for IL-8 (1-66) binding to NT-CXCR1 (39-350), where the residues responsible for the receptor's N-terminal binding site are missing (data not shown). However, no IL-8 (1-66) was detected in the pellet obtained by ultracentrifugation of a sample of the protein suspended in the presence of empty liposomes. This indicates that IL-8 does not interact with or partition to phospholipids. Purified uniformly ^{15}N-labeled IL-8 (1-66) (Fig. 4.2A, lane 2) in aqueous ($^{1}H_2O$) buffer yields a well-resolved ^{15}N-edited ^{1}H solution NMR spectrum of the amide region (Fig. 4.2B), which is similar to that obtained from the wild-type dimeric IL-8 (1-72) [219, 298]. The binding of IL-8 (1-66) to CXCR1 (1-350) in phospholipid bilayers at a molar ratio of 1:1 (Fig. 4.2A, lane 3) results in the broadening of all IL-8 (1-66) ^{1}H amide signals beyond detection by solution NMR (Fig. 4.2C). This demonstrates that the global reorientation of IL-8 (1-66) is highly restricted by binding to CXCR1 embedded in phospholipid bilayers. Similar results were observed for the interaction of wild-type dimeric IL-8 (1-72) with the receptor under the same sample and

spectroscopic conditions (data not shown). Notably, signals from those residues of wild-type dimeric IL-8 (1-72) not directly involved in the interaction with CXCR1 (1-350) could be observed in solution NMR spectra when the protein complexes are in rapidly reorienting isotropic bicelles, but not when they are in slowly and anisotropically reorienting lipid environments, such as magnetically aligned bicelles or proteoliposomes [219]. The slow global reorientation of IL-8 complexed with CXCR1 in phospholipid bilayers severely compromises the application of solution NMR methods to these samples. However, it is possible to use solid-state NMR methods to investigate IL-8 bound to CXCR1 in phospholipid bilayers. Fig. 4.3 compares two-dimensional ^{1}H-^{15}N chemical shift correlation spectra of IL-8 (1-66) obtained under various experimental conditions. The use of uniformly ^{2}H- and ^{15}N-labeled IL-8 (1-66), where the perdeuteration facilitates the suppression of ^{1}H-^{1}H dipolar couplings, is essential to obtain these high-resolution MAS spectra.

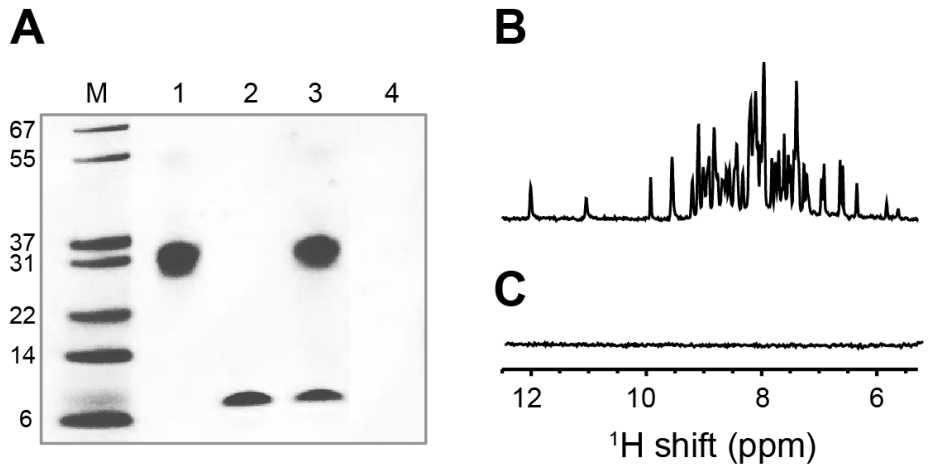

Figure 4.2. IL-8 forms a tight complex with CXCR1 (A) SDS-PAGE analysis of IL-8 (1-66), CXCR1 (1-350), and their 1:1 complex. Lane M: Protein molecular weight marker. Lane 1: CXCR1 (1-350) in phospholipid bilayers. Lane 2: IL-8 (1-66) in aqueous buffer. Lane 3: pellet and Lane 4: supernatant, of a 1:1 molar ratio mixture of IL-8 (1-66) and CXCR1 (1-350) in phospholipid bilayers after 20 h of ultracentrifugation at 645,000 g. Lane 3 demonstrates that IL-8 (1-66) and CXCR1 (1-350) are in the resulting pellet and that neither protein is in the supernatant, indicating that they form a complex in the bilayers. (B and C) One-dimensional ^{15}N-edited ^{1}H solution NMR spectra of uniformly ^{15}N-labeled IL-8 (1-66) obtained at 600 MHz and 40 C. (B) IL-8 (1-66) alone in aqueous solution. (C) 1:1 IL-8 (1-66):CXCR1 (1-350) complex in phospholipid bilayers. The ^{1}H solution NMR signals of IL-8 (1-66) are broadened beyond detection by the slow reorientation of the chemokine bound to CXCR1 in phospholipid bilayers.

4.4.2 Fast-exchanging amide hydrogens of IL-8

A two-dimensional ^{1}H-^{15}N HSQC NMR spectrum of uniformly ^{15}N labeled IL-8 (1-66) in aqueous solution is shown with black contours in Figs. 4.3A and 4.4A. This spectrum was obtained with the sample in a standard 5 mm OD solution NMR sample tube that was not spun. All the amide resonances have been assigned to specific residues, with the exception of the mobile C-terminal residue, 66, whose amide hydrogen exchanges rapidly with water at pH 7.3 [298]. A spectrum of the same solution sample obtained in a 1.3 mm rotor spinning at 60 kHz using the same pulse sequence, with minor

modifications of the τ delay for INEPT transfers and the use of continuous wave irradiation (presaturation) for water signal suppression, is shown with black contours in Fig. 4.3B and with red contours in Fig. 4.4A. The observed line widths of amide ^{1}H resonances of IL-8 (1-66) in aqueous solution obtained by conventional solution NMR and obtained by 60 kHz MAS solid-state NMR are 30 and 50 Hz, respectively. The solution NMR and solid-state NMR spectra in Fig. 4.4 are very similar with extensive overlap of chemical shifts. Importantly, no signals could be observed using CP transfer, indicating that IL-8 (1-66) is not sedimented but remains soluble undergoing isotropic reorientation in solution at 60 kHz MAS, which produces > 106 g centrifugal force toward the rotor wall. Presaturation for water suppression in the solid-state MAS spectrum results in missing or very weak intensity signals from solvent-accessible residues (1–5, 11–15, 18, 20, 33, 35, 37, 44, 45, and 57) compared to the solution NMR spectrum obtained with the WATERGATE pulse sequence [398] for water suppression. This result was verified by amide hydrogendeuterium exchange measurements on IL-8 (1-66) in solution [298]. The residues with fast-exchanging amide hydrogens are represented in green in the IL-8 (1-66) structure (Fig. 4.4B); they are mainly located in the N-terminal and three loop regions (N-loop, 30s loop, and 40s loop) This result is in agreement with the previously measured amide nitrogen relaxation rates of a monomeric IL-8 mutant in aqueous solution, in which a high degree of mobility was observed for the unstructured N-terminal region, and reduced mobility for several residues in the loop regions (residues 11, 12, 33, 35, 45, and 57) [377].

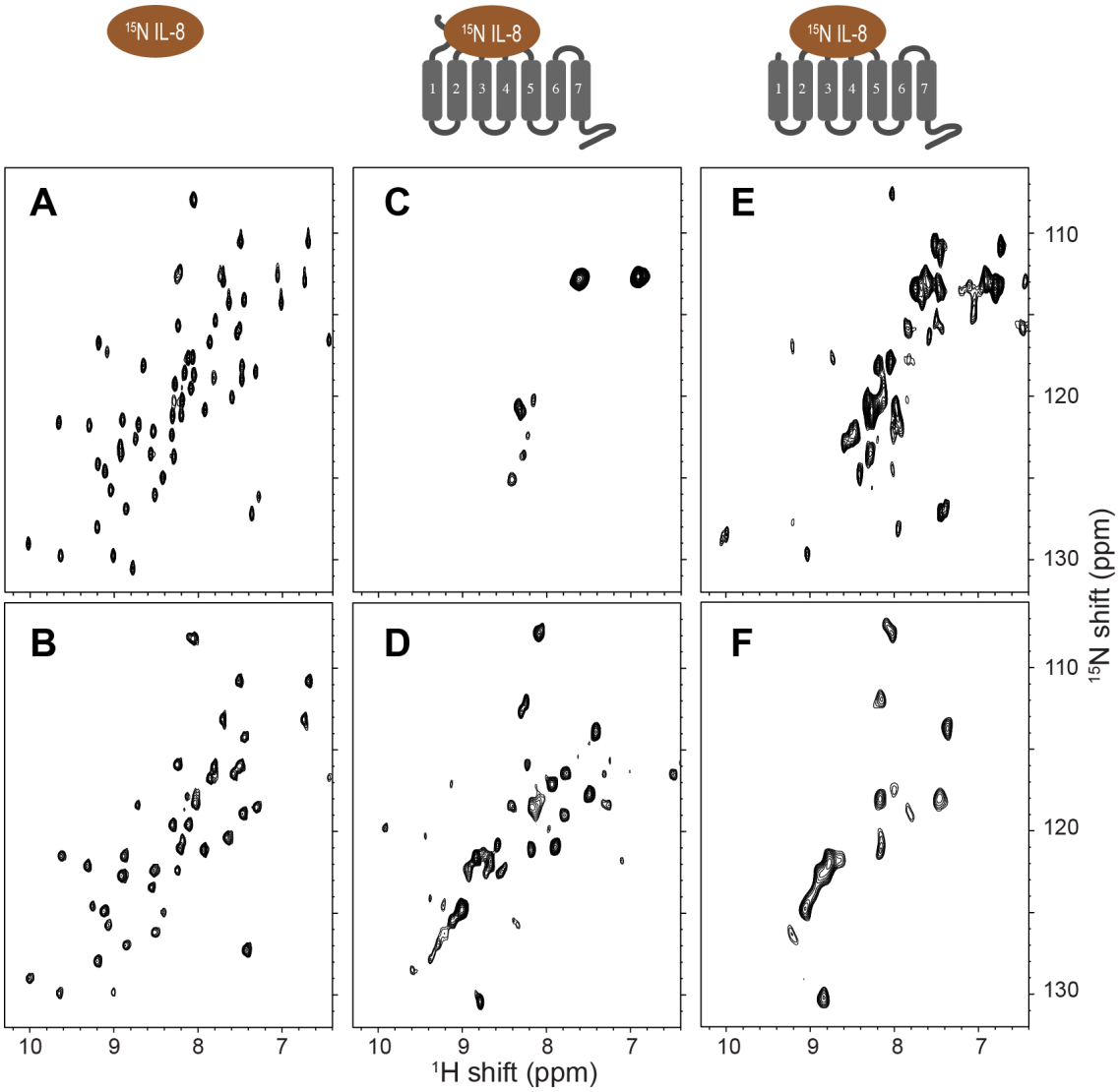

Figure 4.3. Two-dimensional ^{1}H-detected ^{1}H-^{15}N correlation NMR spectra of uniformly [^{2}H, ^{15}N-HN] labeled IL-8 (1-66). The cartoons at the top represent the samples: IL-8 (1-66) alone (left), the IL-8 (1-66):CXCR1(1-350) complex (center), and the IL-8 (1-66):NT-CXCR1(39-350) complex (right). (A) HSQC solution NMR spectrum of IL-8 (1-66) alone in aqueous solution obtained at 600 MHz and 40 C. (B–F) ^{1}H-detected 60 kHz MAS solid-state NMR spectra of IL-8 (1-66) in the absence (B) and presence (C–F) of CXCR1 constructs in phospholipid bilayers obtained at 900 MHz and 30 C. (B) IL-8 (1-66) alone in aqueous solution. (C and D) 1:1 IL-8 (1-66):CXCR1 (1-350) complex in phospholipid bilayers. (E and F) 1:1 IL-8 (1-66):NT-CXCR1 (39-350) in phospholipid bilayers. (A–C and E) were obtained with INEPT and (D and F) with CP magnetization transfers, enabling the separate observation of signals from mobile (A–C and E) and immobile (D and F) sites.

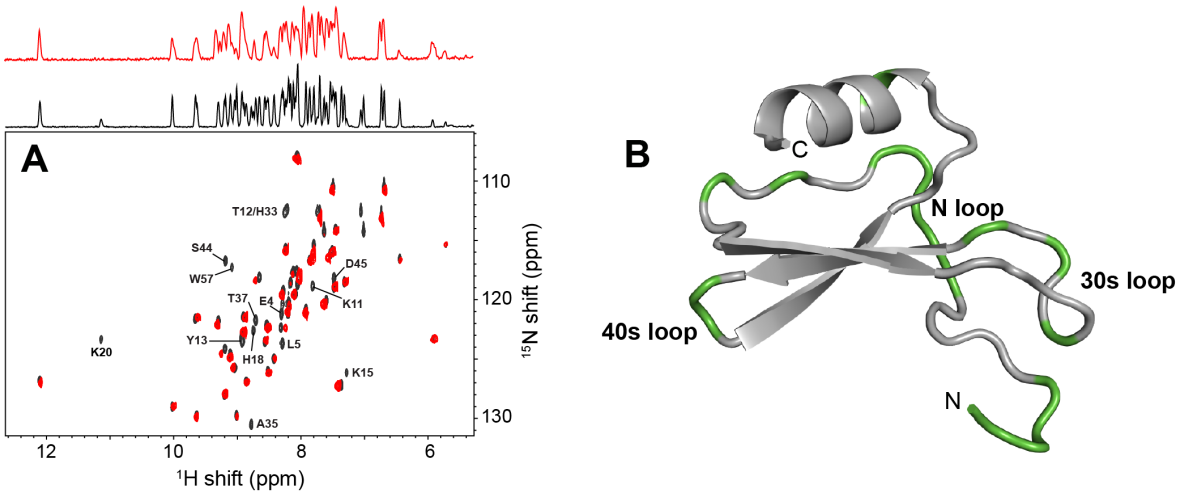

Figure 4.4. Fast-exchanging protons in IL-8 (A) Comparison of one-dimensional ^{15}N-edited ^{1}H NMR and two-dimensional ^{1}H-detected ^{1}H-^{15}N correlation NMR spectra of uniformly ^{15}N-labeled IL-8 (1-66) in aqueous solution obtained by solution NMR (black contours) and solid-state 60 kHz MAS NMR (red contours), respectively. The amide resonances absent in the solid-state MAS NMR spectrum due to fast exchange with water are marked. (B) The fast-exchanging sites in the N-terminal and three loop regions of IL-8 (1-66) are colored in green in the protein structure.

4.4.3 IL-8 Interaction with CXCR1 in Phospholipid Bilayers

Comparison of MAS solid-state NMR spectra obtained with CP and INEPT magnetization transfers enables the qualitative characterization of residue-specific local dynamics of IL-8 (1-66) bound to CXCR1 in phospholipid bilayers (Figs. 4.3, 4.5, and 4.7). Signals from immobilized residues are observed in the spectra obtained with CP transfers whereas signals from mobile residues are observed in the spectra obtained with INEPT transfers. ^{1}H-detected ^{1}H-^{15}N correlation solid-state MAS NMR spectra of ^{2}H and ^{15}N labeled IL-8 (1-66) bound to unlabeled full-length CXCR1 (1-350) show that signals from most of the IL-8 (1-66) amide backbone sites could be observed in the CP spectrum (Fig. 4.3D (black contours) and Fig. 4.5A (red contours)). In contrast, only five backbone and a pair of side-chain signals were observed in the INEPT spectrum (Fig. 4.3C (black

contours), and Fig. 4.5B (green contours). Motionally averaged signals of IL-8 (1-66) bound to CXCR1 in phospholipid bilayers were observed in the MAS solid-state NMR spectrum (Figs. 4.3C and 4.5B), but not in the solution NMR spectrum (Fig. 4.2C) because the severe broadening from the dipole-dipole interactions is suppressed by the combination of fast MAS and perdeuteration. Several residues, including those from the C-terminal helical region, which are not observed in either CP or INEPT solid-state NMR experiments, are marked in gray in Fig. 4.5C. The C-terminal helical region of IL-8 (1-66) does not show evidence of interaction with the receptor. It is known to be responsible for association with the sulfate groups of glycosaminoglycans [399], and local motions might occur on an intermediate timescale, such that neither CP nor INEPT transfers yield signals [400]. The mobile and fast-exchanging IL-8 (1-66) sites in the loops (green sites in Fig. 4.4B) were immobilized along with the three β -strands upon interaction with CXCR1 (red sites in Fig. 4.5C). Several fast-exchanging residues [145, 368-369, 385-386] in the N-loop and the 40s loop of IL-8 (1-66) contribute to its primary binding site [184-187, 192, 219, 295, 377, 401].

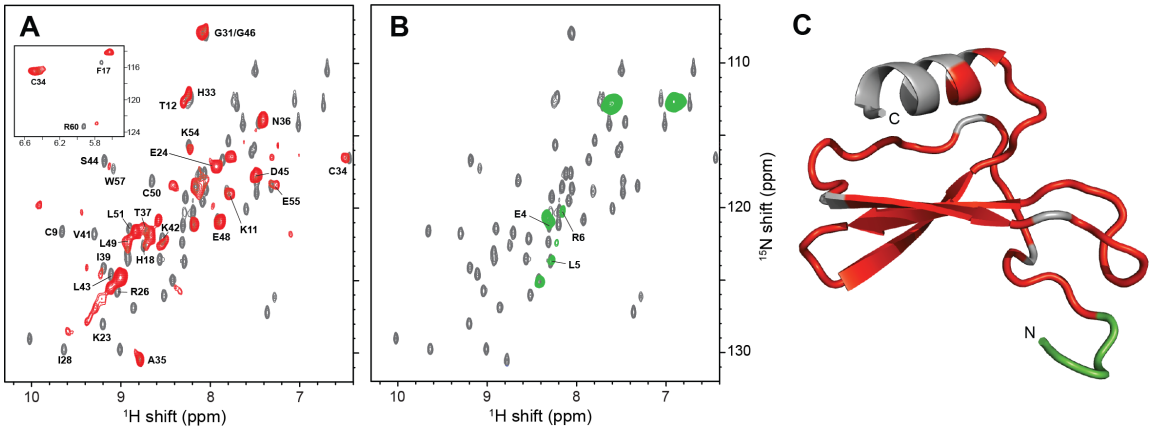

Figure 4.5. (A and B) ^{1}H-detected ^{1}H-^{15}N correlation solid-state 60 kHz MAS NMR spectra of [^{2}H, ^{15}N-HN] labeled IL-8 (1-66) bound to unlabeled CXCR1 (1-350) in phospholipid bilayers obtained with (A) CP (red contours) and (B) INEPT (green contours) magnetization transfers. The solid-state MAS NMR spectra are overlaid on the solution NMR HSQC spectrum (Figs. 3 A and 4 A) of free IL-8 (1-66) (gray contours). Assigned signals are marked. (C) Structure of IL-8 (1-66) with the dynamics of residues in IL-8 (1-66) bound to CXCR1 (1-350) designated by colors. Red represents immobile sites (red contours, A) and green represents mobile sites (green contours, B). Signals from residues in the gray regions are either unassigned or undetected in the solid-state NMR spectra.

Significant chemical shift perturbations of resonances of IL-8 (1-66) upon interaction with CXCR1 (1-350) indicate the locations of the IL-8 (1-66) residues involved in binding. Chemical shift perturbations of five well-resolved resonances of IL-8 (1-66), Gln8, and Lys20 in the downfield (11–12 ppm) region and Phe17, Cys34, and Val58 in the upfield (5.5–6.5 ppm) region are compared in Fig. 4.6. Phe17 and Val58 resonances were significantly perturbed by both CXCR1 (1-350) in phospholipid bilayers and the soluble peptide ND-CXCR1 (1-38) in aqueous buffer, whereas Cys34 was not affected. This result is consistent with solution NMR data on interactions of both monomers and dimers of IL-8 with various N-terminal CXCR1 peptides containing only binding site-I of

the receptor [184]. The Gln8 resonance was slightly perturbed by both receptor constructs, but the Lys20 resonance was only perturbed by ND-CXCR1 (1-38) and not by CXCR1 (1-350), suggesting that the IL-8 (1-66) interaction with CXCR1 (1-350) is different from that with ND-CXCR1 (1-38).

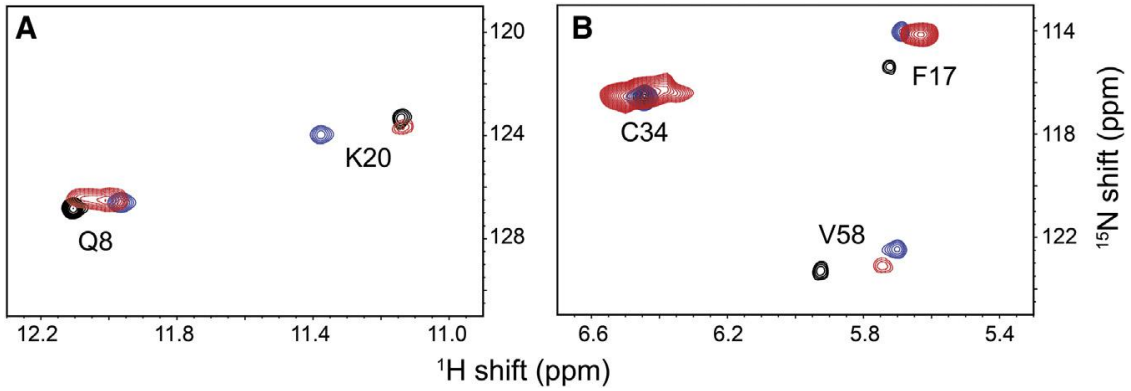

Figure 4.6 Downfield (A) and upfield (B) regions of ^{1}H-^{15}N correlation spectra of IL-8 (1-66). Signals in black contours are from a solution NMR HSQC spectrum of free IL-8 (1-66); blue contours are from a solution NMR HSQC spectrum of IL-8 (1-66) bound to ND-CXCR1 (1-38) [298]; and red contours are from a solid-state MAS NMR spectrum of IL-8 (1-66) bound to CXCR1 (1-350). Assigned residues are marked.

4.4.4 IL-8 interaction with NT-CXCR1 in phospholipid bilayers

IL-8 (1-66) binds to NT-CXCR1 (39-350), which lacks the N-terminal 38 residues of the receptor that contribute to binding site-I, but retains binding site-II associated with extracellular loops of the receptor. Significant differences were observed between the ^{1}H-^{15}N correlation spectra of IL-8 (1-66) bound to NT-CXCR1 (39-350) (Figs. 4.3E and F and 4.7A and B) and to full-length CXCR1 (1-350) (Figs. 4.3C and D and 4.5A and B). From the IL-8 (1-66) and NT-CXCR1 (39-350) complex, 11 backbone amide signals can be

observed in the CP spectrum (Fig. 4.3F, black contours, and Fig. 4.7A, red contours) compared with 18 signals in the INEPT spectrum (Fig. 4.3 E, black contours, and Fig. 4.7B, green contours). Out of the 60 expected backbone amide signals, 31 are not detected in either the CP or the INEPT spectra. The corresponding residues are shown in gray on the structure in Fig. 4.7C. The observed CP signals are located primarily in the 30s loop, 40s loop, and β-3 strand (Fig. 4.7C, red). The chemical shift perturbations of IL-8 (1-66) resonances by interactions with NT-CXCR1 (39-350) in the CP spectrum are generally smaller than those observed for interactions with full-length CXCR1 (1-350), possibly indicating differences in the nature of the interactions with the extracellular loops of the receptor [402-403].

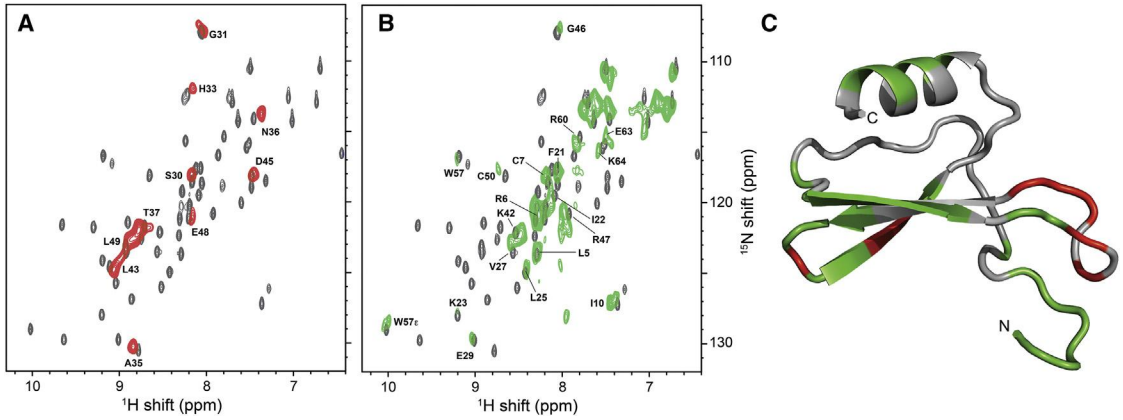

Figure 4.7 (A and B) ^{1}H-detected ^{1}H-^{15}N correlation solid-state 60 kHz MAS NMR spectra of [^{2}H, ^{15}N-HN] labeled IL-8 (1-66) bound to unlabeled NT-CXCR1 (39-350) in phospholipid bilayers obtained with (A) CP (red contours) and (B) INEPT (green contours) magnetization transfers. The solid-state MAS NMR spectra are overlaid on the solution NMR HSQC spectrum (Figs. 3 A and 4 A) of free IL-8 (1-66) (gray contours). Assigned signals are marked. (C) Structure of IL-8 (1-66) with the dynamics of residues in IL-8 (1-66) bound to NT-CXCR1 (39-350) designated by colors. Red represents immobile sites (red signals, A) and green represents mobile sites (green signals, B). Signals from residues in the gray regions are either unassigned or undetected in the solid-state NMR spectra.

4.4.5 Long-range distance restraints from intermolecular PRE of HQA-incorporated CXCR1

The genetic incorporation of the metal-chelating unnatural amino acid HQA [313] into membrane proteins enables the measurement of intra- and intermolecular distance restraints by enabling PRE NMR experiments [222]. The signal intensities in the one-dimensional MAS solid-state ^{15}N-edited ^{1}H NMR spectrum of IL-8 (1-66) bound to W10HQA CXCR1 (1-350) (Fig. 4.8A) were reduced by the broadening effects of the bound paramagnetic Mn^{2+} ion on nearby ^{1}H nuclei (Fig. 4.8 B). Control experiments show that the presence of free manganese ions in solution has negligible effect on the spectrum of IL-8 (1-66) bound to wild-type CXCR1 (1-350) (Fig. 4.8C and D). Most likely this is because the CP transferred ^{1}H signals of IL-8 (1-66), which result from the immobilization of its residues due to interactions with CXCR1 (1-350), are shielded from the free manganese ions. The spectrum of labeled IL-8 (1-66) bound to unlabeled NT-CXCR1(39-350) (Fig. 4.8E), in which the observed signals are primarily from the immobilized IL-8 (1-66) residues interacting with the extracellular loops of the receptor, is similar to that of IL-8 (1-66) bound to W10HQA CXCR1 in the presence of manganese ions (Fig. 4.8 B). This suggests that the intermolecular PREs resulting from the Mn^{2+} bound to residue 10 of CXCR1 selectively broaden the IL-8 (1-66) signals from residues near binding site-I of CXCR1.

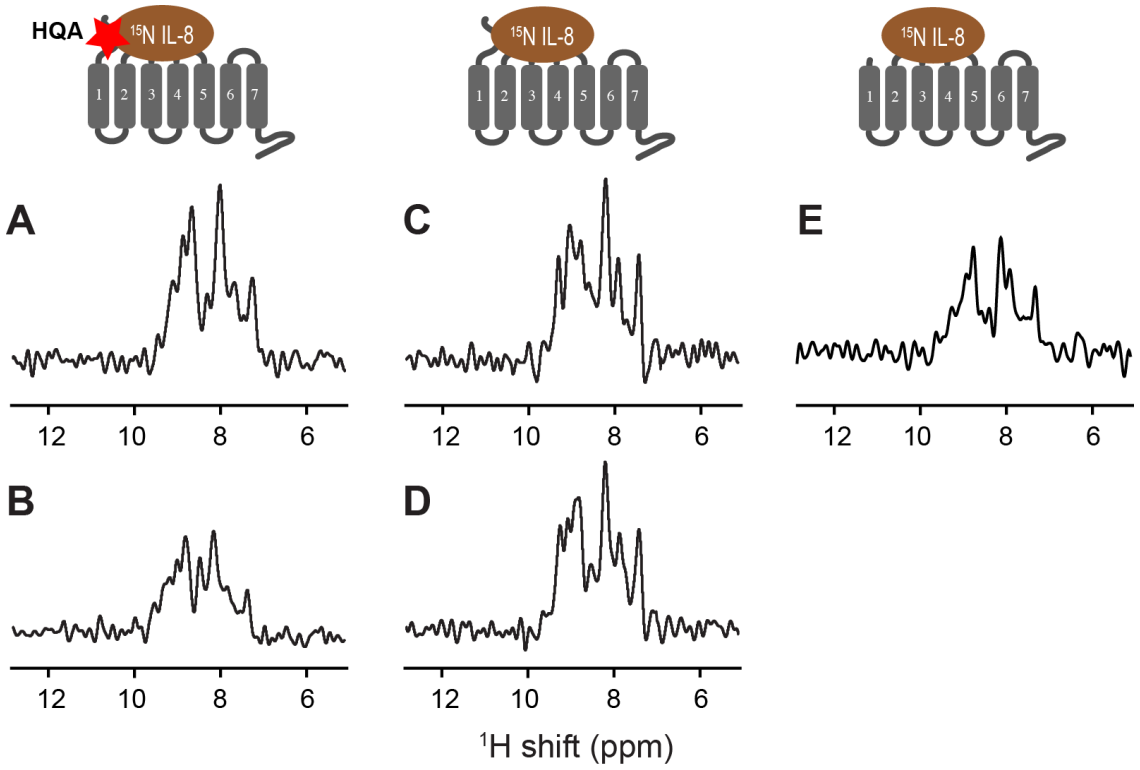

Figure 4.8 One-dimensional ^{15}N-edited ^{1}H-detected 60 kHz MAS solid-state NMR spectra of [^{2}H, ^{15}N-HN] labeled IL-8 (1-66) bound to unlabeled CXCR1 obtained with CP magnetization transfer. The cartoons at the top represent the samples: 1:1 IL-8 (1-66): W10HQA CXCR1 (1-350) complex (left), 1:1 IL-8 (1–66):CXCR1 (1-350) complex (center), and IL-8 (1-66):NT-CXCR1 (39–350) complex (right). The star indicates the location of the metal-chelating unnatural amino acid HQA at residue 10 in the N-terminal domain of CXCR1. (A and B) 1:1 IL-8 (1-66): W10HQA CXCR1 (1-350) complex. (C and D) 1:1 IL-8 (1-66):CXCR1 (1-350) complex. (E) 1:1 IL-8 (1-66):NT-CXCR1 (39-350) complex. (A), (C), and (E) were obtained in the absence of $MnCl_2$. (B) and (D) were obtained in the presence of $MnCl_2$.

4.5 Discussion

Residues in the N-terminal domain (binding site-I) and in extracellular loops (binding site-II) of CXCR1 interact with IL-8 [185-187, 189-192, 219, 295, 377, 403]. Specific residues in the N-terminal domain of CXCR1 contribute to both the selectivity and the affinity of the receptor for IL-8. However, much less is known about how IL-8 interacts with the extracellular loops of CXCR1, or how the binding of IL-8 activates the receptor and

triggers its biological functions. ^{1}H-detected fast MAS solid-state NMR experiments on isotopically labeled IL-8 (1-66) bound to unlabeled constructs of CXCR1 provide new information about the nature of the interactions of IL-8 with CXCR1 in phospholipid bilayers. IL-8 binds to synthesized and expressed polypeptides with sequences corresponding to the N-terminal region of CXCR1 that contains binding site-I. The KD values for IL-8 interacting with only binding site-I are in the submicromolar to submillimolar range [184], which is significantly weaker than for binding to full-length CXCR1, which includes both binding site-I and binding site-II (KD~1–5 nM) [386]. In particular, the binding affinity of IL-8 (1-66) for 1TM-CXCR1 (1-72), which includes N-terminal residues (binding site-I) and the first transmembrane helix of CXCR1, is 12.5 mM in nanodiscs, which is similar to that for the soluble N-terminal domain alone [ND-CXCR1 (1-38)] in aqueous buffer [298]. Notably, not only IL-8 (1-66) bound to full-length CXCR1 (1-350), which includes binding site-I and binding site-II, but also IL-8 (1-66) bound to the shorter constructs 1TM-CXCR1 (1-72), which includes only binding site-I, and NT-CXCR1 (39-350), which includes only binding site-II, are co-pelleted by ultracentrifugation. Thus, ligand-receptor complexes in phospholipid bilayers with as low as micromolar binding affinities are co-pelleted by ultracentrifugation, demonstrating that the complexes are stable and well-suited for NMR experiments. All of the results are consistent with ‘‘slow exchange’’ of the ligand (IL-8) and the receptor (CXCR1) on the relevant NMR timescales.

GPCRs undergo conformational changes as a result of ligand binding and their dynamics are hypothesized to play an important role in the transmission of signals across

membranes [404]. The N- and C-terminal residues of the apo receptor display evidence of mobility in several different sample preparations and NMR experiments. However, it has also been established that they play roles in the interactions with the extracellular ligand IL-8 and intracellular G-proteins, respectively [218, 220], and these residues become ordered upon interaction with the ligands. The data summarized in Fig. 4.9 provide an opportunity to focus on the changes in the structure and dynamics of the chemokine IL-8 that result from interactions with its receptor CXCR1. The data in Fig. 4.9, rows C–F, are derived from the spectra in Fig. 4.3; they show that IL-8 (1-66) undergoes significant changes in dynamics upon interaction with full-length CXCR1 (1-350) and the shorter N-terminal truncated construct NT-CXCR1 (39-350). Previously, the dynamics of monomeric and dimeric IL-8 have been described in the absence and presence of N-terminal CXCR1 peptides by solution NMR [377]; the N-terminus of IL-8, including the conserved ELR motif, is disordered and dynamic, whereas the three loops connecting three β-strands and one C-terminal α -helix are well-structured, even though their amide hydrogens undergo facile exchange with water (the data in row B of Fig. 4.9 are derived from Fig. 4.4). The IL-8 residues that directly interact with various N-terminal CXCR1 constructs, including ND-CXCR1 (1-38) and 1TM-CXCR1 (1-72), are well defined [184, 377]. The residues in the N-loop and 40s loop of IL-8 contribute to its major binding sites and display some evidence of local motions [184-186, 219]. In combination with the solid-state NMR data obtained on IL-8 (1-66) bound to CXCR1 (1-350) and NT-CXCR1 (39-350) in phospholipid bilayers, this suggests that the dynamics of free and bound IL-8 may play important roles in receptor binding selectivity as well as activation.

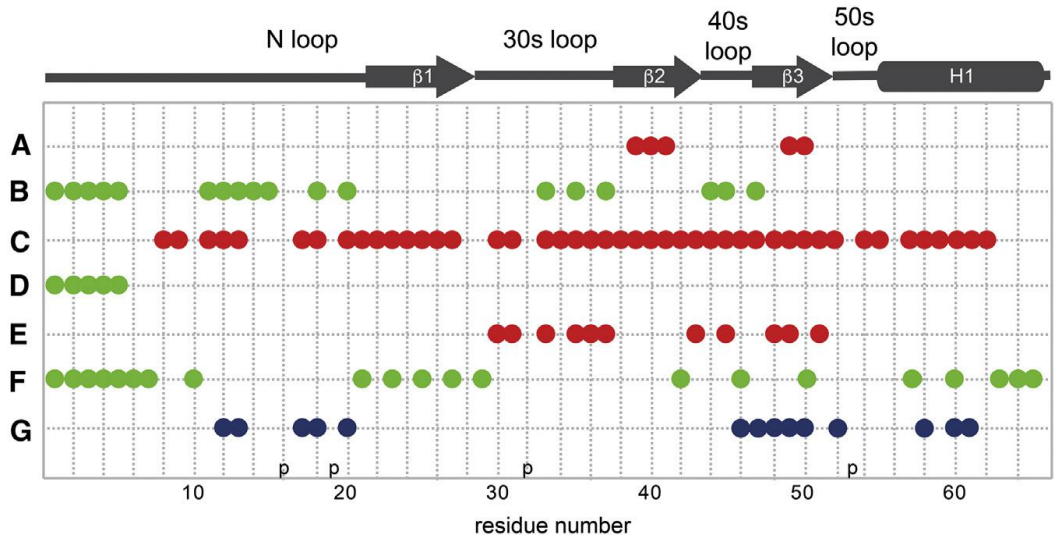

Figure 4.9 Summary of IL-8 (1-66) interactions with CXCR1 (1-350), NT-CXCR1 (39-350), and ND-CXCR1 (1-38). Row A: Non-exchanging amide sites in D_2O. Row B: Fast-exchanging amide sites in H_2O from Fig. 4. (Rows C and D: Immobile and mobile sites by interaction with CXCR1 (1-350), respectively, from Fig. 5. Rows E and F: Immobile and mobile sites by interaction with NT-CXCR1 (39-350), respectively, from Fig. 7. Row G: Most perturbed sites of chemical shifts by interaction with ND-CXCR1 (1-38).

Significant changes in IL-8 (1-66) dynamics occur upon binding to wild-type CXCR1 (1-350). A majority of the residues in IL-8 (1-66), including those in the flexible loop regions, are immobilized upon interaction with CXCR1 (1-350). In addition, residue-specific chemical shift perturbations are observed (Fig. 4.5A). Although many of the resonance assignments of bound IL-8 (1-66) could be obtained by direct comparison to the spectra of unbound IL-8 (1-66), several signals were significantly perturbed by the interaction and independent assignment experiments on the bound form of IL-8 (1-66) will be needed to map out all of the site-specific chemical shift perturbations. This should be feasible using recently developed ^{1}H-detected fast MAS triple resonance solid-state NMR experiments [393]. The solid-state NMR INEPT spectrum in Fig. 4.3C demonstrates that five backbone amide sites are mobile in IL-8 (1-66) bound to CXCR1 (1-350); the signals from

these sites are superimposable on those from the ELR residues of IL-8 (1-66) free in solution as shown in Fig. 4.5B. The signals of Glu4 and Leu5 are absent in the solution NMR INEPT spectrum of unbound IL-8 (1-66) due to their rapid exchange with water (Fig. 4.4A). As a result, their presence in the solid-state NMR INEPT spectrum of bound IL-8 (1-66) demonstrates that these residues are protected from solvent exchange by the interactions of IL-8 with CXCR1. The N-terminal ELR motif of IL-8 has been proposed to interact with the extracellular regions of CXCR1 and trigger receptor activation [193]. However, no chemical shift perturbations are observed, and the mobile ELR signals in bound IL-8 (1-66) suggest that the ELR motif does not interact directly with extracellular or transmembrane helical regions of CXCR1, which is consistent with our previous data on the interactions between wild-type IL-8 dimer and full-length CXCR1 in oriented lipid bilayers [219]. Since the N-terminal truncated form of the receptor is missing binding site-I, NMR spectra of the complex of IL-8 (1-66) and NT-CXCR1 (39-350) are informative about the interactions of IL-8 with binding site-II. The relatively small number of IL-8 (1-66) residues that are immobilized by binding are located mainly within the 30s and 40s loops of IL-8 (1-66). They are likely to be involved in direct interactions with residues in extracellular loops of CXCR1. However, most IL-8 residues undergo sufficient motional averaging to yield signals from INEPT experiments in the absence of binding site-I (Fig. 4.7). Thus, IL-8 interacts with both binding site-I and binding site-II of CXCR1. Other efforts to characterize the two-site model of IL-8 binding to CXCR1 have revealed that the N-loop of IL-8 is the major determinant for CXCR1 activation [405]. In contrast, the N-terminus of IL-8 (ELR and CXC) is essential for CXCR2 activation [406], which suggests

that this approach has the potential to address the selectivity of chemokines for different receptors.

^{1}H-detected fast MAS solid-state NMR enabled the characterization of IL-8 (1-66)-CXCR1 complexes in phospholipid bilayers, providing insight into the molecular events associated with the first step of the CXCR1-mediated signaling cascade. These studies also served to demonstrate that site-specific incorporation of metal-chelating unnatural amino acid HQA into CXCR1 in combination with high-resolution ^{1}H-detected fast MAS solid-state NMR provide site-specific PRE-derived intermolecular distance restraints in ligand-receptor complex. Thus, solid-state NMR can provide measurements of both intra- and intermolecular distances along with the identification of residues directly involved in binding to specific sites on both the ligand and receptor. Demonstrated here on ligand binding to a GPCR, the approach has the potential to be applicable to a broad range of protein complexes in membranes and other biological supramolecular assemblies.

Chapter 4, in full, is a reprint of the material as it appears in Biophysical Journal, “Interaction of Monomeric Interleukin-8 with CXCR1 Mapped by Proton-detected Fast MAS Solid-state NMR and Intermolecular Paramagnetic Relaxation Enhancement” by Park, S. H., Berkamp, S., Radoicic, J., De Angelis, A. A., and Opella, S. J., 2017. The dissertation author was the third author of this paper.

Chapter 5. Macrodiscs Comprising SMALPs for Oriented Sample Solid-State NMR Spectroscopy of Membrane Proteins

5.1 Abstract

Macrodiscs, which are magnetically alignable lipid bilayer discs with diameters >30 nm, were obtained by solubilizing protein-containing liposomes with styrene-maleic acid (SMA) copolymers. Macrodiscs provide a detergent-free phospholipid bilayer environment for biophysical and functional studies of membrane proteins under physiological conditions. The narrow resonance linewidths observed from membrane proteins in SMA macrodiscs advances structure determination by oriented sample solid-state NMR spectroscopy.

5.2 Introduction

Styrene-maleic acid (SMA) macrodiscs advance structure determination of membrane proteins by providing a detergent-free bilayer environment that affords superior alignment in the magnetic field of an NMR spectrometer. Membrane proteins are high profile targets for structure determination. They account for ~30% of all expressed genes and their locations within the membrane barriers of cells, viruses and organelles endow them with unique biological functions, including as receptors, ion channels, and transporters. The need for new techniques for structure determination of membrane proteins is evident in the limited number of structures that have been determined. Moreover, with few exceptions, the accuracy of the available structures is compromised

by the experimental requirements of current methods, e.g., truncated or modified protein sequences, detergent-containing samples, or non-native conditions. Notably, NMR spectroscopy has the potential to be a general method for determining the structures of membrane proteins under near-native conditions. Although earlier studies employed a variety of micelle, bicelle, and amphipol samples, current NMR approaches reflect the availability of protein-containing phospholipid bilayer samples, such as unoriented liposomes studied by magic angle spinning solid-state NMR [220, 407], rapidly reorienting nanodiscs studied by solution NMR [408-409], and aligned bilayers studied by oriented sample (OS) solid-state NMR [109, 126, 380, 410].

The modern-era of bilayer samples for membrane proteins started with the development of nanodiscs by Sligar and coworkers [22]. They introduced a class of amphipathic helical proteins to the role of membrane scaffold proteins (MSP), which self-assemble as a circular "belt" around phospholipids in a bilayer to form nanodiscs with ~10 nm diameter and are suitable for chemical, physical, and functional studies of membrane proteins [24]. Moreover, since protein-containing nanodiscs are a chemically defined system, many parameters can be manipulated, such as lipid composition, diameter, and lipid-to-protein ratio.

Styrene – Maleic Acid (SMA) is an amphipathic copolymer with alternating styrene (hydrophobic) and maleic acid (hydrophilic) moieties that spontaneously solubilizes either native (biological) or synthetic membranes by forming circular boundaries of defined diameter around lipid bilayers [35, 411-412] in a manner similar to a 14-residue amphipathic

polypeptide (14A) [25]. Originally, SMA polymers were used as drug conjugates in cancer therapy [413-414] and once it was established that they interact with lipid bilayers to form discoidal structures they were used as an efficient drug delivery system for hydrophobic molecules [415]. It is thought that the styrene groups of the SMA polymer interact with the lipid head groups and the phenyl groups with the lipid acyl chains [411, 416] to form discs. Due to the pKa's of its two carboxyl groups (pKa ~6 and ~10) [417-418], the SMA polymer is very sensitive to pH; In the charged form, SMA is extended, but as the pH is lowered, it becomes neutral, aggregates, and precipitates [419]. The pH range at which the polymer is stable is determined by the styrene:maleic acid ratio, with lower ratios (i.e. 1:1) being more stable at a broader range of pH values [418]. The SMA polymers are also sensitive to divalent metal cations, especially Mg^{2+} [420-421], however further development has led to similar polymers with greater pH stability and decreased susceptibility to divalent metal cations, among other favorable properties [422-424]. The SMALP discs have been reported to have a circular cross section [416], in contrast to membrane scaffold protein (MSP) discs, which have an elliptical cross-section [425]; this may be a result of the greater flexibility of the polymer chains when wrapping around the lipid bilayer [426]. It has also been found that most efficient membrane solublilisation is achieved with either the 2:1 or 3:1 SMA [421]. SMA will solubilize almost any lipid composition and chain length [418] however the efficiency of SMA solubilisation is increased when lipid chain lengths are shorter and the temperature is increased, especially above the melting temperature (Tm) of the lipid [412].

Following the initial incorporation of PagP and bacteriorhodopsin into SMA nanodiscs [35], a variety of membrane proteins have been studied using similar

preparations [411, 427-428]; Membrane proteins have been extracted from their native membranes using SMALPs as well [429-441]. Membrane proteins embedded in SMALPs are functional and are more stable than proteins solubilized in detergents [421, 427, 430-431, 433]. As a result, SMA polymers offer a detergent-free route to the isolation and purification of membrane proteins. They enable the preparation of samples from purified proteins in liposomes with specified lipid compositions, or from native membranes, and are applicable to a wide variety of biophysical and structural studies. Previously, we described the use of 14A to form both small (nano, ~10 nm diameter) and large (macro, ~30 nm diameter) discs by varying the lipid-to-peptide ratio [25]. In contrast to nanodiscs, macrodiscs are large enough to "immobilize" the proteins on NMR timescales and are magnetically alignable. Higher lipid-to-SMA polymer ratios result in the formation of larger diameter discs [442-445].

Here, we describe the formation of macrodiscs from three different, unmodified, SMA polymers and phospholipids. These discs have favorable properties for OS solid-state NMR spectroscopy, which we demonstrate with one- and two- dimensional spectra that display the narrowest linewidths observed to-date from an aligned protein sample. Highly homogeneous and translucent macrodiscs are obtained by solubilizing liposomes with polymers having average styrene:maleic acid monomer ratios of 1.4:1, 2:1, and 3:1, with molar ratios of lipids to SMA polymers (q_d) of 7.4, 27.7, and 49.1, respectively. Each q_d was optimized by titration of the polymers to the liposomes. The longer the length of the polymer (SMA(3:1) > SMA(2:1) > SMA(1.4:1)), the smaller the amount needed to form macrodiscs. Nanodiscs typically form immediately upon addition of amphipathic peptides

or SMA polymers to liposomes, whereas SMA macrodiscs require many hours to form (Fig. 5.1).

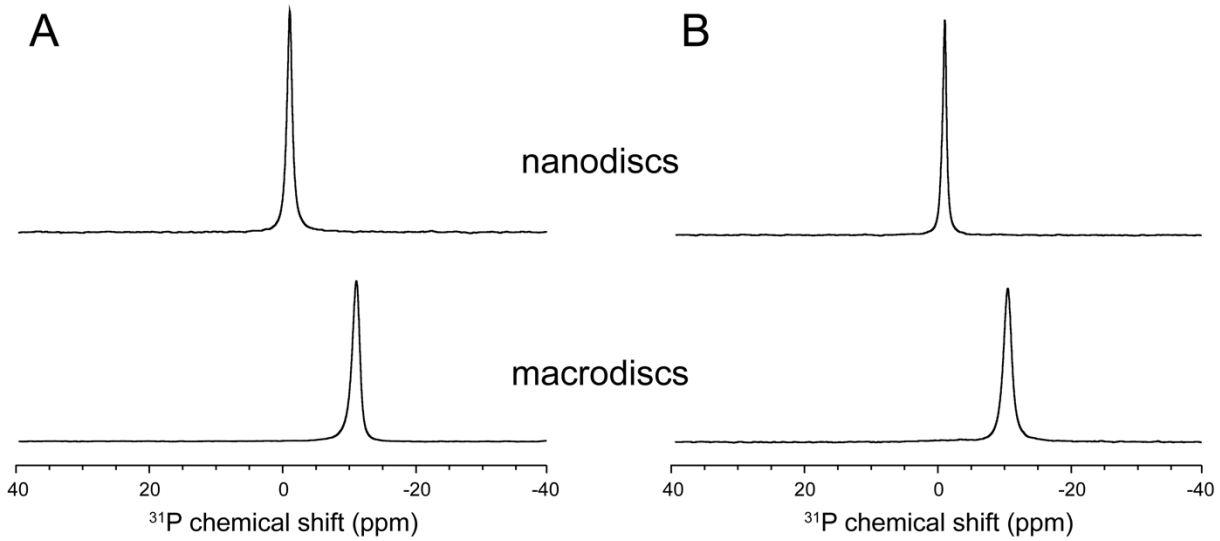

Figure 5.1. ^{31}P chemical shift NMR spectra of DMPC nanodiscs and DMPC macrodiscs at a resonance frequency of 283 MHz with ^{1}H decoupling at 45^{o}C. (A) The weight ratios of DMPC to SMA(1.4:1) were 0.2 and 1.0 for nanodiscs and macrodiscs, respectively. (B) The weight ratios of DMPC to SMA(3:1) were 0.8 and 3.33 for nanodiscs and macrodiscs, respectively.

5.3 Methods and Materials

5.3.1 Sample preparation

1,2-Dimyristoyl-sn-glycero-3-phosphocholine (DMPC) and 1,2-Dimyristoyl-sn-glycero-3-phosphorylglycerol sodium salt (DMPG) were purchased from Anatrace (www.anatrace.com). Triton X-100 was purchased from Sigma-Aldrich (www.sigmaaldrich.com). The 14-residue amphipathic peptide (14A) (>98% purity, Ac-DYLKAFYDKLKEAF-NH_2) was purchased from NeoBioLab (neobiolab.com). Pre-hydrolyzed styrene-maleic acid (SMA) polymers were provided by Polyscope

(www.polyscope.eu). Xiran SL 40005 P20, SL 30010 P20, and SL 25010 P20 correspond to SMA(1.4:1), SMA(2:1), and SMA(3:1), respectively. Average molecular weights (M_w) of SMA(1.4:1), SMA(2:1), and SMA(3:1) were 5 kDa, 7.5 kDa, and 10 kDa, respectively.

The sample preparation of Triton X-100 bicelles [446] and 14A macrodiscs [25] have been described previously. Briefly, 20 mg of dried DMPC film was solubilized with 3.8 mg of Triton X-100 or 3.9 mg of 14A in 200 uL of 50 mM HEPES buffer at pH 8. The molar ratios of DMPC to Triton X-100 and 14A were 5 and 13.3, respectively. The concentration of lipids was 10% (w/v).

SMA macrodiscs were prepared by adding a concentrated solution (~100 mg/mL) of SMA to DMPC liposomes in 50 mM HEPES, pH 8 for a final sample volume of 200 uL. The samples were subjected to heat (42^{o}C) and vortex cycles until the lipids were completely re-suspended, following which they were left to incubate at 25^{o}C overnight. If necessary, the samples were subjected to additional heat (42^{o}C), vortex, and chill (on ice) cycles until they became translucent and homogeneous. The molar ratios of DMPC to SMA(1.4:1), SMA(2:1), and SMA(3:1) were 7.4, 27.7 and 49.1, respectively. The corresponding weight ratios of DMPC to SMA(1.4:1), SMA(2:1), and SMA(3:1) were 1, 2.5, and 3.33, respectively. The concentration of lipids was 10% (w/v).

Uniformly ^{15}N-labeled Pf1 bacteriophage was prepared as described previously [447] and the coat protein was purified and reconstituted into DMPC and DMPG mixtures at a weight ratio of 1:1 to yield proteoliposomes. 2 mg of labeled protein was reconstituted into 40 mg of lipid mixtures in a final lipid concentration of 10 mg/mL in 50 mM HEPES, pH 8.

400 uL of SMA (2:1) or SMA(3:1) polymer (30 mg/mL) was added to the proteoliposome suspension and incubated overnight at 25^{o}C with gentle stirring. Upon formation of Pf1 coat protein -containing SMA macrodiscs, the white dispersion of proteoliposomes become a translucent solution. The dilute solution of Pf1 coat protein -containing macrodiscs was concentrated (Eppendorf 5430 R centrifuge) using a centrifugal filter (Amicon Ultra-15, 50K) at 25^{o}C and 7000 x g for 2-3 hours. The sample volume was monitored every 30 min until the lipid concentration was 16% (w/v). $YbCl_3$ or $TmCl_3$ were added to "flip" the macrodisc samples from perpendicular to parallel orientations at a final concentration of 4-6 mM.

5.3.2 NMR Spectroscopy

^{31}P NMR experiments were performed on a Bruker Avance spectrometer with 16.4 Tesla field and a homebuilt ^{1}H/^{31}P double-resonance probe [448]. The corresponding frequency for ^{31}P nuclei is 243 MHz. Approximately 170 uL of each sample was placed in a 5 mm outer diameter 15 mm long flat-bottomed NMR tube (newera-spectro.com). The samples were equilibrated for at least 10 min at each temperature in the range 5^{o}C to 50^{o}C prior to the measurements. The ^{31}P NMR chemical shift spectra were obtained by direct excitation with a single pulse with a radio frequency field strength of 36 kHz; a 15 ms acquisition time and 3 s recycle delay were used. 64 transients were signal averaged for each spectrum. Continuous wave ^{1}H decoupling was applied during data acquisition at a radiofrequency field strength of 21 kHz. ^{31}P chemical shifts were externally referenced to phosphoric acid solution at 0 ppm.

The solid-state NMR experiments on protein-containing samples were performed at 40°C on a spectrometer with a ^{1}H resonance frequency of 900 MHz. The Bruker Avance III HD console and magnet were interfaced to a home-built ^{1}H/^{15}N double-resonance probe. The one-dimensional ^{15}N chemical shift spectra were obtained using cross-polarization with a contact time of 1 ms, a recycle delay of 6 s, and an acquisition time of 25-30 ms. The ^{1}H and ^{15}N radiofrequency field strengths were 45 kHz. 4096 transients were accumulated. The FID was zero-filled to 16K data points; no apodization was applied prior to Fourier transformation. The two-dimensional PISEMA experiment was performed as described previously [114]. The number of t1 increments was 80-128. Signal averaging was performed with 64 transients for each t1 increment. The NMR data were processed using Bruker Topspin 4.0.2 and NMRPipe/NMRDraw [449]. The data were zero-filled to form a final 2048 x 2048 matrix. ^{15}N chemical shifts were externally referenced to ^{15}N labeled ammonium sulfate powder at 26.8 ppm.

5.4 Results and Discussion

In Fig. 5.2 the alignment and phase behavior of three SMA macrodisc samples are compared to those of samples of high *q* DMPC/Triton X-100 bicelles [446] and DMPC/14A macrodiscs [25]. The ^{31}P NMR spectra of bicelles (Fig. 5.2A), 14A macrodiscs (Fig. 5.2B), and three different SMA macrodiscs (Fig. 5.2C-E) demonstrate that the DMPC bilayers are well aligned between 30°C and 50°C with their normals perpendicular to the direction of the applied magnetic field because they display a single resonance with a chemical shift of -13 ± 2 ppm. However, differences are observed among the samples at temperatures below the gel to liquid crystal phase transition of DMPC. The ^{31}P chemical

shift of DMPC in SMA macrodiscs does not change between 20°C and 50°C for SMA(2:1) macrodiscs, and between 25°C and 50°C for SMA(1.4:1) and SMA(3:1) macrodiscs. This indicates that their magnetic alignments are stable over a wide range of temperatures. Triton X-100 bicelles exist in an isotropic phase below 10°C. The 14A macrodiscs exist in an isotropic phase between 5°C and 15°C. Notably, SMA macrodiscs display no evidence of an isotropic phase and exist as aligned discs above 25°C.

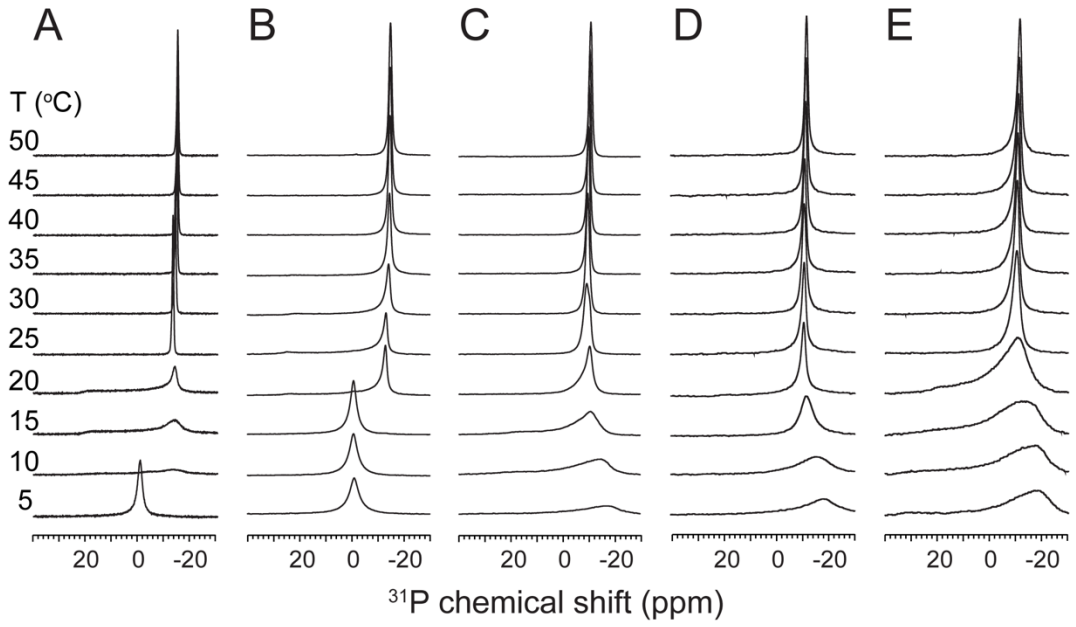

Figure 5.2. ^{31}P chemical shift NMR spectra of DMPC bilayers as a function of temperature at a resonance frequency of 283 MHz with ^{1}H decoupling. (A) Bicelles consisting of DMPC and Triton X-100 with q = 5. (B) Macrodiscs consisting of DMPC and 14A at a molar ratio of 13.3. (C-D) Macrodiscs consisting of DMPC and three different SMA polymers. (C) SMA(1.4:1) with q_d = 7.4. (D) SMA(2:1) with q_d = 27.7. (E) SMA(3:1) with q_d = 49.1. The lipid concentration in all samples is 10% (w/v).

The protein containing SMA macrodiscs were prepared by solubilizing the proteoliposome with SMA polymer. The ^{15}N amide backbone resonances of Pf1 coat protein in SMA macrodiscs (Fig. 5.3A and Fig. 5.4A) have linewidths as narrow as 0.3

ppm, which provides better spectral resolution than previously observed in Triton X-100 bicelles [446] (Fig. 5.4B) and 14A macrodiscs [25]. The chemical shift differences between the spectra of Pf1 coat protein in SMA macrodiscs and in Triton X-100 bicelles are due mainly to the larger order parameter of the SMA macrodiscs (Figs. 5.4 and 5.5). Resonances from residues in the transmembrane helix (60 ppm – 100 ppm) as well as those from residues in the adjacent loop region (110 ppm – 140 ppm) have similar, uniform line shapes, suggesting that the protein adopts a single conformation in SMA macrodiscs.

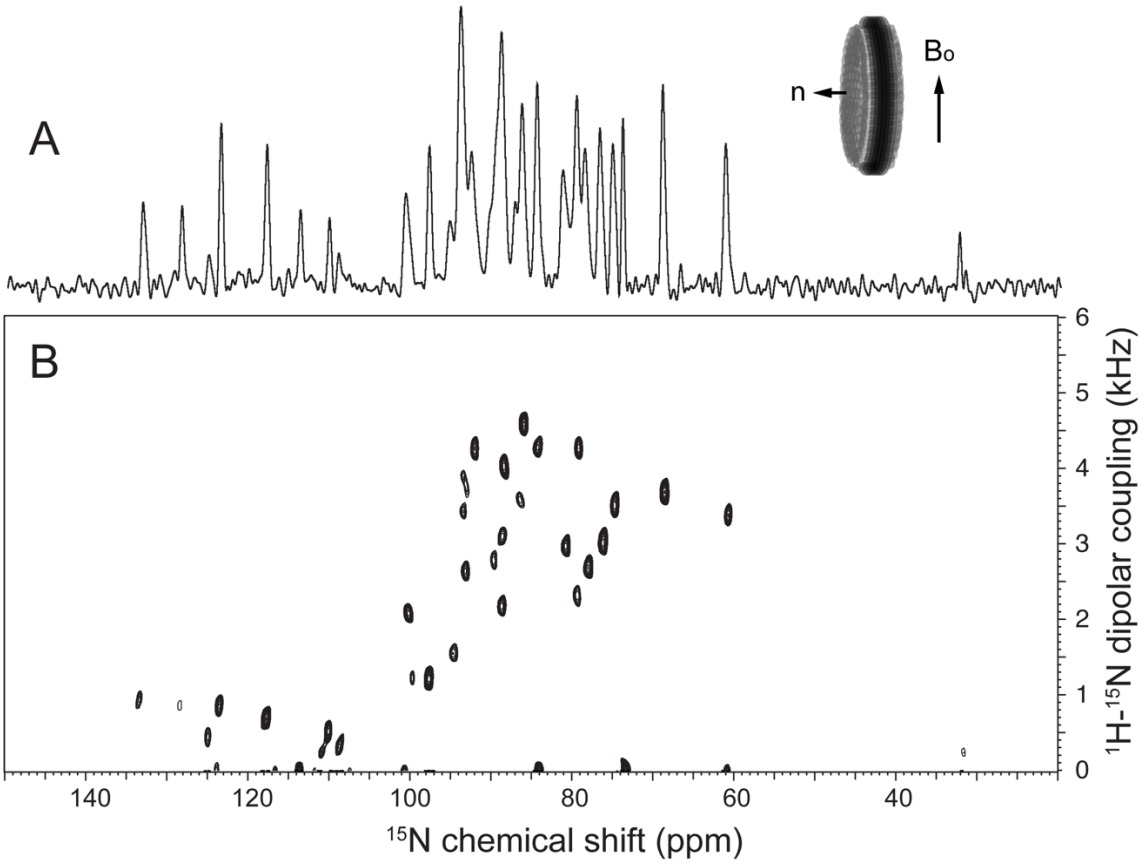

Figure 5.3. Solid-state NMR spectra of the membrane-bound form of uniformly ^{15}N labeled Pf1 coat protein in macrodiscs consisting of DMPC/DMPG (1:1) and SMA(3:1) with q_d = 49.1. The samples are aligned with their bilayer normals (n) perpendicular to the direction of the 21.1 T magnetic field as illustrated in the cartoon. (A) One-dimensional ^{15}N chemical shift spectrum obtained by cross-polarization with a 25 ms acquisition time. (B) Two-dimensional ^{1}H-^{15}N dipolar coupling/^{15}N chemical shift spectrum obtained using PISEMA with 80 t1 increments. Both spectra were obtained at 40 ^{o}C with 45.5 kHz ^{1}H irradiations and 1 ms cross-polarization mix times.

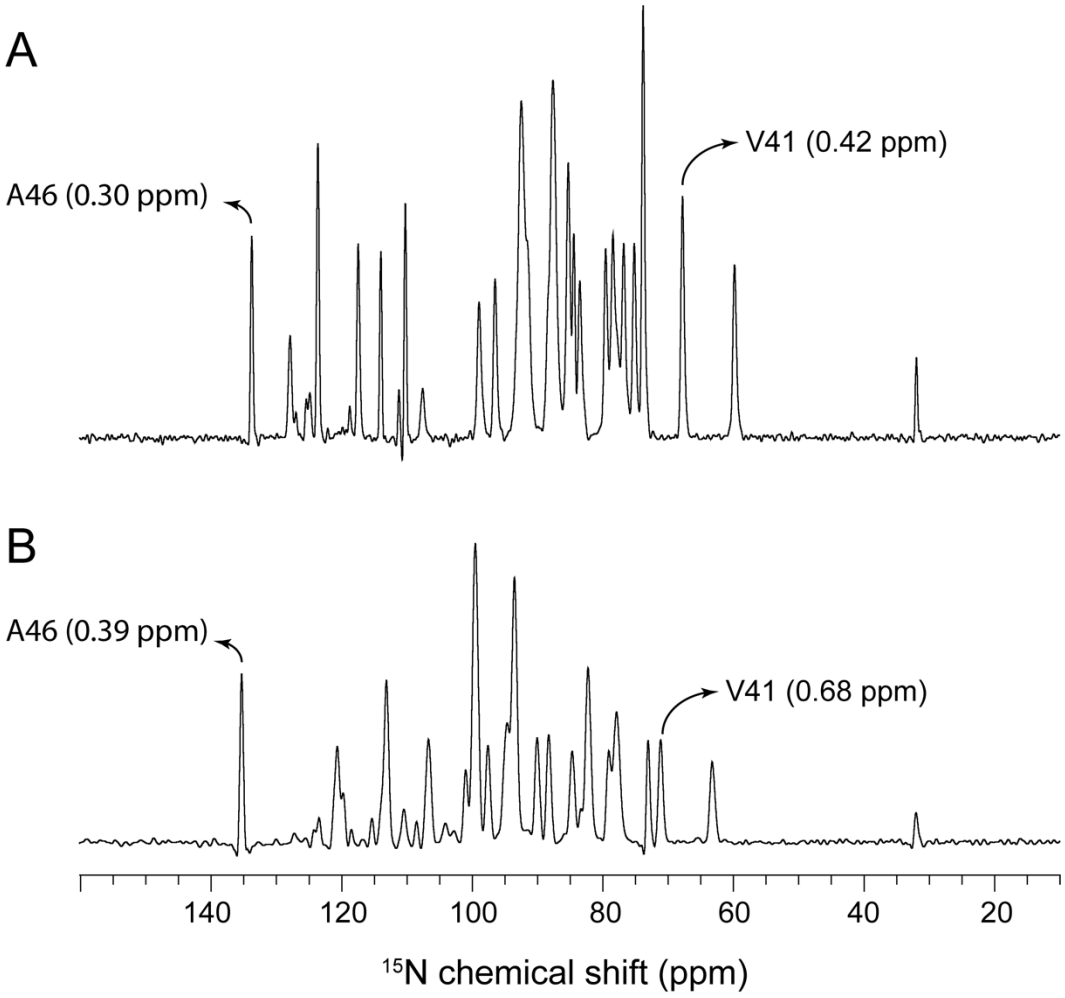

Figure 5.4. Comparison of solid-state ^{15}N chemical shift NMR spectra of the membrane-bound form of uniformly ^{15}N labeled Pf1 coat protein in oriented lipid bilayers with their bilayer normals (n) perpendicular to the direction of the 21.1 T magnetic field at 40°C. (A) Macrodisc sample consisting of DMPC/DMPG(1:1, w/w) and SMA(2:1) with $q_d = 27.7$. (B) Bicelle sample consisting of DMPC:DMPG(1:1, w/w) and Triton X-100 with q = 5. The linewidths of V41 and A46 are indicated.

The two-dimensional $^{1}H/^{15}N$ polarization inversion spin exchange at the magic angle (PISEMA) [114] spectrum shown in Fig. 5.3B is fully resolved with narrow linewidths in both the ^{15}N chemical shift and ^{1}H-^{15}N dipolar coupling frequency dimensions. The orientationally-dependent frequencies of the resonances provide the angular constraints

used in protein structure calculations. We note that two sets of signals (G23/I26 and G24/G28) that overlap in the equivalent spectrum of the protein in Triton X-100 bicelles [25] (Fig. 5.5B) are fully resolved in the spectra in Fig. 5.3B and Fig. 5.5A due to the narrower linewidths observed in SMA macrodiscs.

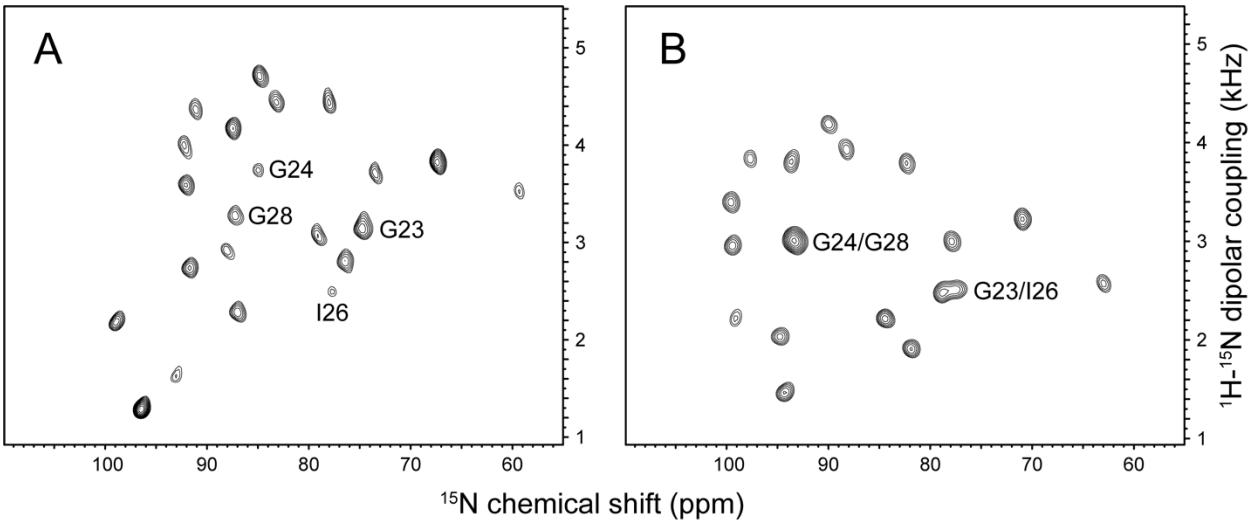

Figure 5.5 Comparison of solid-state ^{1}H-^{15}N dipolar coupling/^{15}N chemical shift spectra of the membrane-bound form of uniformly ^{15}N labeled Pf1 coat protein in oriented lipid bilayers with their bilayer normals (n) perpendicular to the direction of the 21.1 T magnetic field. (A) Macrodisc sample consisting of DMPC/DMPG(1:1, w/w) and SMA(2:1) with q_d = 27.7. (B) Bicelle sample consisting of DMPC:DMPG(1:1, w/w) and Triton X-100 with q = 5. Both spectra were obtained using PISEMA with 128 t1 increments at 40 ^{o}C with 45.5 kHz ^{1}H irradiations and 1 ms cross-polarization mix times. Resonances of G23, G24, I26, and G28 are indicated for comparison.

The lipid bilayer normal of magnetically aligned bicelles and 14A macrodiscs are generally perpendicular to the direction of the magnetic field, as illustrated by the cartoon in Fig. 5.3. However, it is possible to “flip” the normal to the parallel direction with the

addition of lanthanides [31]. This is also the case for SMA macrodiscs, as shown by the spectra of the protein and lipids in Fig. 5.6, which were obtained following the addition of $TmCl_3$ or $YbCl_3$. The total span of the ^{15}N chemical shift frequencies is increased to ~170 ppm (Fig. 5.6A) and that of the ^{31}P chemical shift frequencies to 18.5 ppm (Fig. 5.6B), which is consistent with a 90^o change of the direction of alignment of the SMA macrodiscs. Quantitative titration of $YbCl_3$ to SMA macrodiscs did not yield spectra with any ^{31}P chemical shift values other than those observed in Fig. 5.2E and Fig. 5.6B., thus we find no evidence of intermediate orientations of the bilayer normal in SMA macrodiscs (Fig. 5.7).

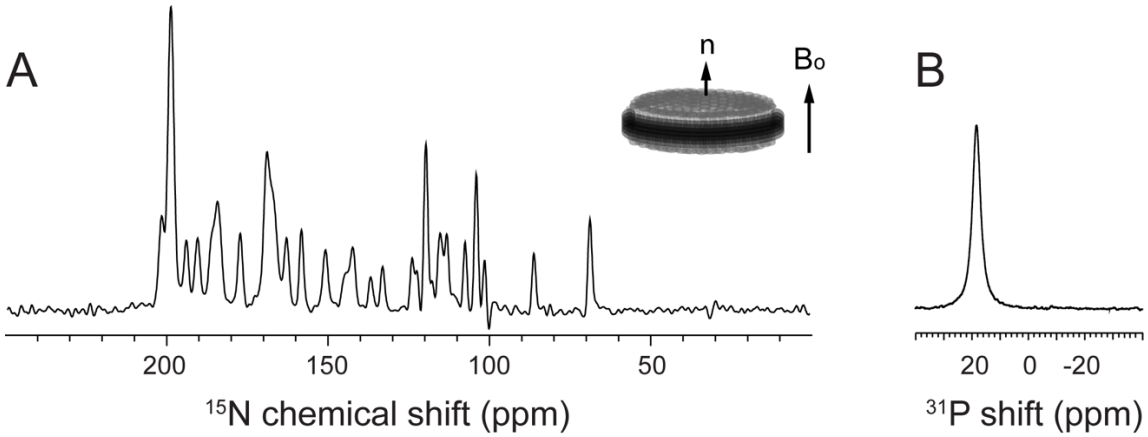

Figure 5.6. (A) ^{15}N chemical shift NMR spectrum of "flipped" Pf1 coat protein in SMA(3:1) macrodiscs was obtained by cross-polarization after addition of 5 mM $TmCl_3$ to the sample used in Fig.2. The membrane normal is parallel to the field, as illustrated in the cartoon. (B) ^{31}P chemical shift NMR spectrum of DMPC:SMA(3:1) macrodiscs in the presence of 4 mM $YbCl_3$. (Also shown in Fig. 5.7).

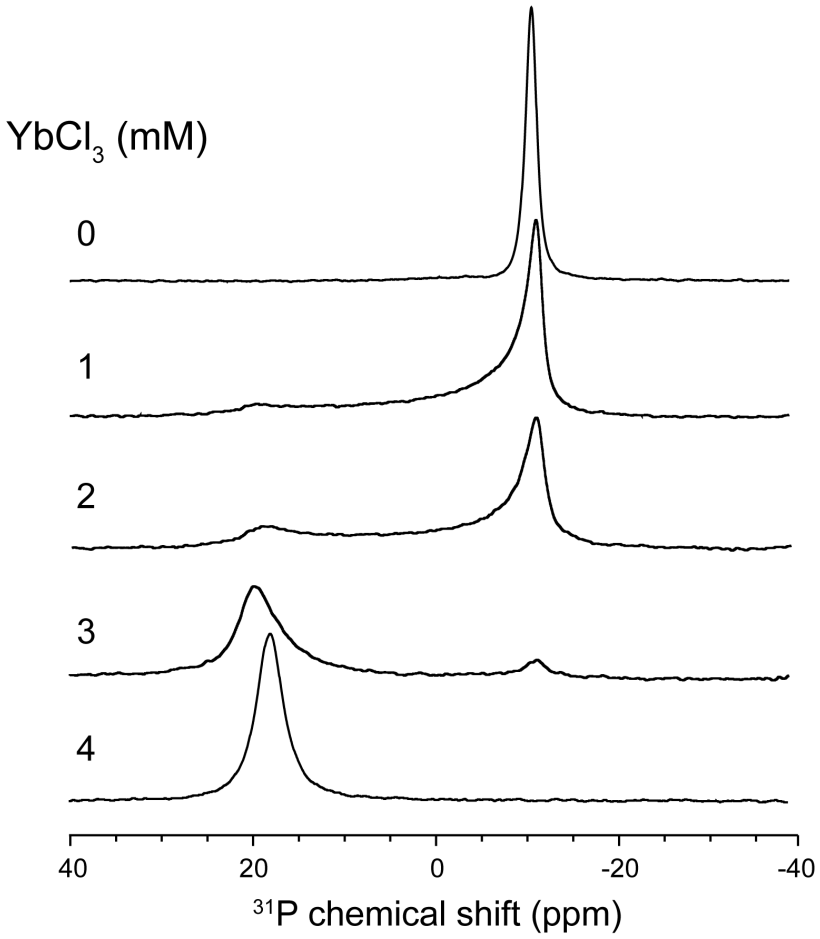

Figure 5.7. ^{31}P chemical shift NMR spectra of DMPC:SMA(3:1) macrodiscs (q_d = 49.1) as a function of $YbCl_3$ concentration at a resonance frequency of 283 MHz with ^{1}H decoupling at 45°C.

SMA macrodiscs provide a stable lipid bilayer environment that is well suited for biophysical and functional studies of membrane proteins. They can be prepared using a variety of phospholipids and a number of different SMA polymers. They are well aligned over a broad range of temperatures and their orientation can be shifted from perpendicular to parallel with the addition of lanthanides. Moreover, they are applicable to membrane proteins and binding partners that are sensitive to detergents. SMA

macrodiscs are particularly well suited for immobilizing and aligning membrane proteins for OS solid-state NMR structure determination. Notably, in these samples the proteins are in a near-native environment under physiological conditions, as required to ensure that their structures represent the functional conformations of the proteins.

Chapter 5, in part, is a reprint of the material as it appears in Biophysical Journal, “Macrodiscs Comprised on Styrene-Maleic Acid Lipid Particles (SMALPs) for Oriented Sample Solid State NMR Spectroscopy of Membrane Proteins” by Radoicic, J., Park, S.H., and Opella, S.J., 2018. The dissertation author was the co-first author of this paper.

Chapter 6. Conclusion

CXCR1 is a class-A rhodopsin-like GPCR which binds to the chemokine Interleukin-8 (IL-8) and activates the G-protein Gi signaling cascade. IL-8 is released as a response to inflammatory stimuli by multiple cell types [139, 142] and it has been shown that IL-8 stimulates self-renewal of breast cancer stem cells [223], making CXCR1 a very attractive drug target [224]. As such, the study of this system is essential. The use of solution and solid-state NMR spectroscopy has allowed for the study of this complex system in near-native membrane environments under physiological conditions.

We have used ^{1}H-detected magic angle spinning (MAS) solid-state NMR to probe the interaction of monomeric IL-8(1-66) and various CXCR1 constructs. INEPT and CP experiments were used to analyze the mobile and immobile regions, respectively, of IL-8(1-66) upon interaction with the receptor. The interactions of the chemokine with the full-length receptor (WT-CXCR1) as well and an N-terminally truncated construct (NT-CXCR1) help to map out the two binding sites. When bound to WT-CXCR1, most of the amide backbone resonances of IL-8 become immobilized and can be observed in the CP spectra, whereas only five backbone residues are observed in the INEPT. In contrast, upon binding to NT-CXCR1, only 11 amide backbone signals (located in the 30s and 40s loops and the β-3 strand) can be detected in the CP spectrum and 18 signals in the INEPT. The chemical shift perturbations of the IL-8(1-66)-NT-CXCR1 interaction in the CP spectra are noticeably smaller than those observed for interaction with WT-CXCR1.

Taken together, these data are indicative of the differences in interaction of the chemokine with the receptor at the two binding sites and enable the characterization of various IL-8(1-66)-CXCR1 complexes.

For our studies on G-proteins we have focused on the alpha subunit as it is well established that this subunit is primarily involved in interaction with the GPCR and there is much literature showing that the extreme C-terminus of the $G\alpha$ subunit is one of the key interaction sites with the receptor. Based on this we made three constructs of the G protein: a CXCR1_$G\alpha_{i22}$ fusion, the full length, unmodified $G\alpha_i$ subunit, and a $G\alpha_{i22}$ peptide corresponding to the last 22 residues of $G\alpha_i$. ^{1}H-^{15}N HSQC spectra of CXCR1_$G\alpha_{i22}$ show that a majority of C-terminal CXCR1 residues become broadened beyond detection in the presence of the G-protein peptide. We also do not observe any additional signals stemming from the attached $G\alpha_{i22}$, further confirming the interaction. INEPT solid-state NMR spectra also showed similar changes in the receptor. Although initially sample purification and stability was an issue for the full-length $G\alpha_{i1}$ and $G\alpha_{i22}$ peptide constructs, high resolution HSQC spectra of both constructs have been recorded showing the proteins to be well folded and stable. Interaction studies with the receptor as well as sample optimization are currently in progress.

Long-range distance restraints have many benefits including the improvement of protein structure resolution, defining the overall folding topology, and identifying residues in the binding sites. A common approach to obtaining these measurements is the use of

paramagnetic relaxation enhancement (PRE) experiments. Although many other methods of incorporation of paramagnetic tags into proteins are available, unnatural amino acid (UAA) incorporation of HQA is the least disruptive to protein structure and function, as it does not require any chemical modifications and the UAA is similar in size and structure to that of amino acids. We have showed, for the first time, that an unnatural amino acid can be incorporated into a membrane protein, in both the loops and termini as well as in the transmembrane portion of the protein without disrupting the integrity of the membrane protein. We have obtained various site-specific intermolecular PREs which have provided specific distance-restraints for the IL8(1-66)-CXCR1 Interaction in both solution NMR and fast-MAS solid-state NMR. Distance restraints for IL-8(1-66) complexed with 1TM-CXCR1, NT-CXCR1, and WT-CXCR1 have been obtained and are being used to aid in structure determination of the complexes.

A common issue when working with membrane proteins is sample preparation and stability. The environment in which membrane proteins are studied is crucial – looking at the same protein in different environments can lead to significant differences in the structure, conformation, and orientation of the protein. [450-452]; the use of detergents can be especially detrimental. We have found that the SMA macrodisc system provides a stable, detergent free environment for the study of membrane proteins using NMR spectroscopy. Integral membrane proteins can be inserted into the central bilayer portion of these discs, and the protein-disc system is soluble and very stable in aqueous solution. The discs can be prepared using a variety of lipids, will align in the presence of a magnetic field, and their normals can be ‘flipped’ from perpendicular to parallel in the presence of

lanthanide ions, making them ideal candidates for the immobilization and study of membrane proteins using oriented-sample solid-state NMR spectroscopy.

Bibliography

1. Cao, J.; Burke, J. E.; Dennis, E. A., Using hydrogen/deuterium exchange mass spectrometry to define the specific interactions of the phospholipase A2 superfamily with lipid substrates, inhibitors, and membranes. *J Biol Chem* **2013,** *288* (3), 1806-13.

2. Wallin, E.; von Heijne, G., Genome-wide analysis of integral membrane proteins from eubacterial, archaean, and eukaryotic organisms. *Protein Sci* **1998,** *7* (4), 1029-38.

3. Sadowski, P. G.; Groen, A. J.; Dupree, P.; Lilley, K. S., Sub-cellular localization of membrane proteins. *Proteomics* **2008,** *8* (19), 3991-4011.

4. Akabas, M. H., Cystic fibrosis transmembrane conductance regulator. Structure and function of an epithelial chloride channel. *J Biol Chem* **2000,** *275* (6), 3729-32.

5. Oldham, W. M.; Hamm, H. E., Heterotrimeric G protein activation by G-protein-coupled receptors. *Nat Rev Mol Cell Biol* **2008,** *9* (1), 60-71.

6. Opella, S. J.; Marassi, F. M., Applications of NMR to membrane proteins. *Arch Biochem Biophys* **2017,** *628*, 92-101.

7. Cross, T. A.; Opella, S. J., NMR of fd coat protein. *J Supramol Struct* **1979,** *11* (2), 139-45.

8. Cross, T. A.; Opella, S. J., Structural properties of fd coat protein in sodium dodecyl sulfate micelles. *Biochem Biophys Res Commun* **1980,** *92*, 478-84.

9. Bosch, C.; Brown, L. R.; Wuthrich, K., Physicochemical characterization of glucagon-containing lipid micelles. *Biochim Biophys Acta* **1980,** *603*, 298-312.

10. Lauterwein, J.; Bosch, C.; Brown, L. R.; Wuthrich, K., Physicochemical studies of the protein-lipid interactions in melittin-containing micelles. *Biochim Biophys Acta* **1979,** *556* (2), 244-64.

11. Bosch, C.; Brown, L. R.; Wuthrich, K., Physicochemical characterization of glucagon-containing lipid micelles. *Biochim Biophys Acta* **1980,** *603* (2), 298-312.

12. Page, R. C.; Moore, J. D.; Nguyen, H. B.; Sharma, M.; Chase, R.; Gao, F. P.; Mobley, C. K.; Sanders, C. R.; Ma, L.; Sonnichsen, F. D.; Lee, S.; Howell, S. C.; Opella, S. J.; Cross, T. A., Comprehensive evaluation of solution nuclear magnetic resonance spectroscopy sample preparation for helical integral membrane proteins. *J Struct Funct Genomics* **2006,** *7* (1), 51-64.

13. Sanders, C. R.; Oxenoid, K., Customizing model membranes and samples for NMR spectroscopic studies of complex membrane proteins. *Biochimica et Biophysica Acta* **2000,** *1508* (1-2), 129-45.

14. Vinogradova, O.; Sonnichsen, F.; Sanders, C. R., 2nd, On choosing a detergent for solution NMR studies of membrane proteins. *J Biomol NMR* **1998,** *11* (4), 381-6.

15. Poget, S. F.; Girvin, M. E., Solution NMR of membrane proteins in bilayer mimics: small is beautiful, but sometimes bigger is better. *Biochim Biophys Acta* **2007,** *1768* (12), 3098-106.

16. Kruger-Koplin, R. D.; Sorgen, P. L.; Druieger-Koplin, S. T.; Rivera-Torres, I. O.; Cahill, S. M.; Krulwich, T. A.; Girvin, M. E., An evaluation of detergents for NMR structural studies of membrane proteins. *J Biomol NMR* **2004,** *28*, 1980-1987.

17. Judge, P. J.; Watts, A., Recent contributions from solid-state NMR to the understanding of membrane protein structure and function. *Curr Opin Chem Biol* **2011,** *15* (5), 690-5.

18. Durr, H. N. U.; Soong, R.; Ramamoorthy, A., When detergent meets bilayer: birth and coming of age of lipid bicelles. *Prog NMR Spec* **2013,** *69*, 1-22.

19. Etzkorn, M.; Zoonens, M.; Catoire, L. J.; Popot, J. L.; Hiller, S., How amphipols embed membrane proteins: global solvent accessibility and interaction with a flexible protein terminus. *J Membr Biol* **2014,** *247* (9-10), 965-70.

20. Tifrea, D. F.; Sun, G.; Pal, S.; Zardeneta, G.; Cocco, M. J.; Popot, J. L.; de la Maza, L. M., Amphipols stabilize the Chlamydia major outer membrane protein and enhance its protective ability as a vaccine. *Vaccine* **2011,** *29* (28), 4623-31.

21. Popot, J. L.; Althoff, T.; Bagnard, D.; Baneres, J. L.; Bazzacco, P.; Billon-Denis, E.; Catoire, L. J.; Champeil, P.; Charvolin, D.; Cocco, M. J.; Cremel, G.; Dahmane, T.; de la Maza, L. M.; Ebel, C.; Gabel, F.; Giusti, F.; Gohon, Y.; Goormaghtigh, E.; Guittet, E.; Kleinschmidt, J. H.; Kuhlbrandt, W.; Le Bon, C.; Martinez, K. L.; Picard, M.; Pucci, B.; Sachs, J. N.; Tribet, C.; van Heijenoort, C.; Wien, F.; Zito, F.; Zoonens, M., Amphipols from A to Z. *Annu Rev Biophys* **2011,** *40*, 379-408.

22. Bayburt, T. H.; Sligar, S. G., Single-molecule height measurements on microsomal cytochrome P450 in nanometer-scale phospholipid bilayer disks. *Proc Natl Acad Sci U S A* **2002,** *99* (10), 6725-30.

23. Denisov, I. G.; Grinkova, Y. V.; Lazarides, A. A.; Sligar, S. G., Directed self-assembly of monodisperse phospholipid bilayer Nanodiscs with controlled size. *J Am Chem Soc* **2004,** *126* (11), 3477-87.

24. Denisov, I. G.; Sligar, S. G., Nanodiscs in Membrane Biochemistry and Biophysics. *Chem Rev* **2017,** *117* (6), 4669-4713.

25. Park, S. H.; Berkamp, S.; Cook, G. A.; Chan, M. K.; Viadiu, H.; Opella, S. J., Nanodiscs versus macrodiscs for NMR of membrane proteins. *Biochemistry* **2011,** *50* (42), 8983-5.

26. Radoicic, J.; Park, S. H.; Opella, S. J., Macrodiscs Comprising SMALPs for Oriented Sample Solid-State NMR Spectroscopy of Membrane Proteins. *Biophys J* **2018**.

27. Opella, S. J.; Nevzorov, A.; Mesleh, M. F.; Marassi, F. M., Structure determination of membrane proteins by NMR spectroscopy. *Biochem Cell Biol* **2002,** *80* (5), 597-604.

28. Nietlispach, D.; Gautier, A., Solution NMR studies of polytopic alpha-helical membrane proteins. *Curr Opin Struc Biol* **2011,** *21* (4), 497-508.

29. Hiller, S.; Wagner, G., The role of solution NMR in the structure determinations of VDAC-1 and other membrane proteins. *Curr Opin Struct Biol* **2009,** *19* (4), 396-401.

30. Prosser, R. S.; Evanics, F.; Kitevski, J. L.; Al-Abdul-Wahid, M. S., Current applications of bicelles in NMR studies of membrane-associated amphiphiles and proteins. *Biochemistry* **2006,** *45* (28), 8453-65.

31. Prosser, R. S.; Hwang, J. S.; Vold, R. R., Magnetically aligned phospholipid bilayers with positive ordering: a new model membrane system. *Biophys J* **1998,** *74* (5), 2405-18.

32. Sanders, C. R.; Prosser, R. S., Bicelles: a model membrane system for all seasons? *Structure* **1998,** *6* (10), 1227-34.

33. Vold, R. R.; Prosser, R. S.; Deese, A. J., Isotropic solutions of phospholipid bicelles: a new membrane mimetic for high-resolution NMR studies of polypeptides. *J Biomol NMR* **1997,** *9* (3), 329-35.

34. Son, W. S.; Park, S. H.; Nothnagel, H. J.; Lu, G. J.; Wang, Y.; Zhang, H.; Cook, G. A.; Howell, S. C.; Opella, S. J., 'q-Titration' of long-chain and short-chain lipids differentiates between structured and mobile residues of membrane proteins studied in bicelles by solution NMR spectroscopy. *J Magn Reson* **2012,** *214* (1), 111-8.

35. Knowles, T. J.; Finka, R.; Smith, C.; Lin, Y. P.; Dafforn, T.; Overduin, M., Membrane proteins solubilized intact in lipid containing nanoparticles bounded by styrene maleic acid copolymer. *J Am Chem Soc* **2009,** *131* (22), 7484-5.

36. Bodenhausen, G.; Ruben, D. J., Natural Abundance N-15 Nmr by Enhanced Heteronuclear Spectroscopy. *Chem Phys Lett* **1980,** *69* (1), 185-189.

37. Marion, D.; Driscoll, P. C.; Kay, L. E.; Wingfield, P. T.; Bax, A.; Gronenborn, A. M.; Clore, G. M., Overcoming the overlap problem in the assignment of 1H NMR spectra of larger proteins by use of three-dimensional heteronuclear 1H-15N Hartmann-Hahn-multiple quantum coherence and nuclear Overhauser-multiple quantum coherence spectroscopy: application to interleukin 1 beta. *Biochemistry* **1989,** *28* (15), 6150-6.

38. Zuiderweg, E. R.; Fesik, S. W., Heteronuclear three-dimensional NMR spectroscopy of the inflammatory protein C5a. *Biochemistry* **1989,** *28* (6), 2387-91.

39. Kay, L. E.; Ikura, M.; Bax, A., Proton Proton Correlation Via Carbon Carbon Couplings - a 3-Dimensional Nmr Approach for the Assignment of Aliphatic Resonances in Proteins Labeled with C-13. *Journal of the American Chemical Society* **1990,** *112* (2), 888-889.

40. Grzesiek, S.; Dobeli, H.; Gentz, R.; Garotta, G.; Labhardt, A. M.; Bax, A., 1H, 13C, and 15N NMR backbone assignments and secondary structure of human interferon-gamma. *Biochemistry* **1992,** *31* (35), 8180-90.

41. Muhandiram, D. R.; Kay, L. E., Gradient-Enhanced Triple-Resonance 3-Dimensional Nmr Experiments with Improved Sensitivity. *J Magn Reson Ser B* **1994,** *103* (3), 203-216.

42. Farmer, B. T., 2nd; Venters, R. A.; Spicer, L. D.; Wittekind, M. G.; Muller, L., A refocused and optimized HNCA: increased sensitivity and resolution in large macromolecules. *J Biomol NMR* **1992,** *2* (2), 195-202.

43. Clubb, R. T.; Wagner, G., A triple-resonance pulse scheme for selectively correlating amide 1HN and 15N nuclei with the 1H alpha proton of the preceding residue. *J Biomol NMR* **1992,** *2* (4), 389-94.

44. Bax, A.; Clore, G. M.; Driscoll, P. C.; Gronenborn, A. M.; Ikura, M.; Kay, L. E., Practical Aspects of Proton Carbon Carbon Proton 3-Dimensional Correlation Spectroscopy of C-13-Labeled Proteins. *Journal of Magnetic Resonance* **1990,** *87* (3), 620-627.

45. Bax, A.; Clore, G. M.; Gronenborn, A. M., H-1-H-1 Correlation Via Isotropic Mixing of C-13 Magnetization, a New 3-Dimensional Approach for Assigning H-1 and C-13 Spectra of C-13-Enriched Proteins. *Journal of Magnetic Resonance* **1990,** *88* (2), 425-431.

46. Olejniczak, E. T.; Xu, R. X.; Fesik, S. W., A 4d-Hcch-Tocsy Experiment for Assigning the Side-Chain H-1-Resonance and C-13-Resonance of Proteins. *Journal of Biomolecular Nmr* **1992,** *2* (6), 655-659.

47. Ikura, M.; Kay, L. E.; Bax, A., Improved three-dimensional 1H-13C-1H correlation spectroscopy of a 13C-labeled protein using constant-time evolution. *J Biomol NMR* **1991,** *1* (3), 299-304.

48. Ma, C.; Opella, S. J., Lanthanide ions bind specifically to an added "EF-hand" and orient a membrane protein in micelles for solution NMR spectroscopy. *J Magn Reson* **2000,** *146* (2), 381-4.

49. Veglia, G.; Opella, S. J., Lanthanide ion binding to adventitious sites aligns membrane proteins in micelles for solution NMR spectroscopy. *Journal of the American Chemical Society* **2000,** *122* (47), 11733-11734.

50. Chou, J. J.; Kaufman, J. D.; Stahl, S. J.; Wingfield, P. T.; Bax, A., Micelle-induced curvature in a water-insoluble HIV-1 Env peptide revealed by NMR dipolar coupling measurement in stretched polyacrylamide gel. *J Am Chem Soc* **2002,** *124* (11), 2450-1.

51. Laws, D. D.; Bitter, H. M.; Jerschow, A., Solid-state NMR spectroscopic methods in chemistry. *Angew Chem Int Ed Engl* **2002,** *41* (17), 3096-129.

52. Cegelski, L., REDOR NMR for drug discovery. *Bioorg. Med. Chem. Lett.* **2013,** *23*, 5767-75.

53. Comellas, G.; Rienstra, C. M., Protein structure determination by magic-angle spinning solid-state NMR, and insights into the formation, structure, and stability of amyloid fibrils. *Annu Rev Biophys* **2013,** *42*, 515 - 536.

54. Goncalves, J. A.; Eilers, M.; South, K.; Opefi, C. A.; Laissue, P.; Reeves, P. J.; Smith, S. O., Magic angle spinning nuclear magnetic resonance spectroscopy of G protein-coupled receptors. *Meth. Enzymol.* **2013,** *522*, 365-389.

55. Hong, M.; Zhang, Y.; Hu, F., Membrane protein structure and dynamics from NMR spectroscopy. *Annu Rev Phys Chem* **2012,** *63*, 1-24.

56. Knight, M. J.; Felli, I. C.; Pierattelli, R.; Emsley, L.; Pintacuda, G., Magic angle spinning NMR of paramagnetic proteins. *Acc Chem Res* **2013,** *46*, 2108-16.

57. Mueller, L. J.; Dunn, M. F., NMR Crystallography of Enzyme Active Sites: Probing Chemically-Detailed, Three-Dimensional Structure in Tryptophan Synthase. *Accounts of Chemical Research* **2013,** *46*, 2008-2017.

58. Murray, D. T.; Das, N.; Cross, T. A., Solid state NMR strategy for characterizing native membrane protein structures. *Acc Chem Res* **2013,** *46* (9), 2172-81.

59. Opella, S., Structure determination of membrane proteins by nuclear magnetic resonance spectrocopy. *Annu Rev Anal Chem* **2013,** *6*, 305-328.

60. Opella, S. J., Structure determination of membrane proteins in their native phospholipid bilayer environment by rotationally aligned solid-state NMR spectroscopy. *Acc Chem Res* **2013,** *46*, 2145-2153.

61. Parthasarathy, S.; Nishiyama, Y.; Ishii, Y., Sensitivity and resolution enhanced solid-state NMR for paramagnetic systems and biomolecules under very fast magic angle spinning. *Acc Chem Res* **2013,** *46*, 2127-2135.

62. Saito, H.; Ando, I.; Ramamoorthy, A., Chemical shift tensor - The heart of NMR: Insights into biological aspects of proteins. *Prog NMR Spec* **2010,** *57*, 181-228.

63. Sengupta, I.; Nadaud, P. S.; Jaroniec, C. P., Protein structure determination with paramagnetic solid-state NMR spectroscopy. *Acc Chem Res* **2013,** *46*, 2117-2126.

64. Shi, L.; Ladizhansky, V., Magic angle spinning solid-state NMR experiments for structural characterization of proteins. *Methods Mol Biol* **2012,** *895*, 153-65.

65. Ullrich, S. J.; Glaubitz, C., Perspectives in enzymology of membrane proteins by solid-state NMR. *Acc Chem Res* **2013,** *46* (9), 2164-71.

66. Ulrich, A. S., Solid state 19G NMR methods for studying biomembranes. *Prog Nucl Magn Reson Spectrosc* **2005,** *46*, 1-21.

67. Weingarth, M.; Baldus, M., Solid-State NMR-Based Approaches for Supramolecular Structure Elucidation. *Acc Chem Res* **2013,** *46* (9), 2037-46.

68. Yan, S.; Suiter, C. L.; Hou, G.; Zhang, H.; Polenova, T., Probing structure and dynamics of protein assemblies by magic angle spinning NMR spectroscopy. *Acc Chem Res* **2013,** *in press*.

69. Seelig, J., 31P nuclear magnetic resonance and the head group structure of phospholipids in membranes. *Biochim Biophys Acta* **1978,** *515* (2), 105-40.

70. Polenova, T.; Gupta, R.; Goldbourt, A., Magic angle spinning NMR spectroscopy: a versatile technique for structural and dynamic analysis of solid-phase systems. *Anal Chem* **2015,** *87* (11), 5458-69.

71. Andrew, E. R.; Bradbury, A.; Eades, R. G., Nuclear Magnetic Resonance Spectra from a Crystal Rotated at High Speed. *Nature* **1958,** *182* (4650), 1659-1659.

72. Lowe, I. J., Free Induction Decays of Rotating Solids. *Phys Rev Lett* **1959,** *2* (7), 285-287.

73. Ladizhansky, V., Recent Advances in Magic-Angle Spinning Solid-State NMR of Proteins. *Isr J Chem* **2014,** *54* (1-2), 86-103.

74. Pauli, J.; Baldus, M.; van Rossum, B.; de Groot, H.; Oschkinat, H., Backbone and side-chain 13C and 15N signal assignments of the alpha-spectrin SH3 domain by magic angle spinning solid-state NMR at 17.6 Tesla. *Chembiochem* **2001,** *2* (4), 272-81.

75. Lange, A.; Luca, S.; Baldus, M., Structural constraints from proton-mediated rare-spin correlation spectroscopy in rotating solids. *J Am Chem Soc* **2002,** *124* (33), 9704-5.

76. Lange, A.; Becker, S.; Seidel, K.; Giller, K.; Pongs, O.; Baldus, M., A concept for rapid protein-structure determination by solid-state NMR spectroscopy. *Angew Chem Int Ed Engl* **2005,** *44* (14), 2089-92.

77. Suter, D.; Ernst, R. R., Spin diffusion in resolved solid-state NMR spectra. *Phys Rev B Condens Matter* **1985,** *32* (9), 5608-5627.

78. Takegoshi, K.; Yano, T.; Takeda, K.; Terao, T., Indirect high-resolution observation of 14N NMR in rotating solids. *J Am Chem Soc* **2001,** *123* (43), 10786-7.

79. Morcombe, C. R.; Gaponenko, V.; Byrd, R. A.; Zilm, K. W., Diluting abundant spins by isotope edited radio frequency field assisted diffusion. *Journal of the American Chemical Society* **2004,** *126* (23), 7196-7197.

80. Andronesi, O. C.; Becker, S.; Seidel, K.; Heise, H.; Young, H. S.; Baldus, M., Determination of membrane protein structure and dynamics by magic-angle-spinning solid-state NMR spectroscopy. *Journal of the American Chemical Society* **2005,** *127* (37), 12965-12974.

81. Franks, W. T.; Kloepper, K. D.; Wylie, B. J.; Rienstra, C. M., Four-dimensional heteronuclear correlation experiments for chemical shift assignment of solid proteins. *Journal of Biomolecular Nmr* **2007,** *39* (2), 107-131.

82. Franks, W. T.; Zhou, D. H.; Wylie, B. J.; Money, B. G.; Graesser, D. T.; Frericks, H. L.; Sahota, G.; Rienstra, C. M., Magic-angle spinning solid-state NMR spectroscopy of the beta 1 immunoglobulin binding domain of protein G (GB1): N-15 and C-13 chemical shift assignments and conformational analysis. *Journal of the American Chemical Society* **2005,** *127* (35), 12291-12305.

83. Zhong, L.; Bamm, V. V.; Ahmed, M. A. M.; Harauz, G.; Ladizhansky, V., Solid-state NMR spectroscopy of 18.5 kDa myelin basic protein reconstituted with lipid vesicles: Spectroscopic characterisation and spectral assignments of solvent-exposed protein fragments. *Bba-Biomembranes* **2007,** *1768* (12), 3193-3205.

84. Li, Y.; Berthold, D. A.; Gennis, R. B.; Rienstra, C. M., Chemical shift assignment of the transmembrane helices of DsbB, a 20-kDa integral membrane enzyme, by 3D magic-angle spinning NMR spectroscopy. *Protein Science* **2008,** *17* (2), 199-204.

85. Shi, L. C.; Ahmed, M. A. M.; Zhang, W. R.; Whited, G.; Brown, L. S.; Ladizhansky, V., Three-Dimensional Solid-State NMR Study of a Seven-Helical Integral Membrane Proton Pump-Structural Insights. *Journal of Molecular Biology* **2009,** *386* (4), 1078-1093.

86. Shi, L. C.; Lake, E. M. R.; Ahmed, M. A. M.; Brown, L. S.; Ladizhansky, V., Solid-state NMR study of proteorhodopsin in the lipid environment: Secondary structure and dynamics. *Bba-Biomembranes* **2009,** *1788* (12), 2563-2574.

87. Schuetz, A.; Wasmer, C.; Habenstein, B.; Verel, R.; Greenwald, J.; Riek, R.; Bockmann, A.; Meier, B. H., Protocols for the Sequential Solid-State NMR Spectroscopic Assignment of a Uniformly Labeled 25 kDa Protein: HET-s(1-227). *Chembiochem* **2010,** *11* (11), 1543-1551.

88. Costa, P. R.; Sun, B. Q.; Griffin, R. G., Rotational resonance NMR: separation of dipolar coupling and zero quantum relaxation. *Journal of Magnetic Resonance* **2003,** *164* (1), 92-103.

89. Ramachandran, R.; Ladizhansky, V.; Bajaj, V. S.; Griffin, R. G., C-13-C-13 rotational resonance width distance measurements in uniformly C-13-labeled peptides. *Journal of the American Chemical Society* **2003,** *125* (50), 15623-15629.

90. van der Wel, P. C. A.; Eddy, M. T.; Ramachandran, R.; Griffin, R. G., Targeted C-13-C-13 Distance Measurements in a Microcrystalline Protein via J-Decoupled Rotational Resonance Width Measurements. *Chemphyschem* **2009,** *10* (9-10), 1656-1663.

91. Williamson, P. T. F.; Verhoeven, A.; Ernst, M.; Meier, B. H., Determination of internuclear distances in uniformly labeled molecules by rotational-resonance solid-state NMR. *Journal of the American Chemical Society* **2003,** *125* (9), 2718-2722.

92. Janik, R.; Peng, X. H.; Ladizhansky, V., C-13-C-13 distance measurements in U-(CN)-C-13-N-15-labeled peptides using rotational resonance width experiment with a homogeneously broadened matching condition. *Journal of Magnetic Resonance* **2007,** *188* (1), 129-140.

93. Peng, X. H.; Libich, D.; Janik, R.; Harauz, G.; Ladizhansky, V., Dipolar chemical shift correlation spectroscopy for homonuclear carbon distance measurements in proteins in the solid state: Application to structure determination and refinement. *Journal of the American Chemical Society* **2008,** *130* (1), 359-369.

94. Hing, A. W.; Vega, S.; Schaefer, J., Transferred-Echo Double-Resonance Nmr. *Journal of Magnetic Resonance* **1992,** *96* (1), 205-209.

95. Helmus, J. J.; Nadaud, P. S.; Hofer, N.; Jaroniec, C. P., Determination of methyl C-13-N-15 dipolar couplings in peptides and proteins by three-dimensional and

four-dimensional magic-angle spinning solid-state NMR spectroscopy. *J Chem Phys* **2008,** *128* (5).

96. Jaroniec, C. P.; Filip, C.; Griffin, R. G., 3D TEDOR NMR experiments for the simultaneous measurement of multiple carbon-nitrogen distances in uniformly C-13, N-15-labeled solids. *Journal of the American Chemical Society* **2002,** *124* (36), 10728-10742.

97. Nieuwkoop, A. J.; Rienstra, C. M., Supramolecular Protein Structure Determination by Site-Specific Long-Range Intermolecular Solid State NMR Spectroscopy. *Journal of the American Chemical Society* **2010,** *132* (22), 7570-+.

98. Franks, W. T.; Wylie, B. J.; Schmidt, H. L. F.; Nieuwkoop, A. J.; Mayrhofer, R. M.; Shah, G. J.; Graesser, D. T.; Rienstra, C. M., Dipole tensor-based atomic-resolution structure determination of a nanocrystalline protein by solid-state NMR. *P Natl Acad Sci USA* **2008,** *105* (12), 4621-4626.

99. Zech, S. G.; Wand, A. J.; McDermott, A. E., Protein structure determination by high-resolution solid-state NMR spectroscopy: Application to microcrystalline ubiquitin. *Journal of the American Chemical Society* **2005,** *127* (24), 8618-8626.

100. Loquet, A.; Bardiaux, B.; Gardiennet, C.; Blanchet, C.; Baldus, M.; Nilges, M.; Malliavin, T.; Bockmann, A., 3D structure determination of the Crh protein from highly ambiguous solid-state NMR restraints. *Journal of the American Chemical Society* **2008,** *130* (11), 3579-3589.

101. Morris, G. A.; Freeman, R., Enhancement of Nuclear Magnetic-Resonance Signals by Polarization Transfer. *Journal of the American Chemical Society* **1979,** *101* (3), 760-762.

102. Bloembergen, N., On the Interaction of Nuclear Spins in a Crystalline Lattice. *Physica* **1949,** *15* (3-4), 386-426.

103. Baldus, M.; Petkova, A. T.; Herzfeld, J.; Griffin, R. G., Cross polarization in the tilted frame: assignment and spectral simplification in heteronuclear spin systems. *Mol Phys* **1998,** *95* (6), 1197-1207.

104. Cross, T. A.; Opella, S. J., Protein-Structure by Solid-State Nmr. *Journal of the American Chemical Society* **1983,** *105* (2), 306-308.

105. Opella, S. J.; Waugh, J. S., 2-Dimensional C-13 Nmr of Highly Oriented Polyethylene. *J Chem Phys* **1977,** *66* (11), 4919-4924.

106. Opella, S. J.; Marassi, F. M., Structure determination of membrane proteins by NMR spectroscopy. *Chem Rev* **2004,** *104* (8), 3587-606.

107. Opella, S. J.; Stewart, P. L.; Valentine, K. G., Protein structure by solid-state NMR spectroscopy. *Q Rev Biophys* **1987,** *19* (1-2), 7-49.

108. Marassi, F. M.; Ramamoorthy, A.; Opella, S. J., Complete resolution of the solid-state NMR spectrum of a uniformly 15N-labeled membrane protein in phospholipid bilayers. *Proc Natl Acad Sci U S A* **1997,** *94* (16), 8551-6.

109. Ketchem, R. R.; Hu, W.; Cross, T. A., High-resolution conformation of gramicidin A in a lipid bilayer by solid-state NMR. *Science* **1993,** *261* (5127), 1457-60.

110. Opella, S. J.; Ma, C.; Marassi, F. M., Nuclear magnetic resonance of membrane-associated peptides and proteins. *Methods Enzymol* **2001,** *339*, 285-313.

111. Howard, K. P.; Opella, S. J., High-resolution solid-state NMR spectra of integral membrane proteins reconstituted into magnetically oriented phospholipid bilayers. *J Magn Reson B* **1996,** *112* (1), 91-4.

112. Waugh, J. S., Uncoupling of local field spectra in nuclear magnetic resonance: determination of atomic positions in solids. *Proc Natl Acad Sci U S A* **1976,** *73* (5), 1394-7.

113. Hester, R. K.; Ackerman, J. L.; Neff, B. L.; Waugh, J. S., Separated Local Field Spectra in Nmr - Determination of Structure of Solids. *Phys Rev Lett* **1976,** *36* (18), 1081-1083.

114. Wu, C. H.; Ramamoorthy, A.; Opella, S. J., High-Resolution Heteronuclear Dipolar Solid-State Nmr-Spectroscopy. *J Magn Reson Ser A* **1994,** *109* (2), 270-272.

115. Nevzorov, A. A.; Opella, S. J., A "magic sandwich" pulse sequence with reduced offset dependence for high-resolution separated local field spectroscopy. *J Magn Reson* **2003,** *164* (1), 182-6.

116. Marassi, F. M.; Opella, S. J., Using pisa pies to resolve ambiguities in angular constraints from PISEMA spectra of aligned proteins. *J Biomol NMR* **2002,** *23* (3), 239-42.

117. Wang, J.; Denny, J.; Tian, C.; Kim, S.; Mo, Y.; Kovacs, F.; Song, Z.; Nishimura, K.; Gan, Z.; Fu, R.; Quine, J. R.; Cross, T. A., Imaging membrane protein helical wheels. *J Magn Reson* **2000,** *144* (1), 162-7.

118. Marassi, F. M.; Opella, S. J., A solid-state NMR index of helical membrane protein structure and topology. *J Magn Reson* **2000,** *144* (1), 150-5.

119. Ramamoorthy, A.; Gierasch, L. M.; Opella, S. J., 4-Dimensional Solid-State Nmr Experiment That Correlates the Chemical-Shift and Dipolar-Coupling Frequencies of 2 Heteronuclei with the Exchange of Dilute-Spin Magnetization. *J Magn Reson Ser B* **1995,** *109* (1), 112-116.

120. Ramamoorthy, A.; Gierasch, L. M.; Opella, S. J., Three-dimensional solid-state NMR correlation experiment with H-1 homonuclear spin exchange. *J Magn Reson Ser B* **1996,** *111* (1), 81-84.

121. Ramamoorthy, A.; Marassi, F. M.; Zasloff, M.; Opella, S. J., 3-Dimensional Solid-State Nmr-Spectroscopy of a Peptide Oriented in Membrane Bilayers. *Journal of Biomolecular Nmr* **1995,** *6* (3), 329-334.

122. Ramamoorthy, A.; Wu, C. H.; Opella, S. J., 3-Dimensional Solid-State Nmr Experiment That Correlates the Chemical-Shift and Dipolar Coupling Frequencies of 2 Heteronuclei. *J Magn Reson Ser B* **1995,** *107* (1), 88-90.

123. Jelinek, R.; Ramamoorthy, A.; Opella, S. J., High-Resolution 3-Dimensional Solid-State Nmr-Spectroscopy of a Uniformly N-15-Labeled Protein. *Journal of the American Chemical Society* **1995,** *117* (49), 12348-12349.

124. Marassi, F. M.; Opella, S. J., Simultaneous assignment and structure determination of a membrane protein from NMR orientational restraints. *Protein Sci* **2003,** *12* (3), 403-11.

125. Park, S. H.; Mrse, A. A.; Nevzorov, A. A.; Mesleh, M. F.; Oblatt-Montal, M.; Montal, M.; Opella, S. J., Three-dimensional structure of the channel-forming trans-membrane domain of virus protein "u" (Vpu) from HIV-1. *J Mol Biol* **2003,** *333* (2), 409-24.

126. Opella, S. J.; Marassi, F. M.; Gesell, J. J.; Valente, A. P.; Kim, Y.; Oblatt-Montal, M.; Montal, M., Structures of the M2 channel-lining segments from nicotinic acetylcholine and NMDA receptors by NMR spectroscopy. *Nat Struct Biol* **1999,** *6* (4), 374-9.

127. Tian, C.; Gao, P. F.; Pinto, L. H.; Lamb, R. A.; Cross, T. A., Initial structural and dynamic characterization of the M2 protein transmembrane and amphipathic helices in lipid bilayers. *Protein Sci* **2003,** *12* (11), 2597-605.

128. Dorsam, R. T.; Gutkind, J. S., G-protein-coupled receptors and cancer. *Nat Rev Cancer* **2007,** *7* (2), 79-94.

129. Fredriksson, R.; Lagerstrom, M. C.; Lundin, L. G.; Schioth, H. B., The G-protein-coupled receptors in the human genome form five main families. Phylogenetic analysis, paralogon groups, and fingerprints. *Mol Pharmacol* **2003,** *63* (6), 1256-72.

130. Venter, J. C.; Adams, M. D.; Myers, E. W.; Li, P. W.; Mural, R. J.; Sutton, G. G.; Smith, H. O.; Yandell, M.; Evans, C. A.; Holt, R. A.; Gocayne, J. D.; Amanatides, P.; Ballew, R. M.; Huson, D. H.; Wortman, J. R.; Zhang, Q.; Kodira, C. D.; Zheng, X. H.; Chen, L.; Skupski, M.; Subramanian, G.; Thomas, P. D.; Zhang, J.; Gabor Miklos, G. L.; Nelson, C.; Broder, S.; Clark, A. G.; Nadeau, J.; McKusick, V. A.; Zinder, N.; Levine, A. J.; Roberts, R. J.; Simon, M.; Slayman, C.; Hunkapiller, M.; Bolanos, R.; Delcher, A.; Dew, I.; Fasulo, D.; Flanigan, M.; Florea, L.; Halpern, A.; Hannenhalli, S.; Kravitz, S.; Levy, S.; Mobarry, C.; Reinert, K.; Remington, K.; Abu-Threideh, J.; Beasley, E.; Biddick, K.; Bonazzi, V.; Brandon, R.; Cargill, M.; Chandramouliswaran, I.; Charlab, R.; Chaturvedi, K.; Deng, Z.; Di Francesco, V.; Dunn, P.; Eilbeck, K.; Evangelista, C.; Gabrielian, A. E.; Gan, W.; Ge, W.; Gong, F.; Gu, Z.; Guan, P.; Heiman, T. J.; Higgins, M. E.; Ji, R. R.; Ke, Z.; Ketchum, K. A.; Lai, Z.; Lei, Y.; Li, Z.; Li, J.; Liang, Y.; Lin, X.; Lu, F.; Merkulov, G. V.; Milshina, N.; Moore, H. M.; Naik, A. K.; Narayan, V. A.; Neelam, B.; Nusskern, D.; Rusch,

D. B.; Salzberg, S.; Shao, W.; Shue, B.; Sun, J.; Wang, Z.; Wang, A.; Wang, X.; Wang, J.; Wei, M.; Wides, R.; Xiao, C.; Yan, C.; Yao, A.; Ye, J.; Zhan, M.; Zhang, W.; Zhang, H.; Zhao, Q.; Zheng, L.; Zhong, F.; Zhong, W.; Zhu, S.; Zhao, S.; Gilbert, D.; Baumhueter, S.; Spier, G.; Carter, C.; Cravchik, A.; Woodage, T.; Ali, F.; An, H.; Awe, A.; Baldwin, D.; Baden, H.; Barnstead, M.; Barrow, I.; Beeson, K.; Busam, D.; Carver, A.; Center, A.; Cheng, M. L.; Curry, L.; Danaher, S.; Davenport, L.; Desilets, R.; Dietz, S.; Dodson, K.; Doup, L.; Ferriera, S.; Garg, N.; Gluecksmann, A.; Hart, B.; Haynes, J.; Haynes, C.; Heiner, C.; Hladun, S.; Hostin, D.; Houck, J.; Howland, T.; Ibegwam, C.; Johnson, J.; Kalush, F.; Kline, L.; Koduru, S.; Love, A.; Mann, F.; May, D.; McCawley, S.; McIntosh, T.; McMullen, I.; Moy, M.; Moy, L.; Murphy, B.; Nelson, K.; Pfannkoch, C.; Pratts, E.; Puri, V.; Qureshi, H.; Reardon, M.; Rodriguez, R.; Rogers, Y. H.; Romblad, D.; Ruhfel, B.; Scott, R.; Sitter, C.; Smallwood, M.; Stewart, E.; Strong, R.; Suh, E.; Thomas, R.; Tint, N. N.; Tse, S.; Vech, C.; Wang, G.; Wetter, J.; Williams, S.; Williams, M.; Windsor, S.; Winn-Deen, E.; Wolfe, K.; Zaveri, J.; Zaveri, K.; Abril, J. F.; Guigo, R.; Campbell, M. J.; Sjolander, K. V.; Karlak, B.; Kejariwal, A.; Mi, H.; Lazareva, B.; Hatton, T.; Narechania, A.; Diemer, K.; Muruganujan, A.; Guo, N.; Sato, S.; Bafna, V.; Istrail, S.; Lippert, R.; Schwartz, R.; Walenz, B.; Yooseph, S.; Allen, D.; Basu, A.; Baxendale, J.; Blick, L.; Caminha, M.; Carnes-Stine, J.; Caulk, P.; Chiang, Y. H.; Coyne, M.; Dahlke, C.; Mays, A.; Dombroski, M.; Donnelly, M.; Ely, D.; Esparham, S.; Fosler, C.; Gire, H.; Glanowski, S.; Glasser, K.; Glodek, A.; Gorokhov, M.; Graham, K.; Gropman, B.; Harris, M.; Heil, J.; Henderson, S.; Hoover, J.; Jennings, D.; Jordan, C.; Jordan, J.; Kasha, J.; Kagan, L.; Kraft, C.; Levitsky, A.; Lewis, M.; Liu, X.; Lopez, J.; Ma, D.; Majoros, W.; McDaniel, J.; Murphy, S.; Newman, M.; Nguyen, T.; Nguyen, N.; Nodell, M.; Pan, S.; Peck, J.; Peterson, M.; Rowe, W.; Sanders, R.; Scott, J.; Simpson, M.; Smith, T.; Sprague, A.; Stockwell, T.; Turner, R.; Venter, E.; Wang, M.; Wen, M.; Wu, D.; Wu, M.; Xia, A.; Zandieh, A.; Zhu, X., The sequence of the human genome. *Science* **2001,** *291* (5507), 1304-51.

131. Lander, E. S.; Linton, L. M.; Birren, B.; Nusbaum, C.; Zody, M. C.; Baldwin, J.; Devon, K.; Dewar, K.; Doyle, M.; FitzHugh, W.; Funke, R.; Gage, D.; Harris, K.; Heaford, A.; Howland, J.; Kann, L.; Lehoczky, J.; LeVine, R.; McEwan, P.; McKernan, K.; Meldrim, J.; Mesirov, J. P.; Miranda, C.; Morris, W.; Naylor, J.; Raymond, C.; Rosetti, M.; Santos, R.; Sheridan, A.; Sougnez, C.; Stange-Thomann, Y.; Stojanovic, N.; Subramanian, A.; Wyman, D.; Rogers, J.; Sulston, J.; Ainscough, R.; Beck, S.; Bentley, D.; Burton, J.; Clee, C.; Carter, N.; Coulson, A.; Deadman, R.; Deloukas, P.; Dunham, A.; Dunham, I.; Durbin, R.; French, L.; Grafham, D.; Gregory, S.; Hubbard, T.; Humphray, S.; Hunt, A.; Jones, M.; Lloyd, C.; McMurray, A.; Matthews, L.; Mercer, S.; Milne, S.; Mullikin, J. C.; Mungall, A.; Plumb, R.; Ross, M.; Shownkeen, R.; Sims, S.; Waterston, R. H.; Wilson, R. K.; Hillier, L. W.; McPherson, J. D.; Marra, M. A.; Mardis, E. R.; Fulton, L. A.; Chinwalla, A. T.; Pepin, K. H.; Gish, W. R.; Chissoe, S. L.; Wendl, M. C.; Delehaunty, K. D.; Miner, T. L.; Delehaunty, A.; Kramer, J. B.; Cook, L. L.; Fulton, R. S.; Johnson, D. L.; Minx, P. J.; Clifton, S. W.; Hawkins, T.; Branscomb, E.;

Predki, P.; Richardson, P.; Wenning, S.; Slezak, T.; Doggett, N.; Cheng, J. F.; Olsen, A.; Lucas, S.; Elkin, C.; Uberbacher, E.; Frazier, M.; Gibbs, R. A.; Muzny, D. M.; Scherer, S. E.; Bouck, J. B.; Sodergren, E. J.; Worley, K. C.; Rives, C. M.; Gorrell, J. H.; Metzker, M. L.; Naylor, S. L.; Kucherlapati, R. S.; Nelson, D. L.; Weinstock, G. M.; Sakaki, Y.; Fujiyama, A.; Hattori, M.; Yada, T.; Toyoda, A.; Itoh, T.; Kawagoe, C.; Watanabe, H.; Totoki, Y.; Taylor, T.; Weissenbach, J.; Heilig, R.; Saurin, W.; Artiguenave, F.; Brottier, P.; Bruls, T.; Pelletier, E.; Robert, C.; Wincker, P.; Smith, D. R.; Doucette-Stamm, L.; Rubenfield, M.; Weinstock, K.; Lee, H. M.; Dubois, J.; Rosenthal, A.; Platzer, M.; Nyakatura, G.; Taudien, S.; Rump, A.; Yang, H.; Yu, J.; Wang, J.; Huang, G.; Gu, J.; Hood, L.; Rowen, L.; Madan, A.; Qin, S.; Davis, R. W.; Federspiel, N. A.; Abola, A. P.; Proctor, M. J.; Myers, R. M.; Schmutz, J.; Dickson, M.; Grimwood, J.; Cox, D. R.; Olson, M. V.; Kaul, R.; Raymond, C.; Shimizu, N.; Kawasaki, K.; Minoshima, S.; Evans, G. A.; Athanasiou, M.; Schultz, R.; Roe, B. A.; Chen, F.; Pan, H.; Ramser, J.; Lehrach, H.; Reinhardt, R.; McCombie, W. R.; de la Bastide, M.; Dedhia, N.; Blocker, H.; Hornischer, K.; Nordsiek, G.; Agarwala, R.; Aravind, L.; Bailey, J. A.; Bateman, A.; Batzoglou, S.; Birney, E.; Bork, P.; Brown, D. G.; Burge, C. B.; Cerutti, L.; Chen, H. C.; Church, D.; Clamp, M.; Copley, R. R.; Doerks, T.; Eddy, S. R.; Eichler, E. E.; Furey, T. S.; Galagan, J.; Gilbert, J. G.; Harmon, C.; Hayashizaki, Y.; Haussler, D.; Hermjakob, H.; Hokamp, K.; Jang, W.; Johnson, L. S.; Jones, T. A.; Kasif, S.; Kaspryzk, A.; Kennedy, S.; Kent, W. J.; Kitts, P.; Koonin, E. V.; Korf, I.; Kulp, D.; Lancet, D.; Lowe, T. M.; McLysaght, A.; Mikkelsen, T.; Moran, J. V.; Mulder, N.; Pollara, V. J.; Ponting, C. P.; Schuler, G.; Schultz, J.; Slater, G.; Smit, A. F.; Stupka, E.; Szustakowki, J.; Thierry-Mieg, D.; Thierry-Mieg, J.; Wagner, L.; Wallis, J.; Wheeler, R.; Williams, A.; Wolf, Y. I.; Wolfe, K. H.; Yang, S. P.; Yeh, R. F.; Collins, F.; Guyer, M. S.; Peterson, J.; Felsenfeld, A.; Wetterstrand, K. A.; Patrinos, A.; Morgan, M. J.; de Jong, P.; Catanese, J. J.; Osoegawa, K.; Shizuya, H.; Choi, S.; Chen, Y. J.; Szustakowki, J.; International Human Genome Sequencing, C., Initial sequencing and analysis of the human genome. *Nature* **2001,** *409* (6822), 860-921.

132. Audet, M.; Bouvier, M., Restructuring G-protein- coupled receptor activation. *Cell* **2012,** *151* (1), 14-23.

133. Pierce, K. L.; Premont, R. T.; Lefkowitz, R. J., Seven-transmembrane receptors. *Nat Rev Mol Cell Biol* **2002,** *3* (9), 639-50.

134. Lee, D. K.; George, S. R.; O'Dowd, B. F., Novel G-protein-coupled receptor genes expressed in the brain: continued discovery of important therapeutic targets. *Expert Opin Ther Targets* **2002,** *6* (2), 185-202.

135. Han, X.; Feng, Y.; Chen, X.; Gerard, C.; Boisvert, W. A., Characterization of G protein coupling mediated by the conserved D134(3.49) of DRY motif, M241(6.34), and F251(6.44) residues on human CXCR1. *FEBS Open Bio* **2015,** *5*, 182-90.

136. Nasser, M. W.; Raghuwanshi, S. K.; Malloy, K. M.; Gangavarapu, P.; Shim, J. Y.; Rajarathnam, K.; Richardson, R. M., CXCR1 and CXCR2 activation and regulation. Role of aspartate 199 of the second extracellular loop of CXCR2 in CXCL8-mediated rapid receptor internalization. *J Biol Chem* **2007,** *282* (9), 6906-15.

137. Koch, A. E.; Polverini, P. J.; Kunkel, S. L.; Harlow, L. A.; DiPietro, L. A.; Elner, V. M.; Elner, S. G.; Strieter, R. M., Interleukin-8 as a macrophage-derived mediator of angiogenesis. *Science* **1992,** *258* (5089), 1798-801.

138. Strieter, R. M.; Polverini, P. J.; Arenberg, D. A.; Kunkel, S. L., The role of CXC chemokines as regulators of angiogenesis. *Shock* **1995,** *4* (3), 155-60.

139. Clark-Lewis, I.; Moser, B.; Walz, A.; Baggiolini, M.; Scott, G. J.; Aebersold, R., Chemical synthesis, purification, and characterization of two inflammatory proteins, neutrophil activating peptide 1 (interleukin-8) and neutrophil activating peptide. *Biochemistry* **1991,** *30* (12), 3128-35.

140. Bergin, D. A.; Reeves, E. P.; Meleady, P.; Henry, M.; McElvaney, O. J.; Carroll, T. P.; Condron, C.; Chotirmall, S. H.; Clynes, M.; O'Neill, S. J.; McElvaney, N. G., alpha-1 Antitrypsin regulates human neutrophil chemotaxis induced by soluble immune complexes and IL-8. *J Clin Invest* **2010,** *120* (12), 4236-50.

141. Burke, S. M.; Issekutz, T. B.; Mohan, K.; Lee, P. W.; Shmulevitz, M.; Marshall, J. S., Human mast cell activation with virus-associated stimuli leads to the selective chemotaxis of natural killer cells by a CXCL8-dependent mechanism. *Blood* **2008,** *111* (12), 5467-76.

142. Baggiolini, M.; Walz, A.; Kunkel, S. L., Neutrophil-activating peptide-1/interleukin 8, a novel cytokine that activates neutrophils. *J Clin Invest* **1989,** *84* (4), 1045-9.

143. Nasser, M. W.; Raghuwanshi, S. K.; Grant, D. J.; Jala, V. R.; Rajarathnam, K.; Richardson, R. M., Differential activation and regulation of CXCR1 and CXCR2 by CXCL8 monomer and dimer. *J Immunol* **2009,** *183* (5), 3425-32.

144. Park, S. H.; Casagrande, F.; Chu, M.; Maier, K.; Kiefer, H.; Opella, S. J., Optimization of purification and refolding of the human chemokine receptor CXCR1 improves the stability of proteoliposomes for structure determination. *Biochim Biophys Acta* **2012,** *1818* (3), 584-91.

145. Holmes, W. E.; Lee, J.; Kuang, W. J.; Rice, G. C.; Wood, W. I., Structure and Functional Expression of a Human Interleukin-8 Receptor. *Science* **1991,** *253* (5025), 1278-1280.

146. Ahuja, S. K.; Lee, J. C.; Murphy, P. M., CXC chemokines bind to unique sets of selectivity determinants that can function independently and are broadly distributed on multiple domains of human interleukin-8 receptor B. Determinants of high affinity binding and receptor activation are distinct. *J Biol Chem* **1996,** *271* (1), 225-32.

147. Murphy, P. M.; Tiffany, H. L., Cloning of complementary DNA encoding a functional human interleukin-8 receptor. *Science* **1991,** *253* (5025), 1280-3.

148. Catusse, J.; Liotard, A.; Loillier, B.; Pruneau, D.; Paquet, J. L., Characterization of the molecular interactions of interleukin-8 (CXCL8), growth related oncogen alpha (CXCL1) and a non-peptide antagonist (SB 225002) with the human CXCR2. *Biochem Pharmacol* **2003,** *65* (5), 813-21.

149. Woehler, A.; Ponimaskin, E. G., G protein--mediated signaling: same receptor, multiple effectors. *Curr Mol Pharmacol* **2009,** *2* (3), 237-48.

150. Baker, J. G.; Hill, S. J., Multiple GPCR conformations and signalling pathways: implications for antagonist affinity estimates. *Trends Pharmacol Sci* **2007,** *28* (8), 374-81.

151. Gudermann, T.; Kalkbrenner, F.; Schultz, G., Diversity and selectivity of receptor-G protein interaction. *Annu Rev Pharmacol Toxicol* **1996,** *36*, 429-59.

152. Bertin, B.; Freissmuth, M.; Jockers, R.; Strosberg, A. D.; Marullo, S., Cellular signaling by an agonist-activated receptor/Gs alpha fusion protein. *Proc Natl Acad Sci U S A* **1994,** *91* (19), 8827-31.

153. Wise, A.; Carr, I. C.; Milligan, G., Measurement of agonist-induced guanine nucleotide turnover by the G-protein Gi1alpha when constrained within an alpha2A-adrenoceptor-Gi1alpha fusion protein. *Biochem J* **1997,** *325 (Pt 1)*, 17-21.

154. Seifert, R.; Wenzel-Seifert, K.; Kobilka, B. K., GPCR-Galpha fusion proteins: molecular analysis of receptor-G-protein coupling. *Trends Pharmacol Sci* **1999,** *20* (9), 383-9.

155. Milligan, G., Insights into ligand pharmacology using receptor-G-protein fusion proteins. *Trends Pharmacol Sci* **2000,** *21* (1), 24-8.

156. Milligan, G., G protein-coupled receptor dimerization: function and ligand pharmacology. *Mol Pharmacol* **2004,** *66* (1), 1-7.

157. Wurch, T.; Pauwels, P. J., Analytical pharmacology of G protein-coupled receptors by stoichiometric expression of the receptor and G(alpha) protein subunits. *J Pharmacol Toxicol Methods* **2001,** *45* (1), 3-16.

158. Hildebrandt, J. D., Bring your own G protein. *Mol Pharmacol* **2006,** *69* (4), 1079-82.

159. Zhang, L.; DiLizio, C.; Kim, D.; Smyth, E. M.; Manning, D. R., The G12 family of G proteins as a reporter of thromboxane A2 receptor activity. *Mol Pharmacol* **2006,** *69* (4), 1433-40.

160. Loisel, T. P.; Ansanay, H.; Adam, L.; Marullo, S.; Seifert, R.; Lagace, M.; Bouvier, M., Activation of the beta(2)-adrenergic receptor-Galpha(s) complex leads to rapid depalmitoylation and inhibition of repalmitoylation of both the receptor and Galpha(s). *J Biol Chem* **1999,** *274* (43), 31014-9.

161. Ward, R. J.; Milligan, G., An Asp79Asn mutation of the alpha2A-adrenoceptor interferes equally with agonist activation of individual Gialpha-family G protein subtypes. *FEBS Lett* **1999,** *462* (3), 459-63.

162. Dupuis, D. S.; Tardif, S.; Wurch, T.; Colpaert, F. C.; Pauwels, P. J., Modulation of 5-MT1A receptor signalling by point-mutation of cysteine(351) in the rat G(alpha o) protein. *Neuropharmacology* **1999,** *38* (7), 1035-1041.

163. Pauwels, P. J.; Colpaert, F. C., Disparate ligand-mediated Ca(2+) responses by wild-type, mutant Ser(200)Ala and Ser(204)Ala alpha(2A)-adrenoceptor: G(alpha15) fusion proteins: evidence for multiple ligand-activation binding sites. *Br J Pharmacol* **2000,** *130* (7), 1505-12.

164. Moon, H. E.; Bahia, D. S.; Cavalli, A.; Hoffmann, M.; Milligan, G., Control of the efficiency of agonist-induced information transfer and stability of the ternary complex containing the delta opioid receptor and the alpha subunit of G(i1) by mutation of a receptor/G protein contact interface. *Neuropharmacology* **2001,** *41* (3), 321-30.

165. Ward, R. J.; Milligan, G., Reciprocal mutations of highly conserved residues in transmembrane helices 2 and 7 of the alpha(2A)-adrenoceptor restore agonist activation of G(i1)alpha. *Cell Signal* **2002,** *14* (2), 139-44.

166. Kellett, E.; Carr, I. C.; Milligan, G., Regulation of G protein activation and effector modulation by fusion proteins between the human 5-hydroxytryptamine(1A) receptor and the alpha subunit of G(i1): differences in receptor-constitutive activity imparted by single amino acid substitutions in G(i1)alpha. *Mol Pharmacol* **1999,** *56* (4), 684-92.

167. Wise, A.; Milligan, G., Rescue of functional interactions between the alpha(2A)-adrenoreceptor and acylation-resistant forms of G(i1)alpha by expressing the proteins from chimeric open reading frames. *Journal of Biological Chemistry* **1997,** *272* (39), 24673-24678.

168. Wang, Y.; Windh, R. T.; Chen, C. A.; Manning, D. R., N-Myristoylation and betagamma play roles beyond anchorage in the palmitoylation of the G protein alpha(o) subunit. *J Biol Chem* **1999,** *274* (52), 37435-42.

169. Stevens, P. A.; Pediani, J.; Carrillo, J. J.; Milligan, G., Coordinated agonist regulation of receptor and G protein palmitoylation and functional rescue of palmitoylation-deficient mutants of the G protein G11alpha following fusion to the alpha1b-adrenoreceptor: palmitoylation of G11alpha is not required for interaction with beta*gamma complex. *J Biol Chem* **2001,** *276* (38), 35883-90.

170. Liu, S.; Carrillo, J. J.; Pediani, J. D.; Milligan, G., Effective information transfer from the alpha 1b-adrenoceptor to Galpha 11 requires both beta/gamma interactions and an aromatic group four amino acids from the C terminus of the G protein. *J Biol Chem* **2002,** *277* (28), 25707-14.

171. Ugur, O.; Onaran, H. O.; Jones, T. L., Partial rescue of functional interactions of a nonpalmitoylated mutant of the G-protein G alpha s by fusion to the beta-adrenergic receptor. *Biochemistry* **2003,** *42* (9), 2607-15.

172. Malik, R. U.; Dysthe, M.; Ritt, M.; Sunahara, R. K.; Sivaramakrishnan, S., ER/K linked GPCR-G protein fusions systematically modulate second messenger response in cells. *Sci Rep* **2017,** *7* (1), 7749.

173. Takeda, S.; Yamamoto, A.; Okada, T.; Matsumura, E.; Nose, E.; Kogure, K.; Kojima, S.; Haga, T., Identification of surrogate ligands for orphan G protein-coupled receptors. *Life Sci* **2003,** *74* (2-3), 367-77.

174. Small, K. M.; Brown, K. M.; Forbes, S. L.; Liggett, S. B., Modification of the beta 2-adrenergic receptor to engineer a receptor-effector complex for gene therapy. *J Biol Chem* **2001,** *276* (34), 31596-601.

175. Molinari, P.; Ambrosio, C.; Riitano, D.; Sbraccia, M.; Gro, M. C.; Costa, T., Promiscuous coupling at receptor-Galpha fusion proteins. The receptor of one covalent complex interacts with the alpha-subunit of another. *J Biol Chem* **2003,** *278* (18), 15778-88.

176. Maeda, Y.; Kuroki, R.; Haase, W.; Michel, H.; Reilander, H., Comparative analysis of high-affinity ligand binding and G protein coupling of the human CXCR1 chemokine receptor and of a CXCR1-Galpha fusion protein after heterologous production in baculovirus-infected insect cells. *Eur J Biochem* **2004,** *271* (9), 1677-89.

177. Seifert, R.; Lee, T. W.; Lam, V. T.; Kobilka, B. K., Reconstitution of beta2-adrenoceptor-GTP-binding-protein interaction in Sf9 cells--high coupling efficiency in a beta2-adrenoceptor-G(s alpha) fusion protein. *Eur J Biochem* **1998,** *255* (2), 369-82.

178. Schneider, E. H.; Seifert, R., Fusion proteins as model systems for the analysis of constitutive GPCR activity. *Methods Enzymol* **2010,** *485*, 459-80.

179. Ichiyama, S.; Nemoto, R.; Tanabe, H.; Haga, T., Interaction of the muscarinic acetylcholine receptor M(2) subtype with G protein Galpha(i/o) isotypes and Gbetagamma subunits as studied with the maltose-binding protein-M(2)-

Galpha(i/o) fusion proteins expressed in Escherichia coli. *J Biochem* **2014,** *156* (5), 259-72.

180. Milligan, G.; Parenty, G.; Stoddart, L. A.; Lane, J. R., Novel pharmacological applications of G-protein-coupled receptor-G protein fusions. *Curr Opin Pharmacol* **2007,** *7* (5), 521-6.

181. Milligan, G.; Feng, G. J.; Ward, R. J.; Sartania, N.; Ramsay, D.; McLean, A. J.; Carrillo, J. J., G protein-coupled receptor fusion proteins in drug discovery. *Curr Pharm Des* **2004,** *10* (17), 1989-2001.

182. Burt, A. R.; Sautel, M.; Wilson, M. A.; Rees, S.; Wise, A.; Milligan, G., Agonist occupation of an alpha2A-adrenoreceptor-Gi1alpha fusion protein results in activation of both receptor-linked and endogenous Gi proteins. Comparisons of their contributions to GTPase activity and signal transduction and analysis of receptor-G protein activation stoichiometry. *J Biol Chem* **1998,** *273* (17), 10367-75.

183. White, C. D.; Coetsee, M.; Morgan, K.; Flanagan, C. A.; Millar, R. P.; Lu, Z. L., A crucial role for Galphaq/11, but not Galphai/o or Galphas, in gonadotropin-releasing hormone receptor-mediated cell growth inhibition. *Mol Endocrinol* **2008,** *22* (11), 2520-30.

184. Joseph, P. R. B.; Rajarathnam, K., Solution NMR characterization of WT CXCL8 monomer and dimer binding to CXCR1 N-terminal domain. *Protein Science* **2015,** *24* (1), 81-92.

185. Ravindran, A.; Joseph, P. R. B.; Rajarathnam, K., Structural Basis for Differential Binding of the Interleukin-8 Monomer and Dimer to the CXCR1 N-Domain: Role of Coupled Interactions and Dynamics. *Biochemistry* **2009,** *48* (37), 8795-8805.

186. Skelton, N. J.; Quan, C.; Reilly, D.; Lowman, H., Structure of a CXC chemokine-receptor fragment in complex with interleukin-8. *Structure* **1999,** *7* (2), 157-68.

187. Clubb, R. T.; Omichinski, J. G.; Clore, G. M.; Gronenborn, A. M., Mapping the binding surface of interleukin-8 complexed with an N-terminal fragment of the type 1 human interleukin-8 receptor. *FEBS Lett* **1994,** *338* (1), 93-7.

188. Clark-Lewis, I.; Schumacher, C.; Baggiolini, M.; Moser, B., Structure-activity relationships of interleukin-8 determined using chemically synthesized analogs. Critical role of NH2-terminal residues and evidence for uncoupling of neutrophil chemotaxis, exocytosis, and receptor binding activities. *J Biol Chem* **1991,** *266* (34), 23128-34.

189. Hebert, C. A.; Chuntharapai, A.; Smith, M.; Colby, T.; Kim, J.; Horuk, R., Partial Functional Mapping of the Human Interleukin-8 Type-a Receptor - Identification of a Major Ligand-Binding Domain. *Journal of Biological Chemistry* **1993,** *268* (25), 18549-18553.

190. Leong, S. R.; Kabakoff, R. C.; Hebert, C. A., Complete mutagenesis of the extracellular domain of interleukin-8 (IL-8) type A receptor identifies charged residues mediating IL-8 binding and signal transduction. *J Biol Chem* **1994,** *269* (30), 19343-8.

191. Suetomi, K.; Rojo, D.; Navarro, J., Identification of a signal transduction switch in the chemokine receptor CXCR1. *Journal of Biological Chemistry* **2002,** *277* (35), 31563-31566.

192. Fernando, H.; Nagle, G. T.; Rajarathnam, K., Thermodynamic characterization of interleukin-8 monomer binding to CXCR1 receptor N-terminal domain. *Febs J* **2007,** *274* (1), 241-251.

193. Rajagopalan, L.; Rajarathnam, K., Structural basis of chemokine receptor function--a model for binding affinity and ligand selectivity. *Biosci Rep* **2006,** *26* (5), 325-39.

194. Milligan, G.; Kostenis, E., Heterotrimeric G-proteins: a short history. *Br J Pharmacol* **2006,** *147 Suppl 1*, S46-55.

195. Joseph, P. R.; Sarmiento, J. M.; Mishra, A. K.; Das, S. T.; Garofalo, R. P.; Navarro, J.; Rajarathnam, K., Probing the role of CXC motif in chemokine CXCL8 for high affinity binding and activation of CXCR1 and CXCR2 receptors. *J Biol Chem* **2010,** *285* (38), 29262-9.

196. Sharma, B.; Singh, S.; Varney, M. L.; Singh, R. K., Targeting CXCR1/CXCR2 receptor antagonism in malignant melanoma. *Expert Opin Ther Targets* **2010,** *14* (4), 435-42.

197. Singh, S.; Nannuru, K. C.; Sadanandam, A.; Varney, M. L.; Singh, R. K., CXCR1 and CXCR2 enhances human melanoma tumourigenesis, growth and invasion. *Br J Cancer* **2009,** *100* (10), 1638-46.

198. Waugh, D. J.; Wilson, C., The interleukin-8 pathway in cancer. *Clin Cancer Res* **2008,** *14* (21), 6735-41.

199. Wu, D.; LaRosa, G. J.; Simon, M. I., G protein-coupled signal transduction pathways for interleukin-8. *Science* **1993,** *261* (5117), 101-3.

200. Richardson, R. M.; Marjoram, R. J.; Barak, L. S.; Snyderman, R., Role of the cytoplasmic tails of CXCR1 and CXCR2 in mediating leukocyte migration, activation, and regulation. *J Immunol* **2003,** *170* (6), 2904-11.

201. Han, M.; Smith, S. O.; Sakmar, T. P., Constitutive activation of opsin by mutation of methionine 257 on transmembrane helix 6. *Biochemistry* **1998,** *37* (22), 8253-61.

202. Fuhrer, D.; Wonerow, P.; Willgerodt, H.; Paschke, R., Identification of a new thyrotropin receptor germline mutation (Leu629Phe) in a family with neonatal onset of autosomal dominant nonautoimmune hyperthyroidism. *J Clin Endocrinol Metab* **1997,** *82* (12), 4234-8.

203. Kim, J. M.; Altenbach, C.; Kono, M.; Oprian, D. D.; Hubbell, W. L.; Khorana, H. G., Structural origins of constitutive activation in rhodopsin: Role of the K296/E113 salt bridge. *Proc Natl Acad Sci U S A* **2004,** *101* (34), 12508-13.

204. Tao, Y. X., Constitutive activation of G protein-coupled receptors and diseases: insights into mechanisms of activation and therapeutics. *Pharmacol Ther* **2008,** *120* (2), 129-48.

205. Preininger, A. M.; Meiler, J.; Hamm, H. E., Conformational flexibility and structural dynamics in GPCR-mediated G protein activation: a perspective. *J Mol Biol* **2013,** *425* (13), 2288-98.

206. Louet, M.; Perahia, D.; Martinez, J.; Floquet, N., A concerted mechanism for opening the GDP binding pocket and release of the nucleotide in hetero-trimeric G-proteins. *J Mol Biol* **2011,** *411* (1), 298-312.

207. Palczewski, K.; Kumasaka, T.; Hori, T.; Behnke, C. A.; Motoshima, H.; Fox, B. A.; Le Trong, I.; Teller, D. C.; Okada, T.; Stenkamp, R. E.; Yamamoto, M.; Miyano, M., Crystal structure of rhodopsin: A G protein-coupled receptor. *Science* **2000,** *289* (5480), 739-45.

208. Cherezov, V.; Rosenbaum, D. M.; Hanson, M. A.; Rasmussen, S. G.; Thian, F. S.; Kobilka, T. S.; Choi, H. J.; Kuhn, P.; Weis, W. I.; Kobilka, B. K.; Stevens, R. C., High-resolution crystal structure of an engineered human beta2-adrenergic G protein-coupled receptor. *Science* **2007,** *318* (5854), 1258-65.

209. Rasmussen, S. G.; Choi, H. J.; Rosenbaum, D. M.; Kobilka, T. S.; Thian, F. S.; Edwards, P. C.; Burghammer, M.; Ratnala, V. R.; Sanishvili, R.; Fischetti, R. F.; Schertler, G. F.; Weis, W. I.; Kobilka, B. K., Crystal structure of the human beta2 adrenergic G-protein-coupled receptor. *Nature* **2007,** *450* (7168), 383-7.

210. Rosenbaum, D. M.; Cherezov, V.; Hanson, M. A.; Rasmussen, S. G.; Thian, F. S.; Kobilka, T. S.; Choi, H. J.; Yao, X. J.; Weis, W. I.; Stevens, R. C.; Kobilka, B. K., GPCR engineering yields high-resolution structural insights into beta2-adrenergic receptor function. *Science* **2007,** *318* (5854), 1266-73.

211. Warne, T.; Serrano-Vega, M. J.; Baker, J. G.; Moukhametzianov, R.; Edwards, P. C.; Henderson, R.; Leslie, A. G.; Tate, C. G.; Schertler, G. F., Structure of a beta1-adrenergic G-protein-coupled receptor. *Nature* **2008,** *454* (7203), 486-91.

212. Wu, B.; Chien, E. Y.; Mol, C. D.; Fenalti, G.; Liu, W.; Katritch, V.; Abagyan, R.; Brooun, A.; Wells, P.; Bi, F. C.; Hamel, D. J.; Kuhn, P.; Handel, T. M.; Cherezov, V.; Stevens, R. C., Structures of the CXCR4 chemokine GPCR with small-molecule and cyclic peptide antagonists. *Science* **2010,** *330* (6007), 1066-71.

213. Chien, E. Y.; Liu, W.; Zhao, Q.; Katritch, V.; Han, G. W.; Hanson, M. A.; Shi, L.; Newman, A. H.; Javitch, J. A.; Cherezov, V.; Stevens, R. C., Structure of the human dopamine D3 receptor in complex with a D2/D3 selective antagonist. *Science* **2010,** *330* (6007), 1091-5.

214. Shimamura, T.; Shiroishi, M.; Weyand, S.; Tsujimoto, H.; Winter, G.; Katritch, V.; Abagyan, R.; Cherezov, V.; Liu, W.; Han, G. W.; Kobayashi, T.; Stevens, R. C.; Iwata, S., Structure of the human histamine H1 receptor complex with doxepin. *Nature* **2011,** *475* (7354), 65-70.

215. Kruse, A. C.; Hu, J.; Pan, A. C.; Arlow, D. H.; Rosenbaum, D. M.; Rosemond, E.; Green, H. F.; Liu, T.; Chae, P. S.; Dror, R. O.; Shaw, D. E.; Weis, W. I.; Wess, J.; Kobilka, B. K., Structure and dynamics of the M3 muscarinic acetylcholine receptor. *Nature* **2012,** *482* (7386), 552-6.

216. Zhang, C.; Srinivasan, Y.; Arlow, D. H.; Fung, J. J.; Palmer, D.; Zheng, Y.; Green, H. F.; Pandey, A.; Dror, R. O.; Shaw, D. E.; Weis, W. I.; Coughlin, S. R.; Kobilka, B. K., High-resolution crystal structure of human protease-activated receptor 1. *Nature* **2012,** *492* (7429), 387-92.

217. Radoicic, J.; Lu, G. J.; Opella, S. J., NMR structures of membrane proteins in phospholipid bilayers. *Q Rev Biophys* **2014,** *47* (3), 249-83.

218. Park, S. H.; Casagrande, F.; Das, B. B.; Albrecht, L.; Chu, M.; Opella, S. J., Local and global dynamics of the G protein-coupled receptor CXCR1. *Biochemistry* **2011,** *50* (12), 2371-80.

219. Park, S. H.; Casagrande, F.; Cho, L.; Albrecht, L.; Opella, S. J., Interactions of interleukin-8 with the human chemokine receptor CXCR1 in phospholipid bilayers by NMR spectroscopy. *J Mol Biol* **2011,** *414* (2), 194-203.

220. Park, S. H.; Das, B. B.; Casagrande, F.; Tian, Y.; Nothnagel, H. J.; Chu, M.; Kiefer, H.; Maier, K.; De Angelis, A. A.; Marassi, F. M.; Opella, S. J., Structure of the chemokine receptor CXCR1 in phospholipid bilayers. *Nature* **2012,** *491* (7426), 779-83.

221. Park, S. H.; Berkamp, S.; Radoicic, J.; De Angelis, A. A.; Opella, S. J., Interaction of Monomeric Interleukin-8 with CXCR1 Mapped by Proton-Detected Fast MAS Solid-State NMR. *Biophys J* **2017,** *113* (12), 2695-2705.

222. Park, S. H.; Wang, V. S.; Radoicic, J.; De Angelis, A. A.; Berkamp, S.; Opella, S. J., Paramagnetic relaxation enhancement of membrane proteins by incorporation of the metal-chelating unnatural amino acid 2-amino-3-(8-hydroxyquinolin-3-yl)propanoic acid (HQA). *J Biomol NMR* **2015,** *61* (3-4), 185-96.

223. Visvader, J. E.; Lindeman, G. J., Cancer stem cells in solid tumours: accumulating evidence and unresolved questions. *Nat Rev Cancer* **2008,** *8* (10), 755-68.

224. Ginestier, C.; Liu, S.; Diebel, M. E.; Korkaya, H.; Luo, M.; Brown, M.; Wicinski, J.; Cabaud, O.; Charafe-Jauffret, E.; Birnbaum, D.; Guan, J. L.; Dontu, G.; Wicha, M. S., CXCR1 blockade selectively targets human breast cancer stem cells in vitro and in xenografts. *J Clin Invest* **2010,** *120* (2), 485-97.

225. Bizzarri, C.; Beccari, A. R.; Bertini, R.; Cavicchia, M. R.; Giorgini, S.; Allegretti, M., ELR+ CXC chemokines and their receptors (CXC chemokine receptor 1 and CXC chemokine receptor 2) as new therapeutic targets. *Pharmacol Ther* **2006,** *112* (1), 139-49.

226. Casilli, F.; Bianchini, A.; Gloaguen, I.; Biordi, L.; Alesse, E.; Festuccia, C.; Cavalieri, B.; Strippoli, R.; Cervellera, M. N.; Di Bitondo, R.; Ferretti, E.; Mainiero, F.; Bizzarri, C.; Colotta, F.; Bertini, R., Inhibition of interleukin-8 (CXCL8/IL-8) responses by repertaxin, a new inhibitor of the chemokine receptors CXCR1 and CXCR2. *Biochem Pharmacol* **2005,** *69* (3), 385-94.

227. Cavalieri, B.; Mosca, M.; Ramadori, P.; Perrelli, M. G.; De Simone, L.; Colotta, F.; Bertini, R.; Poli, G.; Cutrin, J. C., Neutrophil recruitment in the reperfused-injured rat liver was effectively attenuated by repertaxin, a novel allosteric noncompetitive inhibitor of CXCL8 receptors: a therapeutic approach for the treatment of post-ischemic hepatic syndromes. *Int J Immunopathol Pharmacol* **2005,** *18* (3), 475-86.

228. Garau, A.; Bertini, R.; Colotta, F.; Casilli, F.; Bigini, P.; Cagnotto, A.; Mennini, T.; Ghezzi, P.; Villa, P., Neuroprotection with the CXCL8 inhibitor repertaxin in transient brain ischemia. *Cytokine* **2005,** *30* (3), 125-31.

229. Lefkowitz, R. J., G proteins in medicine. *N Engl J Med* **1995,** *332* (3), 186-7.

230. Neves, S. R.; Ram, P. T.; Iyengar, R., G protein pathways. *Science* **2002,** *296* (5573), 1636-9.

231. Spiegel, A. M.; Weinstein, L. S., Inherited diseases involving g proteins and g protein-coupled receptors. *Annu Rev Med* **2004,** *55*, 27-39.

232. Hamm, H. E., The many faces of G protein signaling. *J Biol Chem* **1998,** *273* (2), 669-72.

233. Coleman, D. E.; Berghuis, A. M.; Lee, E.; Linder, M. E.; Gilman, A. G.; Sprang, S. R., Structures of active conformations of Gi alpha 1 and the mechanism of GTP hydrolysis. *Science* **1994,** *265* (5177), 1405-12.

234. Noel, J. P.; Hamm, H. E.; Sigler, P. B., The 2.2 A crystal structure of transducin-alpha complexed with GTP gamma S. *Nature* **1993,** *366* (6456), 654-63.

235. Resh, M. D., Regulation of cellular signalling by fatty acid acylation and prenylation of signal transduction proteins. *Cell Signal* **1996,** *8* (6), 403-12.

236. Lambright, D. G.; Sondek, J.; Bohm, A.; Skiba, N. P.; Hamm, H. E.; Sigler, P. B., The 2.0 A crystal structure of a heterotrimeric G protein. *Nature* **1996,** *379* (6563), 311-9.

237. Lambright, D. G.; Noel, J. P.; Hamm, H. E.; Sigler, P. B., Structural determinants for activation of the alpha-subunit of a heterotrimeric G protein. *Nature* **1994,** *369* (6482), 621-8.

238. Skiba, N. P.; Bae, H.; Hamm, H. E., Mapping of effector binding sites of transducin alpha-subunit using G alpha t/G alpha i1 chimeras. *J Biol Chem* **1996,** *271* (1), 413-24.

239. Sprang, S. R., G protein mechanisms: insights from structural analysis. *Annu Rev Biochem* **1997,** *66*, 639-78.

240. Kjeldgaard, M.; Nyborg, J.; Clark, B. F., The GTP binding motif: variations on a theme. *FASEB J* **1996,** *10* (12), 1347-68.

241. Clapham, D. E.; Neer, E. J., G protein beta gamma subunits. *Annu Rev Pharmacol Toxicol* **1997,** *37*, 167-203.

242. Sondek, J.; Bohm, A.; Lambright, D. G.; Hamm, H. E.; Sigler, P. B., Crystal structure of a G-protein beta gamma dimer at 2.1A resolution. *Nature* **1996,** *379* (6563), 369-74.

243. Chen, J.; DeVivo, M.; Dingus, J.; Harry, A.; Li, J.; Sui, J.; Carty, D. J.; Blank, J. L.; Exton, J. H.; Stoffel, R. H.; et al., A region of adenylyl cyclase 2 critical for regulation by G protein beta gamma subunits. *Science* **1995,** *268* (5214), 1166-9.

244. Cabrera-Vera, T. M.; Vanhauwe, J.; Thomas, T. O.; Medkova, M.; Preininger, A.; Mazzoni, M. R.; Hamm, H. E., Insights into G protein structure, function, and regulation. *Endocr Rev* **2003,** *24* (6), 765-81.

245. Preininger, A. M.; Hamm, H. E., G protein signaling: insights from new structures. *Sci STKE* **2004,** *2004* (218), re3.

246. Hamm, H. E., How activated receptors couple to G proteins. *Proc Natl Acad Sci U S A* **2001,** *98* (9), 4819-21.

247. Wess, J., Molecular basis of receptor/G-protein-coupling selectivity. *Pharmacol Ther* **1998,** *80* (3), 231-64.

248. Rasmussen, S. G.; DeVree, B. T.; Zou, Y.; Kruse, A. C.; Chung, K. Y.; Kobilka, T. S.; Thian, F. S.; Chae, P. S.; Pardon, E.; Calinski, D.; Mathiesen, J. M.; Shah, S. T.; Lyons, J. A.; Caffrey, M.; Gellman, S. H.; Steyaert, J.; Skiniotis, G.; Weis, W. I.; Sunahara, R. K.; Kobilka, B. K., Crystal structure of the beta2 adrenergic receptor-Gs protein complex. *Nature* **2011,** *477* (7366), 549-55.

249. Oldham, W. M.; Van Eps, N.; Preininger, A. M.; Hubbell, W. L.; Hamm, H. E., Mechanism of the receptor-catalyzed activation of heterotrimeric G proteins. *Nat Struct Mol Biol* **2006,** *13* (9), 772-7.

250. Hamm, H. E.; Deretic, D.; Arendt, A.; Hargrave, P. A.; Koenig, B.; Hofmann, K. P., Site of G protein binding to rhodopsin mapped with synthetic peptides from the alpha subunit. *Science* **1988,** *241* (4867), 832-5.

251. Martin, E. L.; Rens-Domiano, S.; Schatz, P. J.; Hamm, H. E., Potent peptide analogues of a G protein receptor-binding region obtained with a combinatorial library. *J Biol Chem* **1996,** *271* (1), 361-6.

252. Choe, H. W.; Kim, Y. J.; Park, J. H.; Morizumi, T.; Pai, E. F.; Krauss, N.; Hofmann, K. P.; Scheerer, P.; Ernst, O. P., Crystal structure of metarhodopsin II. *Nature* **2011,** *471* (7340), 651-5.

253. Scheerer, P.; Park, J. H.; Hildebrand, P. W.; Kim, Y. J.; Krauss, N.; Choe, H. W.; Hofmann, K. P.; Ernst, O. P., Crystal structure of opsin in its G-protein-interacting conformation. *Nature* **2008,** *455* (7212), 497-502.

254. Kostenis, E.; Waelbroeck, M.; Milligan, G., Techniques: promiscuous Galpha proteins in basic research and drug discovery. *Trends Pharmacol Sci* **2005,** *26* (11), 595-602.

255. Orban, T.; Jastrzebska, B.; Gupta, S.; Wang, B.; Miyagi, M.; Chance, M. R.; Palczewski, K., Conformational dynamics of activation for the pentameric complex of dimeric G protein-coupled receptor and heterotrimeric G protein. *Structure* **2012,** *20* (5), 826-40.

256. Chung, K. Y.; Rasmussen, S. G.; Liu, T.; Li, S.; DeVree, B. T.; Chae, P. S.; Calinski, D.; Kobilka, B. K.; Woods, V. L., Jr.; Sunahara, R. K., Conformational changes in the G protein Gs induced by the beta2 adrenergic receptor. *Nature* **2011,** *477* (7366), 611-5.

257. Blahos, J.; Fischer, T.; Brabet, I.; Stauffer, D.; Rovelli, G.; Bockaert, J.; Pin, J. P., A novel site on the Galpha -protein that recognizes heptahelical receptors. *J Biol Chem* **2001,** *276* (5), 3262-9.

258. Kostenis, E.; Degtyarev, M. Y.; Conklin, B. R.; Wess, J., The N-terminal extension of Galphaq is critical for constraining the selectivity of receptor coupling. *J Biol Chem* **1997,** *272* (31), 19107-10.

259. Slessareva, J. E.; Graber, S. G., Reconstitution reveals additional roles for N- and C-terminal domains of g(alpha) in muscarinic receptor coupling. *Biochemistry* **2003,** *42* (24), 7552-60.

260. Preininger, A. M.; Parello, J.; Meier, S. M.; Liao, G.; Hamm, H. E., Receptor-mediated changes at the myristoylated amino terminus of Galpha(il) proteins. *Biochemistry* **2008,** *47* (39), 10281-93.

261. Marin, E. P.; Krishna, A. G.; Sakmar, T. P., Disruption of the alpha5 helix of transducin impairs rhodopsin-catalyzed nucleotide exchange. *Biochemistry* **2002,** *41* (22), 6988-94.

262. Gilchrist, A.; Vanhauwe, J. F.; Li, A.; Thomas, T. O.; Voyno-Yasenetskaya, T.; Hamm, H. E., G alpha minigenes expressing C-terminal peptides serve as specific inhibitors of thrombin-mediated endothelial activation. *J Biol Chem* **2001,** *276* (28), 25672-9.

263. Bae, H.; Cabrera-Vera, T. M.; Depree, K. M.; Graber, S. G.; Hamm, H. E., Two amino acids within the alpha4 helix of Galphai1 mediate coupling with 5-hydroxytryptamine1B receptors. *J Biol Chem* **1999,** *274* (21), 14963-71.

264. Natochin, M.; Granovsky, A. E.; Muradov, K. G.; Artemyev, N. O., Roles of the transducin alpha-subunit alpha4-helix/alpha4-beta6 loop in the receptor and effector interactions. *J Biol Chem* **1999,** *274* (12), 7865-9.

265. Mody, S. M.; Ho, M. K.; Joshi, S. A.; Wong, Y. H., Incorporation of Galpha(z)-specific sequence at the carboxyl terminus increases the promiscuity of galpha(16) toward G(i)-coupled receptors. *Mol Pharmacol* **2000,** *57* (1), 13-23.

266. Hazari, A.; Lowes, V.; Chan, J. H.; Wong, C. S.; Ho, M. K.; Wong, Y. H., Replacement of the alpha5 helix of Galpha16 with Galphas-specific sequences enhances promiscuity of Galpha16 toward Gs-coupled receptors. *Cell Signal* **2004,** *16* (1), 51-62.

267. Ho, M. K.; Chan, J. H.; Wong, C. S.; Wong, Y. H., Identification of a stretch of six divergent amino acids on the alpha5 helix of Galpha16 as a major determinant of the promiscuity and efficiency of receptor coupling. *Biochem J* **2004,** *380* (Pt 2), 361-9.

268. Grishina, G.; Berlot, C. H., A surface-exposed region of G(salpha) in which substitutions decrease receptor-mediated activation and increase receptor affinity. *Mol Pharmacol* **2000,** *57* (6), 1081-92.

269. Taylor, J. M.; Jacob-Mosier, G. G.; Lawton, R. G.; VanDort, M.; Neubig, R. R., Receptor and membrane interaction sites on Gbeta. A receptor-derived peptide binds to the carboxyl terminus. *J Biol Chem* **1996,** *271* (7), 3336-9.

270. Kisselev, O.; Pronin, A.; Ermolaeva, M.; Gautam, N., Receptor-G protein coupling is established by a potential conformational switch in the beta gamma complex. *Proc Natl Acad Sci U S A* **1995,** *92* (20), 9102-6.

271. Yasuda, H.; Lindorfer, M. A.; Woodfork, K. A.; Fletcher, J. E.; Garrison, J. C., Role of the prenyl group on the G protein gamma subunit in coupling trimeric G proteins to A1 adenosine receptors. *J Biol Chem* **1996,** *271* (31), 18588-95.

272. Preininger, A. M.; Funk, M. A.; Oldham, W. M.; Meier, S. M.; Johnston, C. A.; Adhikary, S.; Kimple, A. J.; Siderovski, D. P.; Hamm, H. E.; Iverson, T. M., Helix dipole movement and conformational variability contribute to allosteric GDP release in Galphai subunits. *Biochemistry* **2009,** *48* (12), 2630-42.

273. Kapoor, N.; Menon, S. T.; Chauhan, R.; Sachdev, P.; Sakmar, T. P., Structural evidence for a sequential release mechanism for activation of heterotrimeric G proteins. *J Mol Biol* **2009,** *393* (4), 882-97.

274. Louet, M.; Martinez, J.; Floquet, N., GDP release preferentially occurs on the phosphate side in heterotrimeric G-proteins. *PLoS Comput Biol* **2012,** *8* (7), e1002595.

275. Tesmer, J. J.; Sunahara, R. K.; Gilman, A. G.; Sprang, S. R., Crystal structure of the catalytic domains of adenylyl cyclase in a complex with Gsalpha.GTPgammaS. *Science* **1997,** *278* (5345), 1907-16.

276. Dratz, E. A.; Furstenau, J. E.; Lambert, C. G.; Thireault, D. L.; Rarick, H.; Schepers, T.; Pakhlevaniants, S.; Hamm, H. E., NMR structure of a receptor-bound G-protein peptide. *Nature* **1993,** *363* (6426), 276-81.

277. Rasenick, M. M.; Watanabe, M.; Lazarevic, M. B.; Hatta, S.; Hamm, H. E., Synthetic peptides as probes for G protein function. Carboxyl-terminal G alpha s peptides mimic Gs and evoke high affinity agonist binding to beta-adrenergic receptors. *J Biol Chem* **1994,** *269* (34), 21519-25.

278. Gilchrist, A.; Mazzoni, M. R.; Dineen, B.; Dice, A.; Linden, J.; Proctor, W. R.; Lupica, C. R.; Dunwiddie, T. V.; Hamm, H. E., Antagonists of the receptor-G protein interface block Gi-coupled signal transduction. *J Biol Chem* **1998,** *273* (24), 14912-9.

279. Mazzoni, M. R.; Taddei, S.; Giusti, L.; Rovero, P.; Galoppini, C.; D'Ursi, A.; Albrizio, S.; Triolo, A.; Novellino, E.; Greco, G.; Lucacchini, A.; Hamm, H. E., A galpha(s) carboxyl-terminal peptide prevents G(s) activation by the A(2A) adenosine receptor. *Mol Pharmacol* **2000,** *58* (1), 226-36.

280. Oldham, W. M.; Hamm, H. E., Structural basis of function in heterotrimeric G proteins. *Q Rev Biophys* **2006,** *39* (2), 117-66.

281. Westfield, G. H.; Rasmussen, S. G.; Su, M.; Dutta, S.; DeVree, B. T.; Chung, K. Y.; Calinski, D.; Velez-Ruiz, G.; Oleskie, A. N.; Pardon, E.; Chae, P. S.; Liu, T.; Li, S.; Woods, V. L., Jr.; Steyaert, J.; Kobilka, B. K.; Sunahara, R. K.; Skiniotis, G., Structural flexibility of the G alpha s alpha-helical domain in the beta2-adrenoceptor Gs complex. *Proc Natl Acad Sci U S A* **2011,** *108* (38), 16086-91.

282. Kimple, A. J.; Soundararajan, M.; Hutsell, S. Q.; Roos, A. K.; Urban, D. J.; Setola, V.; Temple, B. R.; Roth, B. L.; Knapp, S.; Willard, F. S.; Siderovski, D. P., Structural determinants of G-protein alpha subunit selectivity by regulator of G-protein signaling 2 (RGS2). *J Biol Chem* **2009,** *284* (29), 19402-11.

283. Singh, G.; Ramachandran, S.; Cerione, R. A., A constitutively active Galpha subunit provides insights into the mechanism of G protein activation. *Biochemistry* **2012,** *51* (15), 3232-40.

284. Liu, P.; Jia, M. Z.; Zhou, X. E.; De Waal, P. W.; Dickson, B. M.; Liu, B.; Hou, L.; Yin, Y. T.; Kang, Y. Y.; Shi, Y.; Melcher, K.; Xu, H. E.; Jiang, Y., The structural basis of the dominant negative phenotype of the Galphai1beta1gamma2 G203A/A326S heterotrimer. *Acta Pharmacol Sin* **2016,** *37* (9), 1259-72.

285. Sammond, D. W.; Eletr, Z. M.; Purbeck, C.; Kimple, R. J.; Siderovski, D. P.; Kuhlman, B., Structure-based protocol for identifying mutations that enhance protein-protein binding affinities. *J Mol Biol* **2007,** *371* (5), 1392-404.

286. Kisselev, O. G.; Downs, M. A., Rhodopsin controls a conformational switch on the transducin gamma subunit. *Structure* **2003,** *11* (4), 367-373.

287. Kisselev, O. G.; Kao, J.; Ponder, J. W.; Fann, Y. C.; Gautam, N.; Marshall, G. R., Light-activated rhodopsin induces structural binding motif in G protein alpha subunit. *P Natl Acad Sci USA* **1998,** *95* (8), 4270-4275.

288. Koenig, B. W.; Kontaxis, G.; Mitchell, D. C.; Louis, J. M.; Litman, B. J.; Bax, A., Structure and orientation of a G protein fragment in the receptor bound state from residual dipolar couplings. *Journal of Molecular Biology* **2002,** *322* (2), 441-461.

289. Maly, J.; Crowhurst, K. A., Expression, purification and preliminary NMR characterization of isotopically labeled wild-type human heterotrimeric G protein alphai1. *Protein Expr Purif* **2012,** *84* (2), 255-64.

290. Mase, Y.; Yokogawa, M.; Osawa, M.; Shimada, I., Backbone resonance assignments for G protein alpha(i3) subunit in the GTP-bound state. *Biomol NMR Assign* **2012,** *6* (2), 217-20.

291. Mase, Y.; Yokogawa, M.; Osawa, M.; Shimada, I., Backbone resonance assignments for G protein alpha(i3) subunit in the GDP-bound state. *Biomol NMR Assign* **2014,** *8* (2), 237-41.

292. Goricanec, D.; Stehle, R.; Egloff, P.; Grigoriu, S.; Pluckthun, A.; Wagner, G.; Hagn, F., Conformational dynamics of a G-protein alpha subunit is tightly regulated by nucleotide binding. *Proc Natl Acad Sci U S A* **2016,** *113* (26), E3629-38.

293. Rajarathnam, K.; Kay, C. M.; Clark-Lewis, I.; Sykes, B. D., Characterization of quaternary structure of interleukin-8 and functional implications. *Methods Enzymol* **1997,** *287*, 89-105.

294. Casagrande, F.; Maier, K.; Kiefer, H.; Opella, S. J.; Park, S. H., Expression and Purification of G-Protein-Coupled Receptors for Nuclear Magnetic Resonance Structural Studies. *Production of Membrane Proteins: Strategies for Expression and Isolation* **2011**, 297-316.

295. Fernando, H.; Chin, C.; Rosgen, J.; Rajarathnam, K., Dimer dissociation is essential for interleukin-8 (IL-8) binding to CXCR1 receptor. *Journal of Biological Chemistry* **2004,** *279* (35), 36175-36178.

296. Rajagopalan, L.; Rajarathnam, K., Ligand selectivity and affinity of chemokine receptor CXCR1. Role of N-terminal domain. *J Biol Chem* **2004,** *279* (29), 30000-8.

297. Burrows, S. D.; Doyle, M. L.; Murphy, K. P.; Franklin, S. G.; White, J. R.; Brooks, I.; Mcnulty, D. E.; Scott, M. O.; Knutson, J. R.; Porter, D.; Young, P. R.; Hensley, P., Determination of the Monomer-Dimer Equilibrium of Interleukin-8 Reveals It Is a Monomer at Physiological Concentrations. *Biochemistry* **1994,** *33* (43), 12741-12745.

298. Berkamp, S.; Park, S. H.; De Angelis, A. A.; Marassi, F. M.; Opella, S. J., Structure of monomeric Interleukin-8 and its interactions with the N-terminal Binding Site-I of CXCR1 by solution NMR spectroscopy. *Journal of Biomolecular Nmr* **2017,** *69* (3), 111-121.

299. Saunders, M.; Wishnia, A.; Kirkwood, J. G., The Nuclear Magnetic Resonance Spectrum of Ribonuclease. *Journal of the American Chemical Society* **1957,** *79* (12), 3289-3290.

300. Meadows, D. H.; Markley, J. L.; Cohen, J. S.; Jardetzky, O., Nuclear magnetic resonance studies of the structure and binding sites of enzymes. I. Histidine residues. *Proc Natl Acad Sci U S A* **1967,** *58* (4), 1307-13.

301. Markley, J. L.; Putter, I.; Jardetzky, O., High-Resolution Nuclear Magnetic Resonance Spectra of Selectively Deuterated Staphylococcal Nuclease. *Science* **1968,** *161* (3847), 1249-+.

302. Cross, T. A.; Opella, S. J., Nmr of Fd Coat Protein. *J Supramol Str Cell* **1979,** *11* (2), 139-145.

303. Cross, T. A.; Opella, S. J., Structural-Properties of Fd Coat Protein in Sodium Dodecyl-Sulfate Micelles. *Biochem Bioph Res Co* **1980,** *92* (2), 478-484.

304. Hagen, D. S.; Weiner, J. H.; Sykes, B. D., Fluorotyrosine-M13 Coat Protein - F-19 Nuclear Magnetic-Resonance Study of Motional Properties of an Integral Membrane-Protein in Phospholipid Vesicles. *Biochemistry* **1978,** *17* (18), 3860-3866.

305. Hagen, D. S.; Weiner, J. H.; Sykes, B. D., Investigation of Solvent Accessibility of the Fluorotyrosyl Residues of M13 Coat Protein in Deoxycholate Micelles and Phospholipid-Vesicles. *Biochemistry* **1979,** *18* (10), 2007-2012.

306. Morrisett, J. D.; Wien, R. W.; McConnell, H. M., The use of spin labels for measuring distances in biological systems. *Ann N Y Acad Sci* **1973,** *222*, 149-62.

307. Wien, R. W.; Morrisett, J. D.; McConnell, H. M., Spin-label-induced nuclear relaxation. Distances between bound saccharides, histidine-15, and tryptophan-123 on lysozyme in solution. *Biochemistry* **1972,** *11* (20), 3707-16.

308. Campbell, I. D.; Dobson, C. M.; Williams, R. J. P.; Xavier, A. V., Determination of Structure of Proteins in Solution - Lysozyme. *Ann Ny Acad Sci* **1973,** *222* (Dec31), 163-174.

309. Chen, H. L.; Ji, F.; Olman, V.; Mobley, C. K.; Liu, Y. Z.; Zhou, Y. P.; Bushweller, J. H.; Prestegard, J. H.; Xu, Y., Optimal Mutation Sites for PRE Data Collection and Membrane Protein Structure Prediction. *Structure* **2011,** *19* (4), 484-495.

310. Ganguly, S.; Weiner, B. E.; Meiler, J., Membrane Protein Structure Determination using Paramagnetic Tags. *Structure* **2011,** *19* (4), 441-443.

311. Opella, S. J., Structure determination of membrane proteins in their native phospholipid bilayer environment by rotationally aligned solid-state NMR spectroscopy. *Acc Chem Res* **2013,** *46* (9), 2145-53.

312. Mesleh, M. F.; Lee, S.; Veglia, G.; Thiriot, D. S.; Marassi, F. M.; Opella, S. J., Dipolar waves map the structure and topology of helices in membrane proteins. *J Am Chem Soc* **2003,** *125* (29), 8928-35.

313. Lee, H. S.; Spraggon, G.; Schultz, P. G.; Wang, F., Genetic Incorporation of a Metal-Ion Chelating Amino Acid into Proteins as a Biophysical Probe. *Journal of the American Chemical Society* **2009,** *131* (7), 2481-+.

314. Liu, W. M.; Overhand, M.; Ubbink, M., The application of paramagnetic lanthanoid ions in NMR spectroscopy on proteins. *Coordin Chem Rev* **2014,** *273*, 2-12.

315. Otting, G., Protein NMR using paramagnetic ions. *Annu Rev Biophys* **2010,** *39*, 387-405.

316. McConnell, H. M.; McFarland, B. G., Physics and chemistry of spin labels. *Q Rev Biophys* **1970,** *3* (1), 91-136.

317. Parthasarathy, S.; Nishiyama, Y.; Ishii, Y., Sensitivity and resolution enhanced solid-state NMR for paramagnetic systems and biomolecules under very fast magic angle spinning. *Acc Chem Res* **2013,** *46* (9), 2127-35.

318. Ullrich, S. J.; Holper, S.; Glaubitz, C., Paramagnetic doping of a 7TM membrane protein in lipid bilayers by Gd(3)(+)-complexes for solid-state NMR spectroscopy. *J Biomol NMR* **2014,** *58* (1), 27-35.

319. Ward, M. E.; Wang, S.; Krishnamurthy, S.; Hutchins, H.; Fey, M.; Brown, L. S.; Ladizhansky, V., High-resolution paramagnetically enhanced solid-state NMR

spectroscopy of membrane proteins at fast magic angle spinning. *J Biomol NMR* **2014,** *58* (1), 37-47.

320. Prestegard, J. H.; al-Hashimi, H. M.; Tolman, J. R., NMR structures of biomolecules using field oriented media and residual dipolar couplings. *Q Rev Biophys* **2000,** *33* (4), 371-424.

321. Balayssac, S.; Bertini, I.; Lelli, M.; Luchinat, C.; Maletta, M., Paramagnetic ions provide structural restraints in solid-state NMR of proteins. *J Am Chem Soc* **2007,** *129* (8), 2218-9.

322. Bertini, I.; Luchinat, C.; Parigi, G.; Pierattelli, R., Perspectives in paramagnetic NMR of metalloproteins. *Dalton Trans* **2008,** (29), 3782-90.

323. Knight, M. J.; Pell, A. J.; Bertini, I.; Felli, I. C.; Gonnelli, L.; Pierattelli, R.; Herrmann, T.; Emsley, L.; Pintacuda, G., Structure and backbone dynamics of a microcrystalline metalloprotein by solid-state NMR. *P Natl Acad Sci USA* **2012,** *109* (28), 11095-11100.

324. Wohnert, J.; Franz, K. J.; Nitz, M.; Imperiali, B.; Schwalbe, H., Protein alignment by a coexpressed lanthanide-binding tag for the measurement of residual dipolar couplings. *J Am Chem Soc* **2003,** *125* (44), 13338-9.

325. Barthelmes, K.; Reynolds, A. M.; Peisach, E.; Jonker, H. R.; DeNunzio, N. J.; Allen, K. N.; Imperiali, B.; Schwalbe, H., Engineering encodable lanthanide-binding tags into loop regions of proteins. *J Am Chem Soc* **2011,** *133* (4), 808-19.

326. Gaponenko, V.; Dvoretsky, A.; Walsby, C.; Hoffman, B. M.; Rosevear, P. R., Calculation of z-coordinates and orientational restraints using a metal binding tag. *Biochemistry* **2000,** *39* (49), 15217-15224.

327. Keizers, P. M.; Ubbink, M., Paramagnetic tagging for protein structure and dynamics analysis. *Prog Nucl Mag Res Sp* **2011,** *58* (1-2), 88-96.

328. Hass, M. A. S.; Ubbink, M., Structure determination of protein-protein complexes with long-range anisotropic paramagnetic NMR restraints. *Curr Opin Struc Biol* **2014,** *24*, 45-53.

329. Knight, M. J.; Felli, I. C.; Pierattelli, R.; Emsley, L.; Pintacuda, G., Magic Angle Spinning NMR of Paramagnetic Proteins. *Accounts Chem Res* **2013,** *46* (9), 2108-2116.

330. Yagi, H.; Pilla, K. B.; Maleckis, A.; Graham, B.; Huber, T.; Otting, G., Three-dimensional protein fold determination from backbone amide pseudocontact shifts generated by lanthanide tags at multiple sites. *Structure* **2013,** *21* (6), 883-90.

331. Liu, W. M.; Skinner, S. P.; Timmer, M.; Blok, A.; Hass, M. A. S.; Filippov, D. V.; Overhand, M.; Ubbink, M., A Two-Armed Lanthanoid-Chelating Paramagnetic NMR Probe Linked to Proteins via Thioether Linkages. *Chem-Eur J* **2014,** *20* (21), 6256-6258.

332. Su, X. C.; Man, B.; Beeren, S.; Liang, H.; Simonsen, S.; Schmitz, C.; Huber, T.; Messerle, B. A.; Otting, G., A dipicolinic acid tag for rigid lanthanide tagging of proteins and paramagnetic NMR spectroscopy. *J Am Chem Soc* **2008,** *130* (32), 10486-7.

333. Jaroniec, C. P., Solid-state nuclear magnetic resonance structural studies of proteins using paramagnetic probes. *Solid State Nucl Mag* **2012,** *43-44*, 1-13.

334. Sengupta, I.; Nadaud, P. S.; Jaroniec, C. P., Protein structure determination with paramagnetic solid-state NMR spectroscopy. *Acc Chem Res* **2013,** *46* (9), 2117-26.

335. Nadaud, P. S.; Sarkar, M.; Wu, B.; MacPhee, C. E.; Magliery, T. J.; Jaroniec, C. P., Expression and purification of a recombinant amyloidogenic peptide from transthyretin for solid-state NMR spectroscopy. *Protein Expr Purif* **2010,** *70* (1), 101-8.

336. Wang, S.; Munro, R. A.; Shi, L.; Kawamura, I.; Okitsu, T.; Wada, A.; Kim, S. Y.; Jung, K. H.; Brown, L. S.; Ladizhansky, V., Solid-state NMR spectroscopy structure determination of a lipid-embedded heptahelical membrane protein. *Nat Methods* **2013,** *10* (10), 1007-12.

337. Wang, S.; Munro, R. A.; Kim, S. Y.; Jung, K. H.; Brown, L. S.; Ladizhansky, V., Paramagnetic relaxation enhancement reveals oligomerization interface of a membrane protein. *J Am Chem Soc* **2012,** *134* (41), 16995-8.

338. Gottstein, D.; Reckel, S.; Dotsch, V.; Guntert, P., Requirements on Paramagnetic Relaxation Enhancement Data for Membrane Protein Structure Determination by NMR. *Structure* **2012,** *20* (6), 1019-1027.

339. Hilty, C.; Wider, G.; Fernandez, C.; Wuthrich, K., Membrane protein-lipid interactions in mixed micelles studied by NMR spectroscopy with the use of paramagnetic reagents. *Chembiochem* **2004,** *5* (4), 467-473.

340. Liang, B. Y.; Bushweller, J. H.; Tamm, L. K., Site-directed parallel spin-labeling and paramagnetic relaxation enhancement in structure determination of membrane proteins by solution NMR spectroscopy. *Journal of the American Chemical Society* **2006,** *128* (13), 4389-4397.

341. Su, Y.; Hu, F.; Hong, M., Paramagnetic Cu(II) for probing membrane protein structure and function: inhibition mechanism of the influenza M2 proton channel. *J Am Chem Soc* **2012,** *134* (20), 8693-702.

342. Yeo, K. J.; Kim, H. Y.; Kim, Y. P.; Hwang, E.; Kim, M. H.; Cheong, C.; Choe, S.; Jeon, Y. H., Rapid exploration of the folding topology of helical membrane proteins using paramagnetic perturbation. *Protein Sci* **2010,** *19* (12), 2409-17.

343. Tang, M.; Berthold, D. A.; Rienstra, C. M., Solid-State NMR of a Large Membrane Protein by Paramagnetic Relaxation Enhancement. *J Phys Chem Lett* **2011,** *2* (14), 1836-1841.

344. Page, R. C.; Lee, S.; Moore, J. D.; Opella, S. J.; Cross, T. A., Backbone structure of a small helical integral membrane protein: A unique structural characterization. *Protein Sci* **2009,** *18* (1), 134-46.

345. Cohen, L. S.; Arshava, B.; Neumoin, A.; Becker, J. M.; Guntert, P.; Zerbe, O.; Naider, F., Comparative NMR analysis of an 80-residue G protein-coupled receptor fragment in two membrane mimetic environments. *Bba-Biomembranes* **2011,** *1808* (11), 2674-2684.

346. Liu, C. C.; Schultz, P. G., Adding New Chemistries to the Genetic Code. *Annual Review of Biochemistry, Vol 79* **2010,** *79*, 413-444.

347. Noren, C. J.; Anthony-Cahill, S. J.; Griffith, M. C.; Schultz, P. G., A general method for site-specific incorporation of unnatural amino acids into proteins. *Science* **1989,** *244* (4901), 182-8.

348. Cook, G. A.; Zhang, H.; Park, S. H.; Wang, Y.; Opella, S. J., Comparative NMR studies demonstrate profound differences between two viroporins: p7 of HCV and Vpu of HIV-1. *Biochim Biophys Acta* **2011,** *1808* (2), 554-60.

349. Liu, Z.; Gong, Z.; Guo, D. C.; Zhang, W. P.; Tang, C., Subtle Dynamics of holo Glutamine Binding Protein Revealed with a Rigid Paramagnetic Probe. *Biochemistry* **2014,** *53* (9), 1403-1409.

350. Loh, C. T.; Ozawa, K.; Tuck, K. L.; Barlow, N.; Huber, T.; Otting, G.; Graham, B., Lanthanide Tags for Site-Specific Ligation to an Unnatural Amino Acid and Generation of Pseudocontact Shifts in Proteins. *Bioconjugate Chem* **2013,** *24* (2), 260-268.

351. Jones, D. H.; Cellitti, S. E.; Hao, X. S.; Zhang, Q.; Jahnz, M.; Summerer, D.; Schultz, P. G.; Uno, T.; Geierstanger, B. H., Site-specific labeling of proteins with NMR-active unnatural amino acids. *Journal of Biomolecular Nmr* **2010,** *46* (1), 89-100.

352. Cellitti, S. E.; Jones, D. H.; Lagpacan, L.; Hao, X. S.; Zhang, Q.; Hu, H. Y.; Brittain, S. M.; Brinker, A.; Caldwell, J.; Bursulaya, B.; Spraggon, G.; Brock, A.; Ryu, Y.; Uno, T.; Schultz, P. G.; Geierstanger, B. H., In vivo incorporation of unnatural amino acids to probe structure, dynamics, and ligand binding in a large protein by nuclear magnetic resonance spectroscopy. *Journal of the American Chemical Society* **2008,** *130* (29), 9268-9281.

353. Deiters, A.; Geierstanger, B. H.; Schultz, P. G., Site-specific in vivo labeling of proteins for NMR studies. *Chembiochem* **2005,** *6* (1), 55-58.

354. Nguyen, T. H.; Ozawa, K.; Stanton-Cook, M.; Barrow, R.; Huber, T.; Otting, G., Generation of pseudocontact shifts in protein NMR spectra with a genetically encoded cobalt(II)-binding amino acid. *Angew Chem Int Ed Engl* **2011,** *50* (3), 692-4.

355. Zhang, W. H.; Otting, G.; Jackson, C. J., Protein engineering with unnatural amino acids. *Curr Opin Struct Biol* **2013,** *23* (4), 581-7.

356. Fleissner, M. R.; Brustad, E. M.; Kalai, T.; Altenbach, C.; Cascio, D.; Peters, F. B.; Hideg, K.; Peuker, S.; Schultz, P. G.; Hubbell, W. L., Site-directed spin labeling of a genetically encoded unnatural amino acid. *P Natl Acad Sci USA* **2009,** *106* (51), 21637-21642.

357. Soroka, K.; Vithanage, R. S.; Phillips, D. A.; Walker, B.; Dasgupta, P. K., Fluorescence Properties of Metal-Complexes of 8-Hydroxyquinoline-5-Sulfonic Acid and Chromatographic Applications. *Anal Chem* **1987,** *59* (4), 629-636.

358. Jacobson, K. A., New paradigms in GPCR drug discovery. *Biochem Pharmacol* **2015,** *98* (4), 541-55.

359. Katritch, V.; Cherezov, V.; Stevens, R. C., Structure-Function of the G Protein-Coupled Receptor Superfamily. *Annu Rev Pharmacol* **2013,** *53*, 531-556.

360. Liang, Y. L.; Khoshouei, M.; Radjainia, M.; Zhang, Y.; Glukhova, A.; Tarrasch, J.; Thal, D. M.; Furness, S. G. B.; Christopoulos, G.; Coudrat, T.; Danev, R.; Baumeister, W.; Miller, L. J.; Christopoulos, A.; Kobilka, B. K.; Wootten, D.; Skiniotis, G.; Sexton, P. M., Phase-plate cryo-EM structure of a class B GPCR-G-protein complex. *Nature* **2017,** *546* (7656), 118-+.

361. Zhang, Y.; Sun, B. F.; Feng, D.; Hu, H. L.; Chu, M.; Qu, Q. H.; Tarrasch, J. T.; Li, S.; Kobilka, T. S.; Kobilka, B. K.; Skiniotis, G., Cryo-EM structure of the activated GLP-1 receptor in complex with a G protein. *Nature* **2017,** *546* (7657), 248-+.

362. Alexander, S. P. H.; Davenport, A. P.; Kelly, E.; Marrion, N.; Peters, J. A.; Benson, H. E.; Faccenda, E.; Pawson, A. J.; Sharman, J. L.; Southan, C.; Davies, J. A.; Aldrich, R.; Attali, B.; Back, M.; Barnes, N. M.; Bathgate, R.; Beart, P. M.; Becirovic, E.; Biel, M.; Birdsall, N. J.; Boison, D.; Brauner-Osborne, H.; Broer, S.; Bryant, C.; Burnstock, G.; Burris, T.; Cain, D.; Calo, G.; Chan, S. L.; Chandy, K. G.; Chiang, N.; Christakos, S.; Christopoulos, A.; Chun, J. J.; Chung, J. J.; Clapham, D. E.; Connor, M. A.; Coons, L.; Cox, H. M.; Dautzenberg, F. M.; Dent, G.; Douglas, S. D.; Dubocovich, M. L.; Edwards, D. P.; Farndale, R.; Fong, T. M.; Forrest, D.; Fowler, C. J.; Fuller, P.; Gainetdinov, R. R.; Gershengorn, M. A.; Goldin, A.; Goldstein, S. A. N.; Grimm, S. L.; Grissmer, S.; Gundlach, A. L.; Hagenbuch, B.; Hammond, J. R.; Hancox, J. C.; Hartig, S.; Hauger, R. L.; Hay, D. L.; Hebert, T.; Hollenberg, A. N.; Holliday, N. D.; Hoyer, D.; Ijzerman, A. P.; Inui, K. I.; Ishii, S.; Jacobson, K. A.; Jan, L. Y.; Jarvis, G. E.; Jensen, R.; Jetten, A.; Jockers, R.; Kaczmarek, L. K.; Kanai, Y.; Kang, H. S.; Karnik, S.; Kerr, I. D.; Korach, K. S.; Lange, C. A.; Larhammar, D.; Leeb-Lundberg, F.; Leurs, R.; Lolait, S. J.; Macewan,

D.; Maguire, J. J.; May, J. M.; Mazella, J.; McArdle, C. A.; McDonnell, D. P.; Michel, M. C.; Miller, L. J.; Mitolo, V.; Monie, T.; Monk, P. N.; Mouillac, B.; Murphy, P. M.; Nahon, J. L.; Nerbonne, J.; Nichols, C. G.; Norel, X.; Oakley, R.; Offermanns, S.; Palmer, L. G.; Panaro, M. A.; Perez-Reyes, E.; Pertwee, R. G.; Pike, J. W.; Pin, J. P.; Pintor, S.; Plant, L. D.; Poyner, D. R.; Prossnitz, E. R.; Pyne, S.; Ren, D.; Richer, J. K.; Rondard, P.; Ross, R. A.; Sackin, H.; Safi, R.; Sanguinetti, M. C.; Sartorius, C. A.; Segaloff, D. L.; Sladek, F. M.; Stewart, G.; Stoddart, L. A.; Striessnig, J.; Summers, R. J.; Takeda, Y.; Tetel, M.; Toll, L.; Trimmer, J. S.; Tsai, M. J.; Tsai, S. Y.; Tucker, S.; Usdin, T. B.; J-P, V.; Vore, M.; Ward, D. T.; Waxman, S. G.; Webb, P.; Wei, A. D.; Weigel, N.; Willars, G. B.; Winrow, C.; Wong, S. S.; Wulff, H.; Ye, R. D.; Young, M.; Zajac, J. M.; Collaborators, C., THE CONCISE GUIDE TO PHARMACOLOGY 2015/16: G protein-coupled receptors. *Brit J Pharmacol* **2015,** *172* (24), 5744-5869.

363. Bendall, L., Chemokines and their receptors in disease. *Histol Histopathol* **2005,** *20* (3), 907-926.

364. Baggiolini, M., CXCL8-the first chemokine. *Front Immunol* **2015,** *6*.

365. Clore, G. M.; Appella, E.; Yamada, M.; Matsushima, K.; Gronenborn, A. M., 3-Dimensional Structure of Interleukin-8 in Solution. *Biochemistry* **1990,** *29* (7), 1689-1696.

366. Baldwin, E. T.; Weber, I. T.; Stcharles, R.; Xuan, J. C.; Appella, E.; Yamada, M.; Matsushima, K.; Edwards, B. F. P.; Clore, G. M.; Gronenborn, A. M.; Wlodawer, A., Crystal-Structure of Interleukin-8 - Symbiosis of Nmr and Crystallography. *P Natl Acad Sci USA* **1991,** *88* (2), 502-506.

367. Das, S. T.; Rajagopalan, L.; Guerrero-Plata, A.; Sai, J.; Richmond, A.; Garofalo, R. P.; Rajarathnam, K., Monomeric and Dimeric CXCL8 Are Both Essential for In Vivo Neutrophil Recruitment. *Plos One* **2010,** *5* (7).

368. Lowman, H. B.; Fairbrother, W. J.; Slagle, P. H.; Kabakoff, R.; Liu, J.; Shire, S.; Hebert, C. A., Monomeric variants of IL-8: Effects of side chain substitutions and solution conditions upon dimer formation. *Protein Science* **1997,** *6* (3), 598-608.

369. Rajarathnam, K.; Clarklewis, I.; Sykes, B. D., H-1-Nmr Solution Structure of an Active Monomeric Interleukin-8. *Biochemistry* **1995,** *34* (40), 12983-12990.

370. Rollins, B. J., Where the Confusion Began: Cloning the First Chemokine Receptors. *Journal of Immunology* **2009,** *183* (5), 2893-2894.

371. Murphy, P. M.; Tiffany, H. L., Cloning of Complementary-DNA Encoding a Functional Human Interleukin-8 Receptor. *Science* **1991,** *253* (5025), 1280-1283.

372. Qin, L.; Kufareva, I.; Holden, L. G.; Wang, C.; Zheng, Y.; Zhao, C.; Fenalti, G.; Wu, H.; Han, G. W.; Cherezov, V.; Abagyan, R.; Stevens, R. C.; Handel, T. M., Structural biology. Crystal structure of the chemokine receptor CXCR4 in complex with a viral chemokine. *Science* **2015,** *347* (6226), 1117-22.

373. Zheng, Y.; Qin, L.; Zacarias, N. V.; de Vries, H.; Han, G. W.; Gustavsson, M.; Dabros, M.; Zhao, C.; Cherney, R. J.; Carter, P.; Stamos, D.; Abagyan, R.; Cherezov, V.; Stevens, R. C.; AP, I. J.; Heitman, L. H.; Tebben, A.; Kufareva, I.; Handel, T. M., Structure of CC chemokine receptor 2 with orthosteric and allosteric antagonists. *Nature* **2016,** *540* (7633), 458-461.

374. Tan, Q.; Zhu, Y.; Li, J.; Chen, Z.; Han, G. W.; Kufareva, I.; Li, T.; Ma, L.; Fenalti, G.; Li, J.; Zhang, W.; Xie, X.; Yang, H.; Jiang, H.; Cherezov, V.; Liu, H.; Stevens, R. C.; Zhao, Q.; Wu, B., Structure of the CCR5 chemokine receptor-HIV entry inhibitor maraviroc complex. *Science* **2013,** *341* (6152), 1387-90.

375. Oswald, C.; Rappas, M.; Kean, J.; Dore, A. S.; Errey, J. C.; Bennett, K.; Deflorian, F.; Christopher, J. A.; Jazayeri, A.; Mason, J. S.; Congreve, M.; Cooke, R. M.; Marshall, F. H., Intracellular allosteric antagonism of the CCR9 receptor. *Nature* **2016,** *540* (7633), 462-465.

376. Burg, J. S.; Ingram, J. R.; Venkatakrishnan, A. J.; Jude, K. M.; Dukkipati, A.; Feinberg, E. N.; Angelini, A.; Waghray, D.; Dror, R. O.; Ploegh, H. L.; Garcia, K. C., Structural biology. Structural basis for chemokine recognition and activation of a viral G protein-coupled receptor. *Science* **2015,** *347* (6226), 1113-7.

377. Kendrick, A. A.; Holliday, M. J.; Isern, N. G.; Zhang, F.; Camilloni, C.; Huynh, C.; Vendruscolo, M.; Armstrong, G.; Eisenmesser, E. Z., The dynamics of interleukin-8 and its interaction with human CXC receptor I peptide. *Protein Sci* **2014,** *23* (4), 464-80.

378. Brown, L. S.; Ladizhansky, V., Membrane proteins in their native habitat as seen by solid-state NMR spectroscopy. *Protein Sci* **2015,** *24* (9), 1333-46.

379. Das, B. B.; Park, S. H.; Opella, S. J., Membrane protein structure from rotational diffusion. *Biochim Biophys Acta* **2015,** *1848* (1 Pt B), 229-45.

380. Hansen, S. K.; Bertelsen, K.; Paaske, B.; Nielsen, N. C.; Vosegaard, T., Solid-state NMR methods for oriented membrane proteins. *Prog Nucl Magn Reson Spectrosc* **2015,** *88-89*, 48-85.

381. Opella, S. J., Solid-state NMR and membrane proteins. *J Magn Reson* **2015,** *253*, 129-37.

382. Lopez, J. J.; Shukla, A. K.; Reinhart, C.; Schwalbe, H.; Michel, H.; Glaubitz, C., The structure of the neuropeptide bradykinin bound to the human G-protein coupled receptor bradykinin B2 as determined by solid-state NMR spectroscopy. *Angew Chem Int Ed Engl* **2008,** *47* (9), 1668-71.

383. Luca, S.; White, J. F.; Sohal, A. K.; Filippov, D. V.; van Boom, J. H.; Grisshammer, R.; Baldus, M., The conformation of neurotensin bound to its G protein-coupled receptor. *Proc Natl Acad Sci U S A* **2003,** *100* (19), 10706-11.

384. Verhoeven, M. A.; Creemers, A. F.; Bovee-Geurts, P. H.; De Grip, W. J.; Lugtenburg, J.; de Groot, H. J., Ultra-high-field MAS NMR assay of a multispin labeled ligand bound to its G-protein receptor target in the natural membrane environment: electronic structure of the retinylidene chromophore in rhodopsin. *Biochemistry* **2001,** *40* (11), 3282-8.

385. Whittaker, C. A.; Patching, S. G.; Esmann, M.; Middleton, D. A., Ligand orientation in a membrane-embedded receptor site revealed by solid-state NMR with paramagnetic relaxation enhancement. *Org Biomol Chem* **2015,** *13* (9), 2664-8.

386. Park, S. H.; Prytulla, S.; De Angelis, A. A.; Brown, J. M.; Kiefer, H.; Opella, S. J., High-resolution NMR spectroscopy of a GPCR in aligned bicelles. *J Am Chem Soc* **2006,** *128* (23), 7402-3.

387. Marchetti, A.; Jehle, S.; Felletti, M.; Knight, M. J.; Wang, Y.; Xu, Z. Q.; Park, A. Y.; Otting, G.; Lesage, A.; Emsley, L.; Dixon, N. E.; Pintacuda, G., Backbone assignment of fully protonated solid proteins by 1H detection and ultrafast magic-angle-spinning NMR spectroscopy. *Angew Chem Int Ed Engl* **2012,** *51* (43), 10756-9.

388. Zhou, D. H.; Shah, G.; Cormos, M.; Mullen, C.; Sandoz, D.; Rienstra, C. M., Proton-detected solid-state NMR spectroscopy of fully protonated proteins at 40 kHz magic-angle spinning. *J Am Chem Soc* **2007,** *129* (38), 11791-801.

389. Andreas, L. B.; Le Marchand, T.; Jaudzems, K.; Pintacuda, G., High-resolution proton-detected NMR of proteins at very fast MAS. *J Magn Reson* **2015,** *253*, 36-49.

390. Nieuwkoop, A. J.; Franks, W. T.; Rehbein, K.; Diehl, A.; Akbey, U.; Engelke, F.; Emsley, L.; Pintacuda, G.; Oschkinat, H., Sensitivity and resolution of proton detected spectra of a deuterated protein at 40 and 60 kHz magic-angle-spinning. *J Biomol NMR* **2015,** *61* (2), 161-71.

391. Park, S. H.; Yang, C.; Opella, S. J.; Mueller, L. J., Resolution and measurement of heteronuclear dipolar couplings of a noncrystalline protein immobilized in a biological supramolecular assembly by proton-detected MAS solid-state NMR spectroscopy. *J Magn Reson* **2013,** *237*, 164-8.

392. Reif, B., Ultra-high resolution in MAS solid-state NMR of perdeuterated proteins: implications for structure and dynamics. *J Magn Reson* **2012,** *216*, 1-12.

393. Barbet-Massin, E.; Pell, A. J.; Retel, J. S.; Andreas, L. B.; Jaudzems, K.; Franks, W. T.; Nieuwkoop, A. J.; Hiller, M.; Higman, V.; Guerry, P.; Bertarello, A.; Knight, M. J.; Felletti, M.; Le Marchand, T.; Kotelovica, S.; Akopjana, I.; Tars, K.; Stoppini, M.; Bellotti, V.; Bolognesi, M.; Ricagno, S.; Chou, J. J.; Griffin, R. G.; Oschkinat, H.; Lesage, A.; Emsley, L.; Herrmann, T.; Pintacuda, G., Rapid proton-detected NMR assignment for proteins with fast magic angle spinning. *J Am Chem Soc* **2014,** *136* (35), 12489-97.

394. Dannatt, H. R.; Taylor, G. F.; Varga, K.; Higman, V. A.; Pfeil, M. P.; Asilmovska, L.; Judge, P. J.; Watts, A., (1)(3)C- and (1)H-detection under fast MAS for the study of poorly available proteins: application to sub-milligram quantities of a 7 trans-membrane protein. *J Biomol NMR* **2015,** *62* (1), 17-23.

395. Mance, D.; Sinnige, T.; Kaplan, M.; Narasimhan, S.; Daniels, M.; Houben, K.; Baldus, M.; Weingarth, M., An Efficient Labelling Approach to Harness Backbone and Side-Chain Protons in (1) H-Detected Solid-State NMR Spectroscopy. *Angew Chem Int Ed Engl* **2015,** *54* (52), 15799-803.

396. Ward, M. E.; Ritz, E.; Ahmed, M. A. M.; Bamm, V. V.; Harauz, G.; Brown, L. S.; Ladizhansky, V., Proton detection for signal enhancement in solid-state NMR experiments on mobile species in membrane proteins. *J Biomol NMR* **2015,** *63* (4), 375-388.

397. Shaka, A. J.; Barker, P. B.; Freeman, R., Computer-Optimized Decoupling Scheme for Wideband Applications and Low-Level Operation. *Journal of Magnetic Resonance* **1985,** *64* (3), 547-552.

398. Piotto, M.; Saudek, V.; Sklenar, V., Gradient-Tailored Excitation for Single-Quantum Nmr-Spectroscopy of Aqueous-Solutions. *Journal of Biomolecular Nmr* **1992,** *2* (6), 661-665.

399. Kuschert, G. S. V.; Hoogewerf, A. J.; Proudfoot, A. E. I.; Chung, C. W.; Cooke, R. M.; Hubbard, R. E.; Wells, T. N. C.; Sanderson, P. N., Identification of a glycosaminoglycan binding surface on human interleukin-8. *Biochemistry* **1998,** *37* (32), 11193-11201.

400. Nowacka, A.; Bongartz, N. A.; Ollila, O. H. S.; Nylander, T.; Topgaard, D., Signal intensities in H-1-C-13 CP and INEPT MAS NMR of liquid crystals. *Journal of Magnetic Resonance* **2013,** *230*, 165-175.

401. Williams, G.; Borkakoti, N.; Bottomley, G. A.; Cowan, I.; Fallowfield, A. G.; Jones, P. S.; Kirtland, S. J.; Price, G. J.; Price, L., Mutagenesis studies of interleukin-8 - Identification of a second epitope involved in receptor binding. *Journal of Biological Chemistry* **1996,** *271* (16), 9579-9586.

402. Wu, L. J.; Ruffing, N.; Shi, X. J.; Newman, W.; Soler, D.; Mackay, C. R.; Qin, S. X., Discrete steps in binding and signaling of interleukin-8 with its receptor. *Journal of Biological Chemistry* **1996,** *271* (49), 31202-31209.

403. Barter, E. F.; Stone, M. J., Synergistic Interactions between Chemokine Receptor Elements in Recognition of Interleukin-8 by Soluble Receptor Mimics. *Biochemistry* **2012,** *51* (6), 1322-1331.

404. Latorraca, N. R.; Venkatakrishnan, A. J.; Dror, R. O., GPCR Dynamics: Structures in Motion. *Chemical Reviews* **2017,** *117* (1), 139-155.

405. Prado, G. N.; Suetomi, K.; Shumate, D.; Maxwell, C.; Ravindran, A.; Rajarathnam, K.; Navarro, J., Chemokine signaling specificity: Essential role for the N-terminal domain of chemokine receptors (vol 46, pg 8961, 2007). *Biochemistry* **2007,** *46* (41), 11660-11660.

406. Sarmiento, J.; Shumate, C.; Suetomi, K.; Ravindran, A.; Villegas, L.; Rajarathnam, K.; Navarro, J., Diverging mechanisms of activation of chemokine receptors revealed by novel chemokine agonists. *Plos One* **2011,** *6* (12), e27967.

407. Wang, S.; Ladizhansky, V., Recent advances in magic angle spinning solid state NMR of membrane proteins. *Prog Nucl Magn Reson Spectrosc* **2014,** *82*, 1-26.

408. Hagn, F.; Nasr, M. L.; Wagner, G., Assembly of phospholipid nanodiscs of controlled size for structural studies of membrane proteins by NMR. *Nat Protoc* **2018,** *13* (1), 79-98.

409. Puthenveetil, R.; Nguyen, K.; Vinogradova, O., Nanodiscs and Solution NMR: preparation, application and challenges. *Nanotechnol Rev* **2017,** *6* (1), 111-126.

410. Leninger, M.; Traaseth, N. J., NMR Spectroscopy Approach to Study the Structure, Orientation, and Mechanism of the Multidrug Exporter EmrE. *Methods Mol Biol* **2018,** *1700*, 83-96.

411. Dorr, J. M.; Scheidelaar, S.; Koorengevel, M. C.; Dominguez, J. J.; Schafer, M.; van Walree, C. A.; Killian, J. A., The styrene-maleic acid copolymer: a versatile tool in membrane research. *Eur Biophys J* **2016,** *45* (1), 3-21.

412. Pollock, N. L.; Lee, S. C.; Patel, J. H.; Gulamhussein, A. A.; Rothnie, A. J., Structure and function of membrane proteins encapsulated in a polymer-bound lipid bilayer. *Biochim Biophys Acta* **2018,** *1860* (4), 809-817.

413. Maeda, H., SMANCS and polymer-conjugated macromolecular drugs: advantages in cancer chemotherapy. *Adv Drug Deliv Rev* **2001,** *46* (1-3), 169-85.

414. Maeda, H.; Takeshita, J.; Kanamaru, R., A lipophilic derivative of neocarzinostatin. A polymer conjugation of an antitumor protein antibiotic. *Int J Pept Protein Res* **1979,** *14* (2), 81-7.

415. Tonge, S. R.; Tighe, B. J., Responsive hydrophobically associating polymers: a review of structure and properties. *Adv Drug Deliv Rev* **2001,** *53* (1), 109-22.

416. Jamshad, M.; Grimard, V.; Idini, I.; Knowles, T. J.; Dowle, M. R.; Schofield, N.; Sridhar, P.; Lin, Y. P.; Finka, R.; Wheatley, M.; Thomas, O. R. T.; Palmer, R. E.; Overduin, M.; Govaerts, C.; Ruysschaert, J. M.; Edler, K. J.; Dafforn, T. R., Structural analysis of a nanoparticle containing a lipid bilayer used for detergent-free extraction of membrane proteins. *Nano Res* **2015,** *8* (3), 774-789.

417. Fiori, M. C.; Jiang, Y.; Zheng, W.; Anzaldua, M.; Borgnia, M. J.; Altenberg, G. A.; Liang, H., Polymer Nanodiscs: Discoidal Amphiphilic Block Copolymer Membranes as a New Platform for Membrane Proteins. *Sci Rep* **2017,** *7* (1), 15227.

418. Scheidelaar, S.; Koorengevel, M. C.; van Walree, C. A.; Dominguez, J. J.; Dorr, J. M.; Killian, J. A., Effect of Polymer Composition and pH on Membrane Solubilization by Styrene-Maleic Acid Copolymers. *Biophys J* **2016,** *111* (9), 1974-1986.

419. Goddard, A. D.; Dijkman, P. M.; Adamson, R. J.; dos Reis, R. I.; Watts, A., Reconstitution of membrane proteins: a GPCR as an example. *Methods Enzymol* **2015,** *556*, 405-24.

420. Lee, S. C.; Pollock, N. L., Membrane proteins: is the future disc shaped? *Biochem Soc Trans* **2016,** *44* (4), 1011-8.

421. Morrison, K. A.; Akram, A.; Mathews, A.; Khan, Z. A.; Patel, J. H.; Zhou, C.; Hardy, D. J.; Moore-Kelly, C.; Patel, R.; Odiba, V.; Knowles, T. J.; Javed, M. U.; Chmel, N. P.; Dafforn, T. R.; Rothnie, A. J., Membrane protein extraction and purification using styrene-maleic acid (SMA) copolymer: effect of variations in polymer structure. *Biochem J* **2016,** *473* (23), 4349-4360.

422. Fiori, M. C.; Jiang, Y.; Altenberg, G. A.; Liang, H., Polymer-encased nanodiscs with improved buffer compatibility. *Sci Rep* **2017,** *7* (1), 7432.

423. Lindhoud, S.; Carvalho, V.; Pronk, J. W.; Aubin-Tam, M. E., SMA-SH: Modified Styrene-Maleic Acid Copolymer for Functionalization of Lipid Nanodiscs. *Biomacromolecules* **2016,** *17* (4), 1516-22.

424. Schmidt, V.; Sturgis, J. N., Modifying styrene-maleic acid co-polymer for studying lipid nanodiscs. *Biochim Biophys Acta* **2018,** *1860* (3), 777-783.

425. Skar-Gislinge, N.; Simonsen, J. B.; Mortensen, K.; Feidenhans'l, R.; Sligar, S. G.; Moller, B. L.; Bjornholm, T.; Arleth, L., Elliptical Structure of Phospholipid Bilayer Nanodiscs Encapsulated by Scaffold Proteins: Casting the Roles of the Lipids and the Protein. *Journal of the American Chemical Society* **2010,** *132* (39), 13713-13722.

426. Lee, S. C.; Khalid, S.; Pollock, N. L.; Knowles, T. J.; Edler, K.; Rothnie, A. J.; O, R. T. T.; Dafforn, T. R., Encapsulated membrane proteins: A simplified system for molecular simulation. *Biochim Biophys Acta* **2016,** *1858* (10), 2549-2557.

427. Logez, C.; Damian, M.; Legros, C.; Dupre, C.; Guery, M.; Mary, S.; Wagner, R.; M'Kadmi, C.; Nosjean, O.; Fould, B.; Marie, J.; Fehrentz, J. A.; Martinez, J.; Ferry, G.; Boutin, J. A.; Baneres, J. L., Detergent-free Isolation of Functional G Protein-Coupled Receptors into Nanometric Lipid Particles. *Biochemistry* **2016,** *55* (1), 38-48.

428. Skrzypek, R.; Iqbal, S.; Callaghan, R., Methods of reconstitution to investigate membrane protein function. *Methods* **2018**.

429. Orwick-Rydmark, M.; Lovett, J. E.; Graziadei, A.; Lindholm, L.; Hicks, M. R.; Watts, A., Detergent-Free Incorporation of a Seven-Transmembrane Receptor Protein into Nanosized Bilayer Lipodisq Particles for Functional and Biophysical Studies. *Nano Lett* **2012,** *12* (9), 4687-4692.

430. Dorr, J. M.; Koorengevel, M. C.; Schafer, M.; Prokofyev, A. V.; Scheidelaar, S.; van der Cruijsen, E. A. W.; Dafforn, T. R.; Baldus, M.; Killian, J. A., Detergent-free isolation, characterization, and functional reconstitution of a tetrameric K+ channel: The power of native nanodiscs. *P Natl Acad Sci USA* **2014,** *111* (52), 18607-18612.

431. Gulati, S.; Jamshad, M.; Knowles, T. J.; Morrison, K. A.; Downing, R.; Cant, N.; Collins, R.; Koenderink, J. B.; Ford, R. C.; Overduin, M.; Kerr, I. D.; Dafforn, T. R.; Rothnie, A. J., Detergent-free purification of ABC (ATP-binding-cassette) transporters. *Biochemical Journal* **2014,** *461*, 269-278.

432. Li, D.; Li, J.; Zhuang, Y. L.; Zhang, L. H.; Xiong, Y.; Shi, P.; Tian, C. L., Nano-size uni-lamellar lipodisq improved in situ auto-phosphorylation analysis of E-coli tyrosine kinase using F-19 nuclear magnetic resonance. *Protein Cell* **2015,** *6* (3), 229-233.

433. Jamshad, M.; Charlton, J.; Lin, Y. P.; Routledge, S. J.; Bawa, Z.; Knowles, T. J.; Overduin, M.; Dekker, N.; Dafforn, T. R.; Bill, R. M.; Poyner, D. R.; Wheatley, M., G-protein coupled receptor solubilization and purification for biophysical analysis and functional studies, in the total absence of detergent. *Bioscience Rep* **2015,** *35*.

434. Komar, J.; Alvira, S.; Schulze, R. J.; Martin, R.; Nijeholt, J. A. L. A.; Lee, S. C.; Dafforn, T. R.; Deckers-Hebestreit, G.; Berger, I.; Schaffitzel, C.; Collinson, I., Membrane protein insertion and assembly by the bacterial holo-translocon SecYEG-SecDF-YajC-YidC. *Biochemical Journal* **2016,** *473*, 3341-3354.

435. Lee, S. C.; Knowles, T. J.; Postis, V. L. G.; Jamshad, M.; Parslow, R. A.; Lin, Y. P.; Goldman, A.; Sridhar, P.; Overduin, M.; Muench, S. P.; Dafforn, T. R., A method for detergent-free isolation of membrane proteins in their local lipid environment. *Nature Protocols* **2016,** *11* (7), 1149-1162.

436. Lee, S. C.; Khalid, S.; Pollock, N. L.; Knowles, T. J.; Edler, K.; Rothnie, A. J.; Thomas, O. R. T.; Dafforn, T. R., Encapsulated membrane proteins: A simplified system for molecular simulation. *Bba-Biomembranes* **2016,** *1858* (10), 2549-2557.

437. Jamshad, M.; Lin, Y. P.; Knowles, T. J.; Parslow, R. A.; Harris, C.; Wheatley, M.; Poyner, D. R.; Bill, R. M.; Thomas, O. R.; Overduin, M.; Dafforn, T. R., Surfactant-free purification of membrane proteins with intact native membrane environment. *Biochem Soc Trans* **2011,** *39* (3), 813-8.

438. Parmar, M.; Rawson, S.; Scarff, C. A.; Goldman, A.; Dafforn, T. R.; Muench, S. P.; Postis, V. L. G., Using a SMALP platform to determine a sub-nm single particle cryo-EM membrane protein structure. *Biochim Biophys Acta* **2018,** *1860* (2), 378-383.

439. Bersch, B.; Dorr, J. M.; Hessel, A.; Killian, J. A.; Schanda, P., Proton-Detected Solid-State NMR Spectroscopy of a Zinc Diffusion Facilitator Protein in Native Nanodiscs. *Angew Chem Int Ed Engl* **2017,** *56* (9), 2508-2512.

440. Swainsbury, D. J. K.; Proctor, M. S.; Hitchcock, A.; Cartron, M. L.; Qian, P.; Martin, E. C.; Jackson, P. J.; Madsen, J.; Armes, S. P.; Hunter, C. N., Probing the local lipid environment of the Rhodobacter sphaeroides cytochrome bc1 and Synechocystis sp. PCC 6803 cytochrome b6f complexes with styrene maleic acid. *Biochim Biophys Acta* **2018,** *1859* (3), 215-225.

441. Long, A. R.; O'Brien, C. C.; Malhotra, K.; Schwall, C. T.; Albert, A. D.; Watts, A.; Alder, N. N., A detergent-free strategy for the reconstitution of active enzyme complexes from native biological membranes into nanoscale discs. *BMC Biotechnol* **2013,** *13*, 41.

442. Vargas, C.; Arenas, R. C.; Frotscher, E.; Keller, S., Nanoparticle self-assembly in mixtures of phospholipids with styrene/maleic acid copolymers or fluorinated surfactants. *Nanoscale* **2015,** *7* (48), 20685-96.

443. Zhang, R.; Sahu, I. D.; Liu, L.; Osatuke, A.; Comer, R. G.; Dabney-Smith, C.; Lorigan, G. A., Characterizing the structure of lipodisq nanoparticles for membrane protein spectroscopic studies. *Biochim Biophys Acta* **2015,** *1848* (1 Pt B), 329-33.

444. Craig, A. F.; Clark, E. E.; Sahu, I. D.; Zhang, R.; Frantz, N. D.; Al-Abdul-Wahid, M. S.; Dabney-Smith, C.; Konkolewicz, D.; Lorigan, G. A., Tuning the size of styrene-maleic acid copolymer-lipid nanoparticles (SMALPs) using RAFT polymerization for biophysical studies. *Biochim Biophys Acta* **2016,** *1858* (11), 2931-2939.

445. Smith, A. A. A.; Autzen, H. E.; Laursen, T.; Wu, V.; Yen, M.; Hall, A.; Hansen, S. D.; Cheng, Y.; Xu, T., Controlling Styrene Maleic Acid Lipid Particles through RAFT. *Biomacromolecules* **2017,** *18* (11), 3706-3713.

446. Park, S. H.; Opella, S. J., Triton X-100 as the "short-chain lipid" improves the magnetic alignment and stability of membrane proteins in phosphatidylcholine bilayers for oriented-sample solid-state NMR spectroscopy. *J Am Chem Soc* **2010,** *132* (36), 12552-3.

447. Thiriot, D. S.; Nevzorov, A. A.; Zagyanskiy, L.; Wu, C. H.; Opella, S. J., Structure of the coat protein in Pf1 bacteriophage determined by solid-state NMR spectroscopy. *J Mol Biol* **2004,** *341* (3), 869-79.

448. Grant, C. V.; Sit, S. L.; De Angelis, A. A.; Khuong, K. S.; Wu, C. H.; Plesniak, L. A.; Opella, S. J., An efficient (1)H/(31)P double-resonance solid-state NMR probe that utilizes a scroll coil. *J Magn Reson* **2007,** *188* (2), 279-84.

449. Delaglio, F.; Grzesiek, S.; Vuister, G. W.; Zhu, G.; Pfeifer, J.; Bax, A., NMRPipe: a multidimensional spectral processing system based on UNIX pipes. *J Biomol NMR* **1995,** *6* (3), 277-93.

450. Zhang, H.; Lin, E. C.; Das, B. B.; Tian, Y.; Opella, S. J., Structural determination of virus protein U from HIV-1 by NMR in membrane environments. *Biochim Biophys Acta* **2015,** *1848* (11 Pt A), 3007-3018.

451. Cook, G. A.; Dawson, L. A.; Tian, Y.; Opella, S. J., Three-dimensional structure and interaction studies of hepatitis C virus p7 in 1,2-dihexanoyl-sn-glycero-3-phosphocholine by solution nuclear magnetic resonance. *Biochemistry* **2013,** *52* (31), 5295-303.

452. OuYang, B.; Xie, S.; Berardi, M. J.; Zhao, X.; Dev, J.; Yu, W.; Sun, B.; Chou, J. J., Unusual architecture of the p7 channel from hepatitis C virus. *Nature* **2013,** *498* (7455), 521-5.